Hydraulic-Test Interpretations for Well DOE-2 at the Waste Isolation Pilot Plant (WIPP) Site

Richard L. Beauheim

SF2900Q(8-81)

1008595/1010483

Hydraulic-Test Interpretations for Well DOE-2 at the Waste Isolation Pilot Plant (WIPP) Site

Richard L. Beauheim
Earth Sciences Division
Sandia National Laboratories
Albuquerque, NM 87185

Abstract

Eleven different zones were tested in Well DOE-2 in five phases of testing between 1984 and 1986. Testing techniques included a constant-head, borehole-infiltration test, drill-stem tests, slug tests, pressure-pulse tests, and multiwell pumping tests. Four of the zones tested—the lower Dewey Lake Red Beds, the Tamarisk Member of the Rustler Formation, the lower unnamed member of the Rustler Formation and Rustler/Salado contact, and the entire Salado Formation—had permeabilities too low to measure with the equipment and test techniques used. The other zones had permeabilities ranging over six orders of magnitude. No saturated strata were encountered above the Rustler Formation, although parts of the middle Dewey Lake Red Beds appear to have appreciable permeability.

In the Rustler Formation, the Culebra Dolomite Member is the most permeable unit, having a transmissivity of ~90 ft²/day. The Culebra behaves hydraulically as a double-porosity system, with the major permeability provided by fractures and the major storage provided by matrix porosity. The Culebra at DOE-2 is well connected hydraulically to the Culebra at Wells H-6b and WIPP-13 to the west, probably by interconnected fractures. Response times between these wells are very short (<1 day/10,000 ft). The Culebra does not appear to be as fractured to the south at Wells WIPP-12 and 18, or to the east at Well H-5b, as indicated by delayed, low-magnitude (or nonexistent) responses to DOE-2 pumping, and by low permeabilities interpreted from other tests conducted at those wells. The other Rustler members at DOE-2, which are not known to be fractured and do not display hydraulic responses typical

Abstract (continued)

of fractured (or double-porosity) media, have permeabilities three to four orders of magnitude lower than that of the Culebra. Hydraulic heads decrease through the Rustler with increasing depth. This implies that the Tamarisk, and indirectly the Magenta and Forty-niner, could act as a source of recharge for the Culebra.

In the Salado Formation, the interval including Marker Beds 138 and 139 and the Waste Isolation Pilot Plant (WIPP) facility horizon has an extremely low average permeability (<0.3 μd), and showed no evidence over about 2 days of testing of containing high-pressure sources of either brine or gas.

In the Bell Canyon Formation, the Hays sandstone was the most permeable unit tested, having an average permeability of about 2.4 md (0.55 ft/day). The Olds and Ramsey sandstones, overlying the Hays, have permeabilities almost two orders of magnitude lower. Hydraulic heads in the Bell Canyon sandstones could not be quantified precisely enough to define vertical gradients within the Bell Canyon.

In freshwater terms, the observed Bell Canyon head is higher than the hydraulic head of the Culebra dolomite. If the Bell Canyon and Culebra were connected by an open borehole, however, salt dissolution in the Salado section would increase the specific gravity of the Bell Canyon fluid so that, *at the elevation of the Culebra*, the Culebra head would be higher than that of the Bell Canyon. In this event, the flow direction would be downwards from the Culebra into the Bell Canyon.

Acknowledgments

Contents

Contents (continued)

Figures

Figures (continued)

Tables

Hydraulic-Test Interpretations for Well DOE-2 at the Waste Isolation Pilot Plant (WIPP) Site

1. Introduction

This report presents the interpretations of hydraulic tests performed in Hole DOE-2 at the Waste Isolation Pilot Plant (WIPP) site in southeastern New Mexico (Figure 1-1). The WIPP is a US Department of Energy (DOE) research and development facility designed to demonstrate safe disposal of radioactive wastes resulting from the nation's defense programs. The WIPP facility will lie in bedded halite in the lower Salado Formation.

Various breach-consequence scenarios have been hypothesized for the WIPP that involve interconnection of the WIPP facility with overlying and/or underlying aquifers through one or more boreholes. To evaluate these scenarios, the aquifers overlying and underlying the facility must be characterized with respect to their relative head potentials, permeabilities, storativities, and water qualities. The intent of the DOE-2 testing program was to provide the necessary hydrologic characterization of all zones in a single borehole that could potentially play a significant role in any breach event. The information gathered from each zone would also assist in the regional characterization of the different aquifers. The hydrologic testing program for Hole DOE-2 was developed through consultation between Sandia National Laboratories, the DOE, the US Geological Survey (USGS), INTERA Technologies, and Westinghouse/IT. The program was outlined for the New Mexico Environmental Evaluation Group for their information, and to solicit their comments. All testing was performed under the direction of Sandia National Laboratories, Albuquerque, NM.

2. Location and Stratigraphy

The WIPP site is located in the northern part of the Delaware Basin in southeastern New Mexico. Hole DOE-2 is in the southeast quarter of Section 8, Township 22 South, Range 31 East, in Eddy County, NM. Ground surface elevation at the DOE-2 drilling pad is ~3418 ft above mean sea level. DOE-2 has a total depth of 4325 ft, and penetrated (in descending order) loose surficial sands, the Mescalero caliche, the Santa Rosa Sandstone, the Dewey Lake Red Beds, the Rustler Formation, the Salado Formation, the Castile Formation, and the Bell Canyon Formation (Figure 2-1). The surficial sands are of Holocene age, the Mescalero caliche is of Pleistocene age, the Santa Rosa is of Triassic age, and the remainder of the formations are of Permian age. Detailed stratigraphic and lithologic information from Hole DOE-2 is contained in Mercer et al. (1986); a brief summary based on that document is presented below. All depths given in this report are below ground surface.

From the surface to a depth of 8 ft, DOE-2 penetrated loose sand and pad-fill material. The Mescalero caliche was encountered from 8 to 13 ft deep. The Santa Rosa Sandstone extends from 13 to 133 ft deep at DOE-2. It is composed of fine- to coarse-grained sandstone interbedded with siltstone and claystone.

The Dewey Lake Red Beds lie from 133 to 639 ft deep, and consist of siltstone with claystone and sandstone interbeds. Numerous bedding plane breaks and fractures at various angles are filled with secondary selenite.

Figure 1-1. Locations of Hole DOE-2 and the WIPP Site
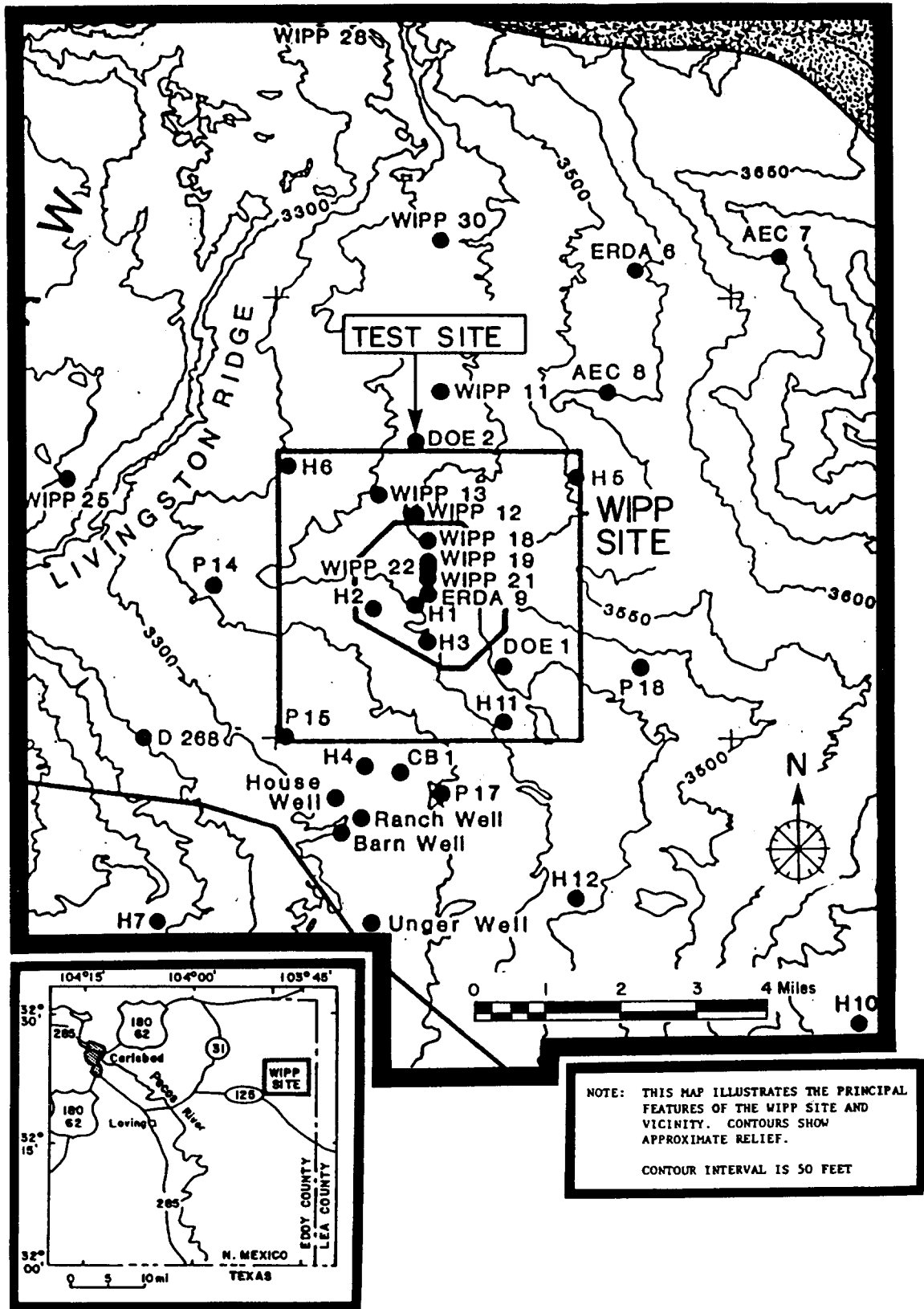
NOTE: THIS MAP ILLUSTRATES THE PRINCIPAL FEATURES OF THE WIPP SITE AND VICINITY. CONTOURS SHOW APPROXIMATE RELIEF.

CONTOUR INTERVAL IS 50 FEET

GROUND SURFACE
DUNE SAND
8'
13'
MESCALERO CALICHE

SANTA ROSA SANDSTONE
133'

DEWEY LAKE RED BEDS

639'

RUSTLER FORMATION
699' FORTY-NINER MEMBER
722' MAGENTA DOLOMITE MEMBER
824' TAMARISK MEMBER
846' CULEBRA DOLOMITE MEMBER
961' UNNAMED MEMBER

SALADO FORMATION

MARKER BED 138
2203'

2303'
2306'
MARKER BED 139

3083'

CASTILE FORMATION

ANHYDRITES
III AND II

3801'
3809'
HALITE I
ANHYDRITE I

4071'

BELL CANYON FORMATION
4103' LAMAR LIMESTONE MEMBER
4174' RAMSEY SANDSTONE
4183' FORD SHALE
4218' OLDS SANDSTONE
HAYS SANDSTONE

TOP OF CASING 1.2' ABOVE GROUND
G.S. ELEVATION
3418.35' a.m.s.l.

9-5/8" O.D., J-55, 36 lb/ft CASING

822'
848'
873.2'
868.6'
SHOT-PERFORATED, 4 shots/ft
BAKER INFLATABLE BRIDGE PLUG

1009'

WELL CONFIGURATION
AS OF 04/02/86

7-7/8" OPEN BOREHOLE

NOT TO SCALE

T.D. 4325'

Figure 2-1. Stratigraphy and As-Built Diagram for DOE-2

11

The Rustler Formation lies from 639 to 961 ft deep and is subdivided into five members. In descending order, they are the Forty-niner Member, the Magenta Dolomite Member, the Tamarisk Member, the Culebra Dolomite Member, and the lower unnamed member. The Forty-niner Member lies from 639 to 699 ft deep and consists of two anhydrite/gypsum units and one claystone unit. The Magenta Dolomite Member lies from 699 to 722 ft deep and is a silty, gypsiferous, laminated dolomite. The Tamarisk Member lies from 722 to 824 ft deep and consists of two gypsum and anhydrite units separated by a gypsiferous siltstone/claystone unit. The Culebra Dolomite Member lies from 824 to 846 ft deep and is a silty, vuggy dolomite. The Culebra is highly fractured at DOE-2, as evidenced by core and acoustic-televiewer logs. The unnamed lower member lies from 846 to 961 ft deep and consists of anhydrite, gypsum, clay(stone), siltstone, and halite.

The Salado Formation lies from 961 to 3083 ft deep and is composed largely of halite, with minor amounts of interspersed clay and polyhalite. The Salado also contains interbeds of anhydrite, polyhalite, clay, sylvite, and langbeinite. Jones et al. (1960) labeled several of the anhydrite and/or polyhalite interbeds that are traceable over most of the Delaware Basin as "Marker Beds" and gave them numbers ranging from 101 to 145 (increasing downward). The WIPP facility horizon lies between Marker Beds 138 and 139.

The Castile Formation lies from 3083 to 4071 ft deep and is composed of anhydrite and halite. At and near the WIPP site, the Castile typically has five members: three anhydrite beds, labeled Anhydrites I, II, and III in ascending order; and two halite interbeds, labeled Halites I and II in ascending order. At DOE-2, Halite II is totally absent, and Halite I is only 8 ft thick.

The Bell Canyon Formation lies from 4071 ft deep to beyond the total depth of DOE-2 at 4325 ft deep. One formal member and four informal members of the Bell Canyon were identified at DOE-2 in descending order as the Lamar Limestone Member, the Ramsey sandstone, the Ford shale, the Olds sandstone, and the Hays sandstone. The Lamar limestone lies from 4071 to 4103 ft deep and consists of grayish-black limestone with minor shale. The Ramsey sandstone lies from 4103 to 4174 ft deep and is fine to medium grained, with a calcareous cement. The calcareous Ford shale lies from 4174 to 4183 ft deep. The Olds sandstone lies from 4183 to 4218 ft deep and is fine to medium grained, with discontinuous clay laminae and noncalcareous cement. The Hays sandstone begins 4218 ft deep and continues beyond the total depth of DOE-2

at 4325 ft. It is fine to medium grained, has a noncalcareous cement, and contains thin (<0.1 ft) shale interbeds. The contacts between the Bell Canyon sandstones are gradational, and are marked by an increase in silt and clay content.

3. Selection and Preparation of Test Intervals

Eleven different zones were tested in DOE-2 in five phases of testing. These zones were, in descending order: the lower part of the Dewey Lake Red Beds; portions or all of the Forty-niner, Magenta, Tamarisk, Culebra, and unnamed members of the Rustler Formation; an interval of the Salado Formation including Marker Beds 138 and 139; the bulk of the Salado Formation; and the Ramsey, Olds, and Hays sandstones of the Bell Canyon Formation. All of these zones were tested in the open drillhole during the first four phases of testing. The Culebra dolomite was also retested after the hole was cased, perforated, and acidized for the fifth phase of testing.

3.1 During Drilling

During the drilling of DOE-2, four stop-points were scheduled to permit hydraulic testing of the most recently penetrated strata. The first stop-point was at the top of the Rustler Formation to allow testing of the overlying Dewey Lake Red Beds. Although a water table exists in the Dewey Lake locally south of the WIPP site, no evidence of saturation of the Dewey Lake at DOE-2 was observed in core samples. Nevertheless, the Dewey Lake *is* permeable, as evidenced by a loss of circulation at a depth of ~245 ft, and could conceivably provide a flow path in the event of a breach of the WIPP facility involving upward movement of fluid to this level or above.

The original Field Operations Plan for the Phase I investigations (Mercer et al., 1986) called for three tests in the Dewey Lake: one in the Dewey Lake sandstone estimated to lie between ~200 and 250 ft deep, one in the Dewey Lake gypsiferous zone between ~250 and 400 ft deep, and one in the lower Dewey Lake from ~400 ft to just below the Dewey Lake-Rustler contact. Unfavorable drilling conditions, however, required reaming the upper Dewey Lake to too large a diameter to be tested with the available equipment. Hence, the decision was made to attempt to test only the lower Dewey Lake from a depth of 490 ft to

the bottom of the hole at 641 ft deep, ~2 ft below the contact with the Rustler Formation. When a reliable packer seat could not be obtained at 490 ft, the top of the test interval was moved down to 539 ft.

The second stop-point, which was at the top of the Salado Formation, coincided with the end of the Phase I drilling and allowed testing of the overlying Rustler Formation. Portions or all of the five members of the Rustler were selected for testing: the lower claystone part of the unnamed member and the Rustler-Salado contact from 945 to 967 ft deep, the Culebra Dolomite Member from 824 to 846 ft deep, the claystone/siltstone portion of the Tamarisk Member from 796 to 817 ft deep, the Magenta Dolomite Member from 700 to 722 ft deep, and the claystone/siltstone portion of the Forty-niner Member from 664 to 686 ft deep. The untested portions of the Tamarisk and Forty-niner members consist of intact anhydrite and gypsum; the untested portion of the lower unnamed member consists of clay, anhydrite, gypsum, and halite. These zones were judged, from examination of core, to have permeabilities too low to measure with the available equipment.

Phase Ia testing of the Culebra dolomite also occurred at the second stop-point, albeit after the hole was reamed. The results of the Phase I testing of the Culebra, discussed below, indicated the need for additional testing before Phase II drilling.

The third stop-point was at the top of the Castile Formation to allow testing of the overlying Salado Formation. The first zone tested in the Salado Formation extended from 2196 to 2308 ft deep; it included Marker Beds 138 and 139 and the WIPP facility horizon. This zone was selected because of the pressurized gas and brine occurrences noted in the 50-ft coreholes into the roof and floor of the facility (US DOE, 1983). The bulk of the Salado (including the Salado-Castile contact) from 1041 to 3095 ft deep was also tested. This interval was tested to determine if there were significant pressure-producing zones within the Salado. Because no such zones were detected while the interval was isolated for several days, no further tests were performed in the Salado.

The fourth stop-point was at the final total depth of the hole, ~254 ft into the Bell Canyon Formation, and allowed testing of portions of the upper Bell Canyon and the Castile Formation. This stop-point was selected because it was beneath the typical stop-point for gas exploration drilling in the Bell Canyon and was about the same distance into the Bell Canyon that hole Cabin Baby-1 extended (Beauheim et al., 1983). Hence, the same Bell Canyon zones that were tested in Cabin Baby-1 could be tested in DOE-2. The Bell Canyon intervals tested in DOE-2 were, in as-

cending order, the Hays sandstone from 4220 to 4325 ft deep, the Olds sandstone from 4177 to 4218 ft deep, and the Ramsey sandstone from 4138 to 4180 ft deep. The Lamar limestone, which was tested in Cabin Baby-1, was not tested in DOE-2 because examination of the core indicated very low permeability. Evaluation of core and caliper logs indicated a total lack of open fractures in the Castile and very low permeability. Thus, testing in the Castile was deemed unwarranted.

All intervals listed above are actual tested intervals, i.e., the intervals between straddle packers or between a single packer and the bottom of the hole. As the individual test results are presented below (Chapter 7), differences between the estimated producing thicknesses and the total tested thicknesses will be discussed.

3.2 After Drilling

After all the drilling and Phases I, Ia, II, and III testing of DOE-2 were finished, the hole was recompleted as a Culebra dolomite observation well to allow for additional Culebra testing and monitoring. This recompletion was accomplished by perforating the casing across the Culebra interval between the depths of 822 and 848 ft with 0.5-in. bullets using four shots/ft. A bridge plug was set in the casing below the Culebra from 868.6 to 873.2 ft deep to isolate the Culebra from the open hole below (Mercer et al., 1986).

Subsequent efforts at well development revealed a very low well efficiency; the maximum sustainable pumping rate was only ~2 gpm. On May 27, 1986, the casing perforations were acidized by first "spotting" ~85 gal of 20% hydrochloric acid at the level of the perforations in the casing for slightly over 1 hr and then by injecting 2000 gal of 20% HCl. The Culebra accepted the acid at a rate of ~25 gpm, with no excess surface pressure beyond hydrostatic exerted on the system. After several hours, most of the spent acid was swabbed from the hole. The hole was also cleaned and developed by pumping and surging before further testing. After acid treatment, the well could sustain a pumping rate of >35 gpm.

4. Test Methods

A variety of testing methods were employed at DOE-2 because both saturated and unsaturated media were tested and because permeabilities ranging over six orders of magnitude were encountered. A constant-head, borehole-infiltration test was

attempted in the unsaturated Dewey Lake Red Beds. For the saturated intervals to be tested, drill-stem tests (DSTs), rising-head "slug" tests, pressure-pulse tests, and pumping tests were selected as the most appropriate means of quantifying hydraulic properties.

4.1 Constant-Head, Borehole-Infiltration Tests

Constant-head, borehole-infiltration tests, as described by Stephens and Neuman (1980), involve isolating a zone to be tested above a water table with inflatable packers, then applying a constant fluid pressure to the zone and monitoring the rate at which water flows into the formation. Where the unsaturated strata to be tested overlie a relatively impermeable layer rather than a water table, the same type of test may be suitable, depending on whether or not steady-state flow conditions are reached before boundary effects from the impermeable layer come into play. If boundary effects begin to influence the data before steady-state conditions are reached, observation wells are required to interpret the response.

When a constant-head, borehole-infiltration test begins, the flow rate into the formation will be relatively high as the rock around the borehole begins to saturate. At this time, flow is largely horizontal because the strongest gradient is oriented normal to the axis of the borehole. With increasing time and saturation, the flow rate decreases and downward vertical flow becomes increasingly important. As the horizontal area of saturation widens, the area over which vertical flow occurs also increases. When the downward vertical flow balances the horizontal flow, steady state is reached and the flow rate stabilizes. The stabilized flow rate can then, in theory, be used to calculate the saturated permeability of the formation.

In practice, complete stabilization of the flow rate can take an unreasonably long time. Stephens and Neuman (1980) determined that when flow rate was plotted versus the inverse of the square root of flow time, a straight line would eventually develop that could be extrapolated to infinite time. The flow-rate intercept at infinite time corresponds to the saturated flow rate within ~10%. In the field, this plotting technique can be used to determine when a valid extrapolation can be made and the test terminated, reducing total test time significantly.

4.2 Drill-Stem Tests

DSTs (and slug and pressure-pulse tests) require a packer assembly mounted at the bottom of a tubing string in the hole that isolates the interval to be tested. For a test of the lower portion of the hole, a single packer may be used. To test a discrete zone in a hole, a straddle-packer arrangement is required. Other necessary equipment includes a shut-in tool to isolate the test interval from the tubing, transducers reading pressures above, between, and below the packers, and a data-acquisition system (DAS). Instrumentation specifications are discussed below.

The first step in a DST is to select the interval to be tested. The packer separation, or straddle, is then adjusted to correspond to interval thickness. Next, the packer assembly, including transducers, is run into the hole to the desired depth, and the packers are inflated. The test interval is then shut-in (isolated from the tubing above), and the fluid in the tubing above the tool is removed by swabbing while the pressure in the test interval stabilizes.

The actual DST begins with opening the shut-in tool, which allows the water in the isolated interval to enter the tubing. Because of the large pressure differential normally existing between the evacuated tubing and the isolated interval, water under the initial formation pressure flows towards the borehole and up the tubing string. This is the first flow period (FFL; see Figure 4-1). This period begins with a drop in pressure from pretest conditions (shut-in tool closed) to a pressure corresponding to the weight of the water remaining in the tubing (after swabbing) above the transducer. As water rises up the tubing string, the pressure exerted downward on the isolated interval increases, reducing the pressure differential and thus the flow rate.
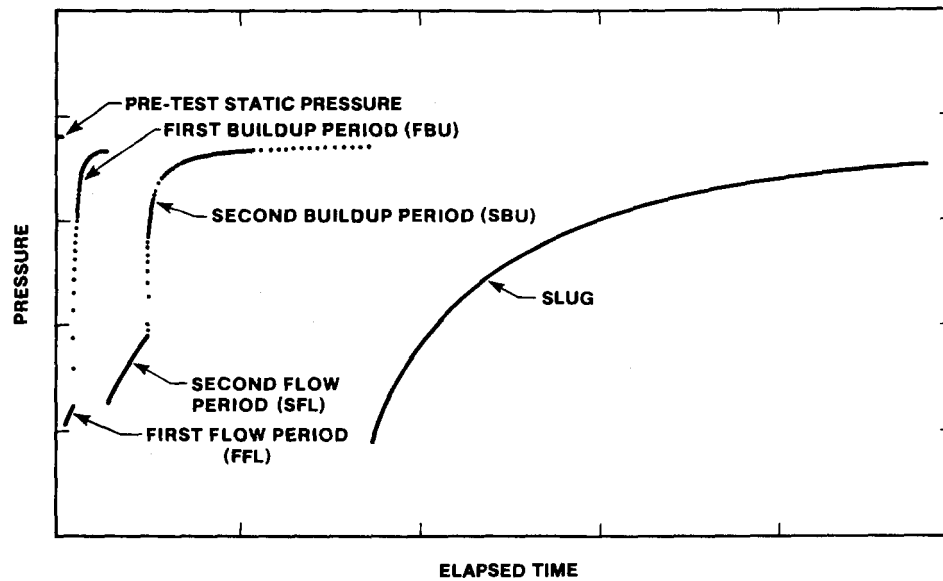
Figure 4-1. Components of a Drill-Stem Test and Slug Test

When the flow rate has decreased by $\sim 10\%$ to 20% from its initial value, the shut-in tool is closed, stopping the flow of water up the tubing. This is the beginning of the first pressure buildup period (FBU). The pressure in the test interval, which was increasing relatively slowly during the FFL, builds back up toward the pretest formation pressure more quickly now that the interval is once again isolated. Initially, the pressure builds up rapidly because of the differential between the pressure in the test interval at the end of the FFL and that in the surrounding formation. As this pressure differential decreases, the rate of pressure buildup decreases. On an arithmetic plot of pressure versus time, the pressure "bends over" and starts to level out (Figure 4-1). The longer the FBU is allowed to run, the more definitive the data become for estimating formation hydraulic parameters, and conditions become more ideal for the start of the second flow period. In practical terms, the FBU should generally last at least four times as long as the FFL. In very low permeability formations, an FBU duration more than 10 times as long as the FFL may be necessary.

Following the FBU, the shut-in tool is reopened to initiate the second flow period (SFL). The water level in the tubing will not have changed since the end of the FFL, and so a pressure differential will exist between the test interval and the tubing. The SFL typically lasts somewhat longer than the FFL, but again the flow rate is allowed to decrease by only 10% to 20%. At the conclusion of the SFL, the shut-in tool is closed and the second buildup period (SBU) begins. Like the FBU, the SBU continues until the pressure

starts to "level out." As with the FBU, the data become more definitive the longer the SBU continues, and conditions improve for the next phase of testing. These four periods, the FFL, FBU, SFL, and SBU, generally constitute a single complete DST.

4.3 Rising-Head Slug Tests

Ater the second buildup of the DST, and while the shut-in tool is still closed, the fluid is swabbed out of the tubing to allow a rising-head slug test. A rising-head slug test is performed in exactly the same manner as the DST flow periods, except that the test is not terminated after the flow rate changes by 10% to 20% (Figure 4-1). Ideally, the slug test should continue until the initial pressure differential has decreased by 80% to 90%. Practically, 40% recovery is generally adequate to define the shape of the recovery curve, particularly if log-log plotting techniques are used (Ramey et al., 1975).

4.4 Pressure-Pulse Tests

Pressure-pulse tests can take the form of either pulse-withdrawal or pulse-injection tests. For either type, the test interval is first shut-in and the pressure allowed to stabilize. The tubing string is either swabbed for a pulse-withdrawal test, or filled to the surface or otherwise pressurized for a pulse-injection test. The shut-in tool is then opened only long enough for the underpressure (pulse-withdrawal) or overpressure (pulse-injection) to be transmitted to the test zone, and then the shut-in tool is closed. In practical

15

terms, it typically takes ∼1 min to open the tool, verify over several pressure readings that the pressure pulse has been transmitted, and close the tool. The dissipation of the resultant pressure differential between the test zone and the formation is then monitored for the actual test. As with a slug test, the pressure differential should be allowed to decrease by 80% to 90%. However, pressure-pulse tests proceed much more rapidly than slug tests because equilibration is caused by compression of fluid rather than by filling a volume of tubing; hence, attaining 80% to 90% recovery is generally practical during a pressure-pulse test.

4.5 Pumping Tests

Pumping tests are performed by lowering a pump into the hole, isolating the interval to be tested, and pumping water from the formation at a nominally constant rate while monitoring the decline in water level or pressure in the pumped well and in any nearby available observation wells. Durations of pumping periods are highly variable and are primarily a function of what volume (or areal extent) of the aquifer one wishes to test. After the pumping period, the recovery (rise) of water levels or pressures in the wells is monitored, typically through at least 95% recovery.

4.6 Isolation Verification

Pressures above and below the tested interval are monitored during all tests so as to detect any leakage around packers or other types of flow into or out of the test interval from/to above or below. Slow, uniform pressure changes of a few psi in the borehole intervals above and below the test interval are not uncommon because fluids from these intervals may seep into the adjacent formations, or formation fluids may flow into relatively underpressurized intervals. Abrupt, higher magnitude pressure changes may indicate faulty packer seats or other malfunctions.

Even when inflated to 2000 psi above ambient borehole pressures, packers exhibit a degree of compliance, or "give." Because some shut-in tools require an up-or-down movement of the tubing string with several tons of force, packers may shift very slightly upward or downward. In an isolated interval of the borehole, such as below the bottom packer, the increase or decrease in volume caused by the packer compliance is translated into a detectable pressure change. Packer-compliance effects should not be confused with pressure changes having other causes. Differentiation is possible because packer compliance typically causes abrupt pressure changes at the time of tool movements or after packer inflation, followed by a return to the predisturbance pressure, whereas packer leaks or bad seals usually result in continuous pressure changes or equilibration between test-interval pressure and annulus or bottomhole pressure.

5. Instrumentation

Five different sets of instrumentation were used during the DOE-2 testing: one set during the Phase I testing of the Dewey Lake Red Beds, a second set during the Phase I testing of the Rustler Formation, a third set during the Phase Ia testing of the Culebra dolomite, a fourth set during the Phase II and Phase III testing of the Salado and Bell Canyon Formations, and a fifth set during the 1986 testing of the Culebra dolomite. The fourth set of instrumentation, which used quartz-crystal transducers, produced the highest-quality (high resolution, low noise) data.

NOTE: The use of brand names in this report is for identification only and does not imply endorsement of specific products by Sandia National Laboratories.

5.1 Phase I Testing—The Dewey Lake Red Beds

A schematic drawing of the downhole and uphole instrumentation for the Phase I constant-head, borehole-infiltration testing of the Dewey Lake Red Beds is presented in Figure 5-1. The downhole equipment consisted of a Baski air-inflatable packer with a feedthrough line for a transducer on 2.375-in. tubing. Two Bell and Howell CEC 1000 strain-gage transducers were strapped to the tubing, one connected to the zone below the packer by means of the feedthrough line and the other measuring the pressure in the borehole annulus above the packer. The uphole equipment consisted of a positive-displacement Bean pump to supply pressure to the tubing, a CertainTeed water meter to measure the flow rate, an Ashcroft 0- to 100-psi pressure gage to measure the injection pressure, a ball valve to control the backpressure, and a bypass line to divert the water produced by the pump in excess of that which the formation could accept.

The transducers and other data-acquisition equipment for the Phase I Dewey Lake and Rustler testing were provided by the USGS and are described in detail by Basler (1983). The USGS DAS is shown schematically in Figure 5-2. A Validyne CD19 carrier demodulator amplifier provided ac excitation and a variable high-level output for the transducers. Data

were recorded with a Soltec VP-6723S strip-chart recorder and an Esterline Angus PD2064 digital data logger. A Validyne DB-199 digital barometer was used to monitor and record barometric pressure. A Datel DVC-8500 voltage calibrator was used to verify calibration of recorders and digital meters. Transducer calibration was performed before and after each installation using a Chandler 23-1 dead-weight tester.
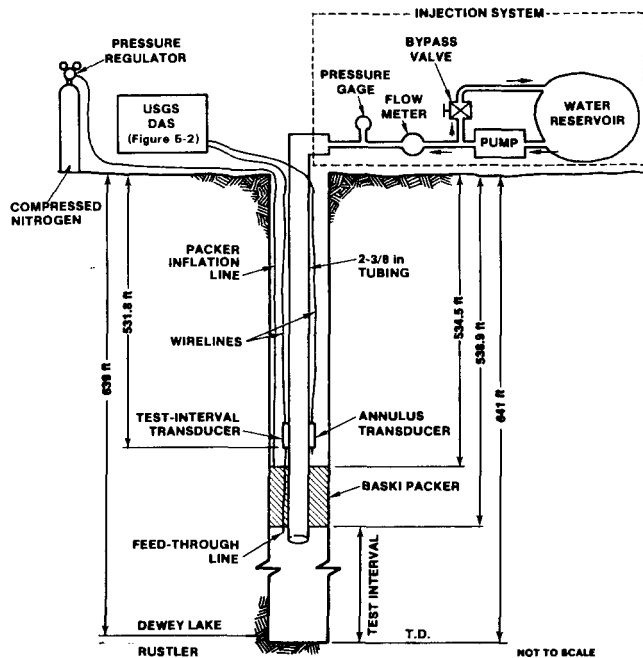
Figure 5-1. Dewey Lake Test Equipment Configuration
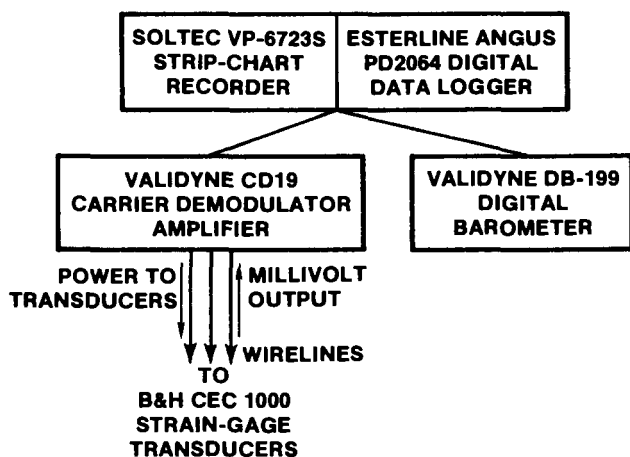
Figure 5-2. USGS Data-Acquisition System

5.2 Phase I Testing—The Rustler Formation

For the Phase I DSTs of the Rustler Formation, the downhole equipment consisted of a Baski straddle-packer DST tool and three Bell and Howell CEC 1000 strain-gage transducers. The DST tool consisted of two air-inflatable packers separated by a perforated spacing shroud, with a section of blank pipe containing an air-inflatable shut-in or "valve" packer set above the upper straddle packer (Figure 5-3). This entire assembly was lowered to the desired test depth on 2.375-in. tubing. The DST tool has feedthrough fittings for inflation lines for the three packers and for pressure-transmittal lines from the zone beneath the lower packer and from the straddled interval to the transducers, which were strapped to the tubing just above the DST tool. A third transducer, which measured the wellbore annulus pressure above the upper packer, was also strapped to the tubing. Each transducer was connected to the DAS at the surface (described in Section 5.1) with a separate wireline.

5.3 Phase Ia Testing— The Culebra Dolomite Member

For the Phase Ia pumping test of the Culebra dolomite, the downhole equipment consisted of a 3-hp Red Jacket 32BC pump suspended below a Baski air-inflatable packer on 2.375-in. tubing, with two Druck PDCR-10 strain-gage transducers strapped to the tubing above the packer (Figure 5-4). One of the transducers measured the pressure below the packer in the test interval by means of a feedthrough line through the packer; the second measured the pressure in the wellbore above the packer. A 0.25-in. nylon line for collecting fluid samples was teed off from the main discharge line just above the pump and fed through the packer to the surface. A Lynes water-inflatable resettable bridge plug was set below the Culebra to seal off the lower portion of the hole. No measurements were made of fluid pressure below the bridge plug. The uphole equipment consisted of a Rockwell flow meter, a pressure gage, and a ball valve to maintain adequate backpressure on the flow meter.

17

PACKER-INFLATION LINES — WIRELINES TO DAS

ANNULUS TRANSDUCER

WIRELINE TO DAS

PACKER-INFLATION LINE

TEST-INTERVAL TRANSDUCER

BOTTOM-HOLE TRANSDUCER

2-3/8 in TUBING

ADAPTOR

NIPPLE

ADAPTOR

CONNECTOR WITH HOLES FOR WATER PASSAGE

SHORT NIPPLE

PACKER-INFLATION LINE

PACKER-INFLATION LINE

VALVE PACKER

TRANSDUCER FEED-THROUGH LINE

TOP PACKER

ADAPTOR

FLUID PORTS

COUPLER

SPACERS

PACKER-INFLATION LINE

BOTTOM PACKER

TRANSDUCER FEED-THROUGH LINE

NOT TO SCALE

NOSE CONE

Figure 5-3. Baski DST Tool

18

Figure 5-4. Phase Ia Culebra Pumping Test Equipment Configuration

The DAS at the surface for the Phase Ia testing consisted of Tektronix PS503A dual power supplies to provide power to the transducers, an HP-3495A signal scanner for channel switching, an HP-3456A digital voltmeter (DVM) to measure the transducer output, an EDC-501J programmable voltage standard to verify the accuracy of the DVM, an HP-9845B desktop computer for system control, and HP-9885M and S floppy disk drives for data storage (Figure 5-5). The HP-3456A DVM and EDC-501J voltage standard are calibrated by the Sandia Standards Laboratory every 6 mo, and the transducers were calibrated in the field using a Heise gage before installation in the well. The data-acquisition software was written and is maintained by Sandia. Additional information on this DAS can be found in INTERA Technologies and Hydro-GeoChem (1985).
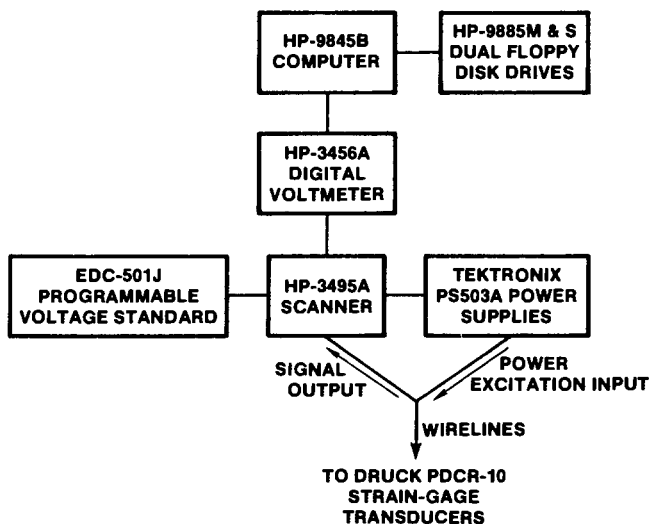
Figure 5-5. Sandia Data-Acquisition System

At the H-5b and H-6b observation wells monitored during the Phase Ia testing at DOE-2, Baski air-inflatable packers were set in the well casing above the Culebra to minimize wellbore-storage effects during the testing. Druck PDCR-10 strain-gage transducers measured pressures in the Culebra intervals by means of feedthrough lines through the packers. Additional transducers measured pressures in the wellbores above the packers. The DASs used were identical to

that at DOE-2, except that at H-5b, no HP-9845b computer was available. Millivolt output from the H-5b transducers was read manually from the HP-3456A DVM and entered into log books. The data were converted to pressures after having been hand-entered into computer files.

5.4 Phases II and III Testing—The Salado and Bell Canyon Formations

For the Phase II and Phase III drill-stem, slug, and pressure-pulse testing of the Salado and Bell Canyon formations, the downhole equipment was supplied by Baker Production Technology (formerly Lynes, Inc.). This consisted of a Baker Hydrological Test Tool comprising two water-inflatable straddle packers, spacers, a circulating valve, a shut-in tool, a J-slot tool used for packer inflation and deflation, various crossovers, and a sensor carrier containing three quartz-crystal pressure-temperature transducers (Figure 5-6). The transducers are ported through the tool to the hole below, between, and above the packers. A seamless, stainless-steel wireline connects the transducers to the DAS at the surface. For tests of the lower portion of the hole, the bottom packer was removed, and the tool was run in a single-packer configuration. The Hydrological Test Tool was lowered to the desired test depth on 2.375-in. tubing.

The DAS used with the Baker tool consisted of a Baker SC-2 interface unit that linked the transducers with the rest of the system, an HP-5316A universal counter that measured the frequencies of the current pulses sent by the transducers, an HP-59306A relay actuator or an HP-3497A data acquisition/control unit for channel switching, an HP-85 computer with tape drive for system control and data recording, an Epson LX-80 or HP-2225A printer for real-time listing of the data, and an HP-9872 plotter for real-time plotting of the data (Figure 5-7). The quartz-crystal transducers were calibrated by Baker before being sent to the field. The transducer calibration coefficients were entered into the data-acquisition program for automatic data conversion to pressure and temperature before recording. The data-acquisition software was written and is maintained by G-Tech Corp. of Houston.

2-3/8 in TUBING
CROSS-OVER SUB
CIRCULATING VALVE
  (BALL BAR SLEEVE)
CROSS-OVER SUB
SHUT-IN TOOL
  2.87 ft CLOSED
  3.22 ft OPEN
CROSS-OVER SUB
SENSOR CARRIER
P3
TRIPLE TRANSDUCER
SAFETY JOINT
"J" SLOT TOOL
  1.37 ft THROW
ELEMENT CONNECTOR
PACKER ELEMENT
ELEMENT CONNECTOR
STAINLESS STEEL TUBING
P2
MANDRIL
SPACERS
ELEMENT CONNECTOR
PACKER ELEMENT
ELEMENT CONNECTOR
TAIL PIPE
BIT SUB

WIRELINE

0.83 ft
0.83 ft

~5.25 ft

FLUID PORTS

STAINLESS STEEL TUBING

~5.25 ft

P1

NOTE:
P1 IS PRESSURE BELOW THE TESTED INTERVAL;
P2 IS PRESSURE IN THE TESTED INTERVAL;
P3 IS PRESSURE IN THE WELL ANNULUS ABOVE
  THE TESTED INTERVAL.

Figure 5-6. Baker DST Tool

DATA-ACQUISITION PROGRAM
DATA STORAGE

```
CASSETTE
TAPE DRIVE
```

```
HP-85
COMPUTER
```

```
EPSON LX-80
OR HP-2225A
PRINTER
```
→ REAL-TIME
DATA LISTING

```
HP-9872
PLOTTER
```
→ REAL-TIME
DATA PLOTTING

```
HP-5316A
UNIVERSAL
COUNTER
```

```
HP-3497A DATA
ACQUISITION/CONTROL
UNIT OR HP-59306A
RELAY ACTUATOR
```

```
BPT
SC-2
INTERFACE
```

POWER TO
PROBE

8 CHANNEL
FREQUENCY DATA
(MULTIPLEX)

WIRELINE
TO
QUARTZ-CRYSTAL
TRANSDUCERS

Figure 5-7. Baker DST Data-Acquisition System

5.5 1986 Testing—The Culebra Dolomite Member

For the 1986 pumping test of the Culebra dolomite, the downhole equipment consisted of a 15-hp Hitachi pump motor with a Red Jacket 15LB6 fluid intake suspended below a Baski air-inflatable packer on 2.375-in. tubing, with three Druck PDCR-10D strain-gage transducers strapped to the tubing above the packer (Figure 5-8). Two transducers measured the pressure below the packer by means of feed-through lines through the packer; the third measured the pressure in the wellbore above the packer. A Baker water-inflatable resettable bridge plug was set below the Culebra to seal off the lower portion of the hole. The uphole equipment consisted of a Hays totalizing flow meter, a calibrated standpipe to provide an independent means of measuring flow rate, a ball valve, and a Dole 50-gpm orifice valve to maintain adequate backpressure on the flow meter.

The DAS at the surface for the 1986 Culebra testing was identical to that used for the Phase Ia testing of the Culebra (Section 5.3).

6. Methods of Analyzing the Test Data

The analyses of the hydraulic test data were to produce answers to the following questions:

- Do the tested intervals behave hydraulically as single-porosity, double-porosity, or fractured media?

- What are the hydraulic properties of the tested intervals?

- What are the static formation pressures in the tested intervals?

The analytical methods used to interpret the types of tests listed in Chapter 4 and that were found to best answer these questions are discussed below.

6.1 Constant-Head, Borehole-Infiltration Test Analysis

Stephens and Neuman (1980) report that the analytical techniques for interpreting constant-head, borehole-infiltration tests, such as those of the US Bureau of Reclamation (1974, 1977), Glover (1953), and others, lead to an underestimation of saturated permeability because they disregard that part of the flow region that is unsaturated. Stephens and Neuman (1980) recommend a numerical approach to the problem that includes both saturated and unsaturated conditions. No analyses are presented in this report because the lower Dewey Lake proved to have too low a permeability for field testing by this method (Section 7.1). The interested reader is referred to Stephens and Neuman (1980).

6.2 Multiwell Pumping-Test Analysis

The analysis of data from multiwell pumping tests may be divided into analysis of the pumping-well data and analysis of the observation-well data. The different techniques used for the DOE-2 analyses are presented below.
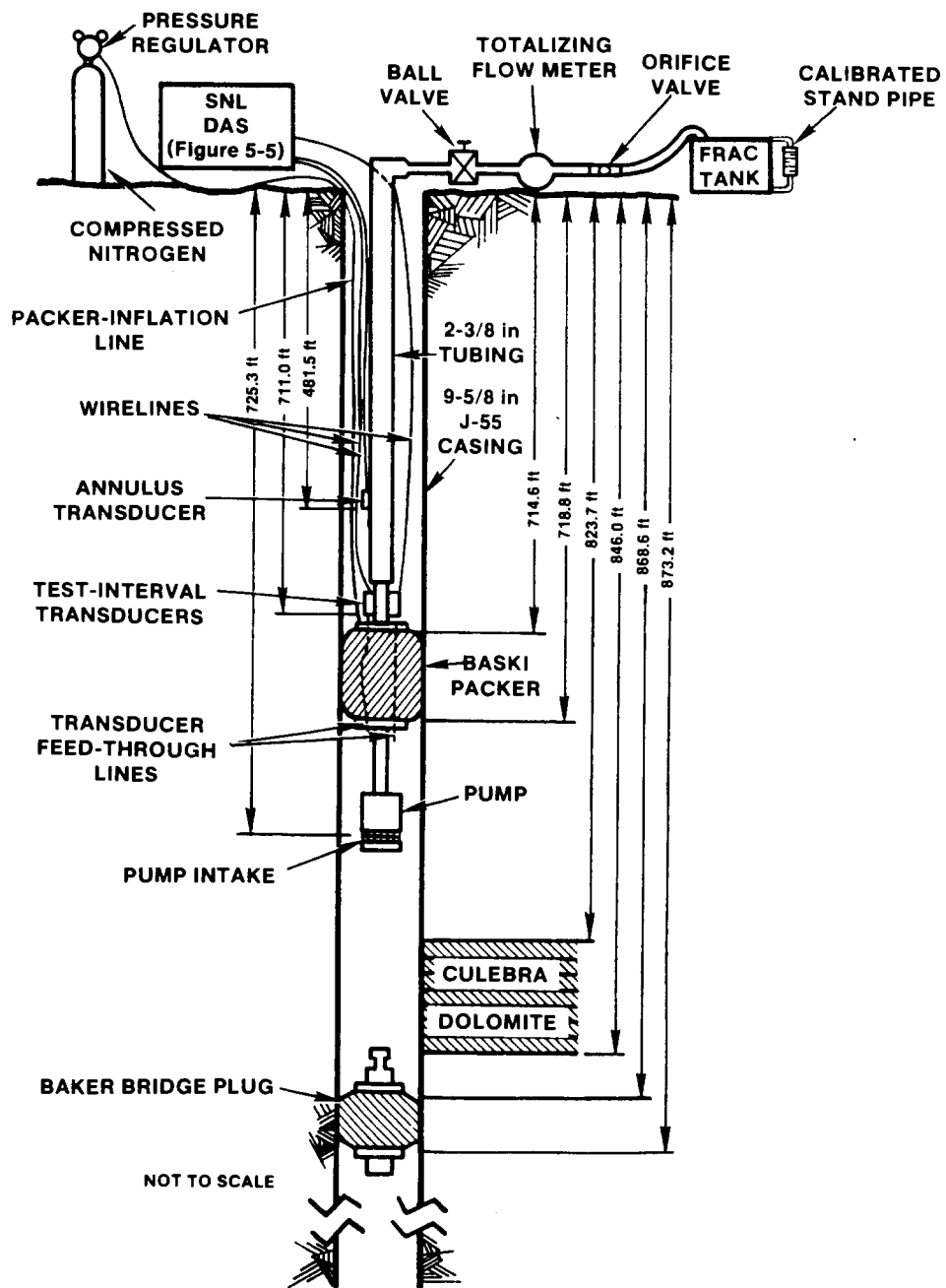
Figure 5-8. 1986 Culebra Pumping Test Equipment Configuration

6.2.1 Pumping-Well Data Analysis

Pumping-well data may be analyzed using either single-porosity or double-porosity interpretation techniques and using log-log and semi-log plotting techniques. These are described below. The well-test interpretation code INTERPRET, which was used to interpret the DOE-2 pumping-test data, is also described below.

6.2.1.1 Single-Porosity Log-Log Analysis

Single-porosity log-log analysis of the DOE-2 drawdown and buildup data was performed using a method presented by Gringarten et al. (1979), modified to include the pressure-derivative technique of Bourdet et al. (1984). This method applies to both the drawdown and buildup (recovery) of a well that fully penetrates a homogeneous, isotropic, horizontal, confined, porous medium during or after a constant-rate flow period. Gringarten et al. (1979) constructed a family of log-log type curves of dimensionless pressure, p_D, versus a dimensionless time group defined as dimensionless time, t_D, divided by dimensionless wellbore storage, C_D, where:

$$p_D = \frac{kh}{141.2qB\mu}\Delta p , \qquad (6.1)$$

$$t_D = \frac{0.000264kt}{\phi\mu c_t r_w^2} , \qquad (6.2)$$

$$C_D = \frac{0.8936C}{\phi c_t hr_w^2} , \qquad (6.3)$$

$$\frac{t_D}{C_D} = \frac{0.000295kht}{\mu C} , \text{ and} \qquad (6.4)$$

k = permeability in millidarcies (md)
h = test interval thickness (ft)
Δp = change in pressure (psi)
q = flow rate in barrels/day (BPD)
B = formation volume factor ($B = 1.0$ in single-phase water reservoir)
μ = fluid viscosity in centipoises (cp)
t = elapsed time (hr)
ϕ = porosity
c_t = total system compressibility, 1/psi
r_w = wellbore radius (ft)
C = wellbore storage coefficient (barrels/psi).

Each type curve in the family of curves (Figure 6-1) is characterized by a distinct value of the parameter $C_D e^{2s}$, where

s = skin factor.

A positive value of s indicates wellbore damage, or a wellbore with a lower permeability as a result of drilling effects than the formation as a whole. A negative value of s indicates a wellbore with enhanced permeability, usually caused by one or more fractures intersecting the wellbore.
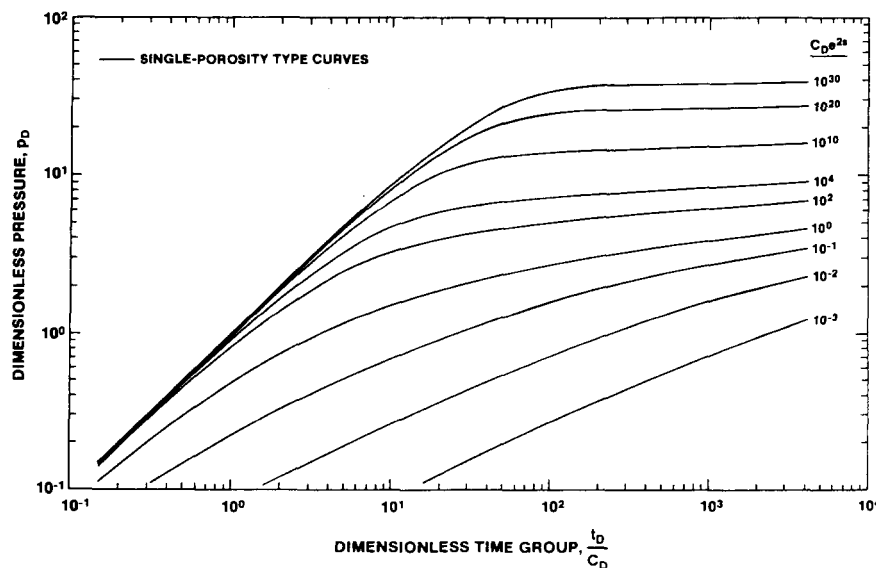
Figure 6-1. Single-Porosity Type Curves for Wells With Wellbore Storage and Skin

Most of the type curves begin with an initial segment having a unit slope corresponding to early-time wellbore storage and skin effects. The duration of this unit slope segment is proportional to the amount of wellbore storage and skin present; curves with $C_D e^{2s}$ values representative of negative skins (i.e., $C_D e^{2s} < 1$) do not show this unit slope. At late time, the curves flatten as infinite-acting, radial-flow effects dominate.

Bourdet et al. (1984) added the pressure derivative to the analysis procedure by constructing a family of type curves of the semi-log slope of the dimensionless pressure response versus the same dimensionless time group, t_D/C_D. The semi-log slope of the dimensionless pressure response is defined as

$$\frac{dp_D}{d\ln(t_D/C_D)} = \frac{t_D}{C_D}\frac{dp_D}{d(t_D/C_D)} = \frac{t_D}{C_D}p'_D , \qquad (6.5)$$

where

p'_D = dimensionless pressure derivative.

These curves are plotted on the same log-log graphs as the type curves of Gringarten et al. (1979), with the vertical axis now being also labeled $(t_D/C_D)p'_D$ (Figure 6-2). Again, each individual type curve is characterized by a distinct value of $C_D e^{2s}$. Pressure-derivative type curves begin with an initial segment with unit slope reflecting early-time wellbore storage and positive skin effects. This segment reaches a maximum that is proportional to the amount of wellbore storage and skin; then the curve declines and

stabilizes at a dimensionless pressure/semi-log slope value of 0.5, reflecting late-time, infinite-acting, radial flow effects.

Pressure-derivative data in combination with pressure data are much more sensitive indicators of double-porosity and boundary effects, nonstatic antecedent test conditions, and other phenomena than are pressure data alone. For this reason, pressure-derivative data are useful in choosing between conflicting phenomenological models that often cannot be differentiated on the basis of pressure data alone. Pressure-derivative data are also useful in determining when infinite-acting radial-flow conditions occur during a test, because these conditions cause the pressure derivative to stabilize at a constant value.

For any given point, the pressure derivative is calculated as the linear-regression slope of a semi-log line fit through that point and any chosen number of neighboring points on either side. The equation for the derivative is

$$p' = \frac{n\sum_{i=1}^{n}x_iy_i - \sum_{i=1}^{n}x_i\sum_{i=1}^{n}y_i}{n\sum_{i=1}^{n}x_i^2 - \sum_{i=1}^{n}x_i^2} , \qquad (6.6)$$

where, for a single, constant-rate flow period,
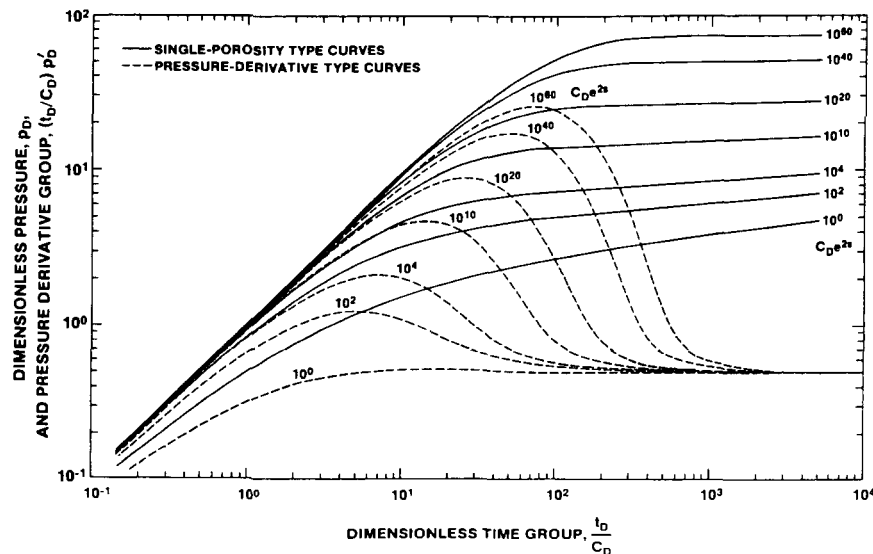
Figure 6-2. Single-Porosity Type Curves and Pressure-Derivative Type Curves for Wells With Wellbore Storage and Skin

n $\quad$ = number of points to be fitted
x_i $\quad$ = ln Δt_i
y_i $\quad$ = Δp_i
Δt_i $\quad$ = elapsed test time at point i (hr)
Δp_i $\quad$ = pressure change at Δt_i (psi).

For a multirate flow period or a buildup period, the time parameter is calculated as

$$x_i = \left\{ \sum_{i=1}^{n-1} (q_i - q_{i-1}) \log\left[\left(\sum_{j=i}^{n-1} \Delta t_j\right) + \Delta t\right]\right\}$$
$$+ (q_n - q_{n-1}) \log \Delta t \ , \tag{6.7}$$

where

q $\quad$ = flowrate (BPD)
Δt $\quad$ = elapsed time during a flow period (hr)

with subscripts

i $\quad$ = individual flow period
j $\quad$ = individual flow period
n $\quad$ = number of flow periods considered.

In general, the fewer the number of points used in calculating the derivative, the more precise it will be. Three-point derivatives, calculated using only the nearest neighbor on either side of a point, usually provide enough resolution to distinguish most important features. However, excessive noise in the data sometimes makes it necessary to use five- or seven-point derivatives, or various "windowing" procedures, to obtain a smooth curve. Unfortunately, this may also smooth out some of the features sought.

The type curves published by both Gringarten et al. (1979) and Bourdet et al. (1984) were derived for flow-period (drawdown) analysis. In general, the curves can also be used for buildup-period analysis, so long as it is recognized that, at late time, buildup data will plot below the drawdown type curves.

If the test analysis is to be performed manually, the buildup data are plotted as pressure change since buildup began (Δp) versus elapsed time since buildup began (t) on log-log paper of the same scale as the type curves. The derivative of the pressure change is also plotted using the same vertical axis as the Δp data. The data plot is then laid over the type curves and moved both laterally and vertically, so long as the axes remain parallel, until a fit is achieved between the data and pressure and pressure-derivative curves with the same $C_D e^{2s}$ value. When the data fit the curves, an arbitrary match point is selected, and the coordinates

of that point on both the data plot, t and Δp, and the type-curve plot, p_D and t_D/C_D, are noted. The permeability-thickness product is then calculated from a rearrangement of Eq (6.1):

$$kh = 141.2qB\mu \ \frac{p_D}{\Delta p} \ . \tag{6.8}$$

The groundwater-hydrology parameter transmissivity, T, is related to the permeability-thickness product by the following relationship, modified from Freeze and Cherry (1979):

$$T = kh\rho g/\mu \ , \tag{6.9}$$

where

ρ $\quad$ = fluid density, M/L^3
g $\quad$ = gravitational acceleration, L/T^2
μ $\quad$ = fluid viscosity, M/LT.

When T is given in ft^2/day, kh is given in millidarcy-ft, ρ is given in g/cm^3, g is set equal to 980.665 cm/s^2, and μ is given in centipoises, Eq (6.9) becomes

$$T = 2.7435 \times 10^{-3} \ kh\rho/\mu \ . \tag{6.10}$$

The wellbore storage coefficient is calculated from a rearrangement of Eq (6.4):

$$C = \frac{0.000295kht}{\mu t_D/C_D} \ . \tag{6.11}$$

Finally, if estimates of porosity and total system compressibility are available, the skin factor can be calculated from the value of the $C_D e^{2s}$ curve selected and Eq (6.3) as

$$s = 0.5 \ln\left[\frac{C_D e^{2s}}{0.8936C/\phi c_t hr_w^2}\right] \ . \tag{6.12}$$

6.2.1.2 Double-Porosity Log-Log Analysis

Double-porosity media have two porosity sets that differ in terms of storage volume and permeability. Typically, the two porosity sets are (1) a fracture network with higher permeability and lower storage, and (2) the primary porosity of the rock matrix with lower permeability and higher storage. During a hydraulic test, these two porosity sets respond differently. With high-quality test data, the hydraulic parameters of both porosity sets can be quantified.

During a hydraulic test in a double-porosity medium, the fracture system responds first. Initially, most of the water pumped comes from the fractures, and the pressure in the fractures drops accordingly. With time, the matrix begins to supply water to the fractures, causing the fracture pressure to stabilize and the matrix pressure to drop. As the pressures in the fractures and matrix equalize, both systems produce water to the well. The total system response is then observed for the balance of the test.

The initial fracture response and the final total system response both follow the single-porosity type curves described above. Simultaneously fitting the fracture response and the total system response to two different $C_D e^{2s}$ curve allows fracture-system and total-system properties to be derived. Information on the matrix, and additional information on the fracture system, can be obtained by interpretation of the data from the transition period when the matrix begins to produce to the fractures. Two different sets of type curves can be used to try to fit the transition-period data.

Transition-period data are affected by the nature, or degree, of interconnection between the matrix and the fractures. Warren and Root (1963) published the first line-source solution for well tests in double-porosity systems. They assumed that flow from the matrix to the fractures (interporosity flow) occurred under pseudosteady-state conditions; that is, that the flow between the matrix and the fractures was directly proportional to the average head difference between those two systems. Other authors, such as Kazemi (1969) and de Swaan (1976), derived solutions using the diffusivity equation to govern interporosity flow. These are known as *transient* interporosity flow solutions. Mavor and Cinco-Ley (1979) added wellbore storage and skin to the double-porosity solution but still used pseudosteady-state interporosity flow. Bourdet and Gringarten (1980) modified Mavor and Cinco-Ley's (1979) theory to include transient interporosity flow and generated type curves for double-porosity systems with both pseudosteady-state and transient interporosity flow.

Pseudosteady-state and transient interporosity flow represent two extremes; intermediate behavior is also possible. Gringarten (1984), however, indicates that most of the tests he has seen exhibit pseudosteady-state interporosity flow behavior.

In recent years, Gringarten (1984, 1986) has suggested that the terms "restricted" and "unrestricted" interporosity flow replace the terms "pseudosteady-state" and "transient" interporosity flow. He believes that all interporosity flow is transient in the sense that

it is governed by the diffusivity equation. But in the case where the fractures possess a positive skin similar to a wellbore skin (caused, for example, by secondary mineralization on the fracture surfaces) that restricts the flow from the matrix to the fractures, the observed behavior is similar to that described by the pseudosteady-state formulation (Moench, 1984; Cinco-Ley et al., 1985). Transient interporosity flow is observed when there are no such restrictions. Hence, the terms "restricted" and "unrestricted" more accurately describe conditions than do the terms "pseudosteady-state" and "transient." The recent terminology of Gringarten will be followed in this report.

Restricted Interporosity Flow

Warren and Root (1963) defined two parameters to aid in characterizing double-porosity behavior. These are the storativity ratio, ω, and the interporosity flow coefficient, λ. The storativity ratio is defined as

$$\omega = \frac{(\phi V c_t)_f}{(\phi V c_t)_{f+m}}, \qquad (6.13)$$

where

ϕ = ratio of the pore volume in the system to the total system volume

V = the ratio of the total volume of one system to the bulk volume

c_t = total compressibility of the system,

and the subscripts f and m refer to the fracture system and the matrix, respectively.

The interporosity flow coefficient is defined as

$$\lambda = \alpha r_w^2 \frac{k_m}{k_f}, \qquad (6.14)$$

where α is a shape factor characteristic of the geometry of the system and other terms are as defined above.

The shape factor, α, is defined as

$$\alpha = \frac{4n(n+2)}{\ell^2}, \qquad (6.15)$$

where

n = number of normal sets of fracture planes limiting the matrix

ℓ = characteristic dimension of a matrix block (ft).

Bourdet and Gringarten (1980) constructed a family of transition type curves for restricted inter-porosity flow on the same axes as the $C_D e^{2s}$ curves of Gringarten et al. (1979), with each transition curve being characterized by a distinct value of the parameter λe^{-2s}. Together, the single-porosity type curves and the transition type curves comprise double-porosity type curves (Figure 6-3).

In manual double-porosity type curve matching, a log-log plot of the data is prepared as in single-porosity type curve matching. The data plot is then laid over the double-porosity type curves and moved both laterally and vertically, so long as the axes remain parallel, until the early-time (fracture flow only) data fall on one $C_D e^{2s}$ curve, the middle portion of the transition data fall on a λe^{-2s} curve, and the late-time (total-system) data fall on a lower $C_D e^{2s}$ curve.

In computer-aided analysis, pressure-derivative curves for double-porosity systems may also be prepared (Gringarten, 1986). The number of possible curve combinations, however, precludes preparation of generic curves for manual curve fitting.

When a fit of the data plot to the type curves is achieved, an arbitrary match point is selected and the coordinates of that point on both the data plot, t and Δp, and the type-curve plot, p_D and t_D/C_D, are noted. The values of $C_D e^{2s}$ and λe^{-2s} of the matched curves are also noted. The permeability-thickness product of the fracture system near the well (and also of the total system because fracture permeability dominates) and the wellbore storage coefficient are calculated from Eqs (6.8) and (6.11). The storativity ratio, ω, is calculated from

$$\omega = \frac{(C_D e^{2s})_{f+m}}{(C_D e^{2s})_f} . \tag{6.16}$$

The dimensionless wellbore storage coefficient for the matrix is calculated as

$$(C_D)_m = \frac{0.8936 \; C}{(V\phi c_t)_m h r_w^2} . \tag{6.17}$$

This leads to the dimensionless wellbore storage coefficient for the total system:

$$(C_D)_{f+m} = (C_D)_m \cdot (1-\omega) . \tag{6.18}$$

Then the skin factor is calculated as

$$s = 0.5 \ln \left[\frac{(C_D e^{2s})_{f+m}}{(C_D)_{f+m}} \right] . \tag{6.19}$$

The interporosity flow coefficient is calculated from

$$\lambda = \frac{\lambda e^{-2s}}{e^{-2s}} . \tag{6.20}$$

If matrix permeability and geometry are known independently, Eqs (6.14) and (6.15) can be used to determine the effective dimensions of the matrix blocks.
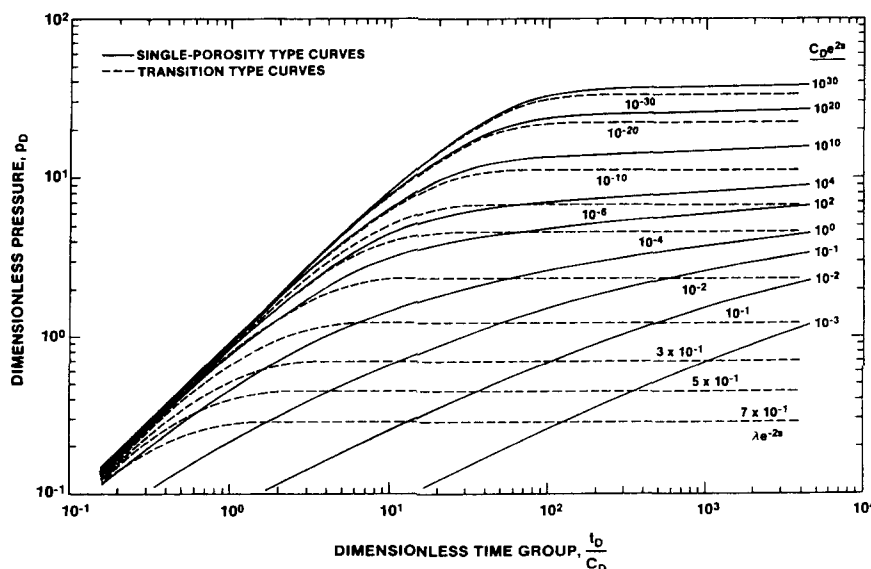
Figure 6-3. Double-Porosity Type Curves for Wells With Wellbore Storage, Skin, and Restricted Interporosity Flow

Unrestricted Interporosity Flow

Matrix geometry is more important for unrestricted interporosity flow than for restricted interporosity flow, because unrestricted flow is governed by the diffusivity equation. A different set of type curves is used, therefore, to match transition-period data when unrestricted interporosity flow conditions exist (Figure 6-4). Bourdet and Gringarten (1980) characterize each of these curves with a different value of the parameter β, the exact definition of which is a function of the matrix geometry. For example, for slab-shaped matrix blocks, they give

$$\beta = \frac{6}{\gamma^2} \frac{(C_D e^{2s})_{f+m}}{\lambda e^{-2s}} , \tag{6.21}$$

and for sphere-shaped blocks they give

$$\beta = \frac{10}{3\gamma^2} \frac{(C_D e^{2s})_{f+m}}{\lambda e^{-2s}} , \tag{6.22}$$

where

γ = exponential of Euler's constant (= 1.781).

Moench (1984) provides an extensive discussion on the effects of matrix geometry on unrestricted interporosity flow.

Manual double-porosity type curve matching with unrestricted interporosity flow transition curves is performed in exactly the same manner as with restricted interporosity flow transition curves, described above. The same equations are used to derive the fracture and matrix parameters, except that the matrix geometry must now be known or assumed to obtain the interporosity flow coefficient, λ, from rearrangement of Eqs (6.21) or (6.22).

6.2.1.3 Semi-Log Analysis of Buildup Data

Horner (1951) provided a method of checking the permeability value obtained from log-log type-curve matching. Horner's method applies to the buildup (recovery) of the pressure in a well that fully penetrates a homogeneous, isotropic, horizontal, infinite, confined reservoir following a constant-rate flow period. Horner's solution is

$$p(t) = p_s - \frac{162.6qB\mu}{kh} \log\left[\frac{t_p + dt}{dt}\right] , \tag{6.23}$$

where

$p(t)$ = pressure at time t (psi)
p_s = static formation pressure (psi)
t_p = duration of previous flow period (hr)
dt = time elapsed since end of flow period (hr),

and other terms are as defined above under Eq (6.4).
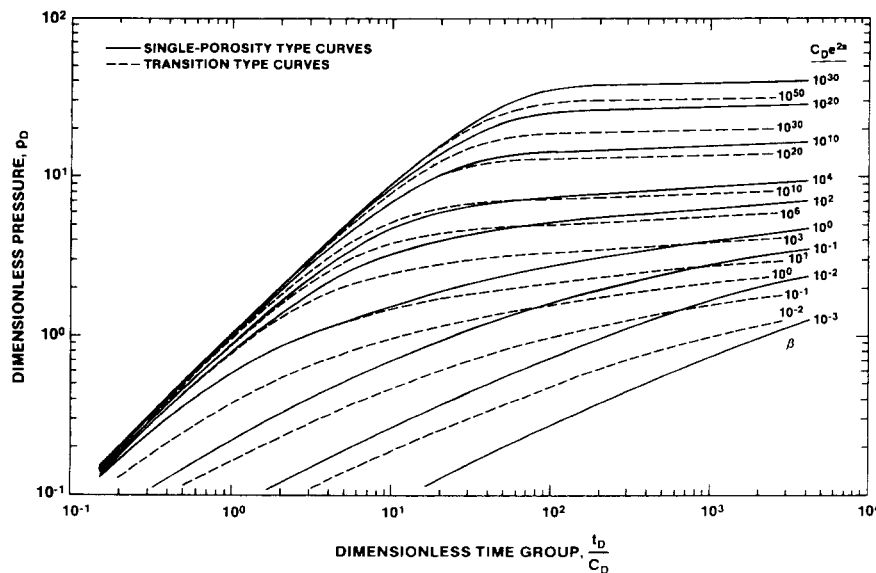
Figure 6-4. Double-Porosity Type Curves for Wells With Wellbore Storage, Skin, and Unrestricted Interporosity Flow

The permeability-thickness product (kh) is obtained by plotting p(t) versus log $[(t_p + dt)/dt]$, drawing a straight line through the data determined from the log-log pressure-derivative plot to be representative of infinite-acting radial flow, and measuring the change in p(t) on this line over one log cycle of time (m). Equation (6.23) can then be rearranged and reduced to

$$kh = 162.6qB\mu/m \ . \qquad (6.24)$$

Static formation pressure is estimated by extrapolating the radial-flow straight line to the pressure axis where log $[(t_p + dt)/dt] = 1$, representing infinite recovery time. The pressure intercept at that time should equal the static formation pressure.

Horner (1951) also suggested a modification of his method for the case where the flow rate was not held constant. This modification was later theoretically verified for the case of constant-pressure, variable-rate production by Ehlig-Economides (1979). The modification entails calculating a modified production time

$$t_p^* = V/q_f \ , \qquad (6.25)$$

where

V = total flow produced (bbl)
q_f = final flow rate (bbl)/hr.

The modified production time, t_p^*, is substituted for the actual production time, t_p, in Eq (6.23), and the analysis proceeds as before. The modified production time can also be used for calculating buildup type curves for log-log analysis.

6.2.1.4 INTERPRET Well-Test Interpretation Code

Manual type-curve fitting is a time-consuming process limited by the published type curves available and subject to the opinion of the analyst as to what constitutes a good fit. The analyses presented in this report were not done manually, but by using the well-test analysis code INTERPRET developed by A. C. Gringarten and Scientific Software-Intercomp (SSI). INTERPRET is a proprietary code and can be leased from SSI.

INTERPRET can be used to analyze drawdown (flow) and buildup (recovery) tests in single-porosity, double-porosity, and fractured (i.e., a fracture as a singularity) media. It incorporates the analytical techniques discussed above and additional techniques discussed in Gringarten et al. (1974), Bourdet and Grin-

garten (1980), and Gringarten (1984). Rather than relying on a finite number of drawdown type curves, INTERPRET calculates the precise drawdown or buildup type curve corresponding to the match point and data point selected by the user.

After type-curve selection, INTERPRET simulates the test with the chosen parameters so that the user can see how good the match truly is. Through an iterative parameter-adjustment process, the user "fine-tunes" the simulation until satisfied with the results. Both log-log and semi-log (Horner) plotting techniques are used to ensure that the final model is as consistent as possible with the data in every respect. Once the final model is selected, INTERPRET carries out all necessary calculations and provides final parameter values. Analyses obtained using INTERPRET have been verified by performing manual checks.

In addition to standard type-curve analysis, INTERPRET allows the incorporation of constant-pressure and no-flow boundaries in analysis, using the theory of superposition and image wells discussed by Lohman (1979) and others. A constant-pressure boundary can be simulated by adding a recharge (image) well to the model. A no-flow boundary can be simulated by adding a discharge (image) well to the model. Drawdowns/rises from multiple discharge/recharge wells are additive. In INTERPRET, an image well, either discharge or recharge, is included by specifying a dimensionless distance for the image well from the production well and using the line-source solution of Theis (1935) to calculate the drawdown or recovery caused by that well at the production well (see Section 6.2.2). The dimensionless distance is related to the actual distance, d, by

$$d = \frac{(C_D D_D)^{0.5} r_w}{2} \ , \qquad (6.26)$$

where

D_D = dimensionless distance, and other terms are as defined above.

Without observation wells also responding to the same boundary effects, no information is obtained on the direction to boundaries. Geologic information must be used to evaluate the reasonableness, and possible locations, of the proposed boundaries.

6.2.2 Observation-Well Data Analysis

For the observation wells monitored during the DOE-2 pumping tests, the drawdown and recovery

data were analyzed together using a method described by Ramey (1980) for single-porosity systems, and also using INTERPRET. Use of a single-porosity interpretation technique for an observation well in a double-porosity aquifer is justified when the observation well is far enough from the pumping well that only total system responses are observed. Deruyck et al. (1982) provide the following criterion for being able to measure double-porosity responses at an observation well:

$$\ln\left[\frac{2}{\gamma(\lambda r_D^2)^{0.5}}\right] > \text{gage resolution} + \text{noise}, \qquad (6.27)$$

where

$$r_D = r/r_w \qquad (6.28)$$

r = radial distance to pumping well (ft),

and other terms are as defined above. Generally, this criterion limits observable double-porosity responses to a maximum distance of tens to perhaps hundreds of feet from the pumping well.

Ramey (1980) created a log-log drawdown type curve of p_D versus t_D/r_D^2 using the exponential integral solution for drawdown caused by a line-source well developed by Theis (1935)

$$p_D = -0.5 \, Ei(-r_D^2/4t_D), \qquad (6.29)$$

where

$$\frac{t_D}{r_D^2} = \frac{0.000264kht}{\phi\mu c_t hr^2}, \qquad (6.30)$$

p_D and t_D are defined by Eqs (6.1) and (6.2), respectively, and other terms are as defined in Section 6.2.1. Theis's solution describes the response that will be observed at an observation well lacking wellbore storage and skin in an infinite, confined, homogeneous, isotropic aquifer when pumping from another well completed in the same aquifer.

By the principle of superposition, water-level or pressure recovery after a pump is turned off is the same as if (1) the pump is left on, and (2) a recharge well injecting water at the same rate as water being pumped out is turned on. That is, the recovery response induced by the recharge well is *added* to the drawdown response induced by the discharge well. Ramey (1980) added a family of recovery curves to the drawdown curve of Theis using various values of the parameter t_{pD}/r_D^2, where

t_{pD} = dimensionless total production time.

To use Ramey's method, a log-log plot is prepared, to the same scale as the type curves (Figure 6-5), of *pressure change* since the beginning of pumping versus *elapsed time* since the beginning of pumping, including both drawdown and recovery data. The data plot is laid over the type curves and translated both vertically and horizontally, with the axes of both plots remaining parallel, until the data match both the drawdown type curve and one of the recovery curves. An arbitrary match point is selected, and the coordinates of that point on both plots are used with Eqs (6.8) and (6.30) to calculate the permeability-thickness product and the porosity-compressibility-thickness product, respectively.
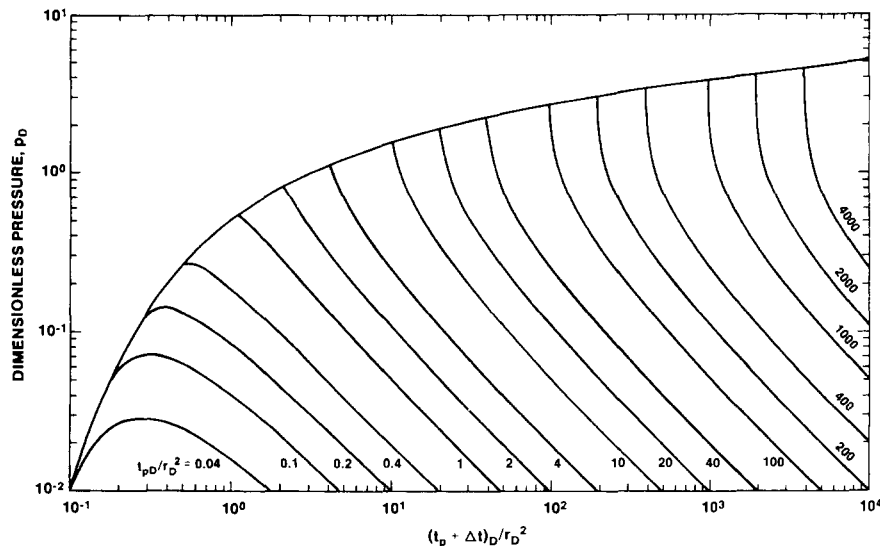
Figure 6-5. Composite Line-Source Solution Type Curves for Drawdown and Recovery

These values are representative of the average aquifer properties between the pumping well and the observation well, with an underlying assumption of aquifer homogeneity and isotropy. In a heterogeneous aquifer, these values are valid only for the specific flow path under investigation.

The permeability-thickness product is related to transmissivity through Eqs (6.9) and (6.10). Narasimhan and Kanehiro (1980) give the relationship between the porosity-compressibility-thickness product and the groundwater-hydrology parameter storativity, S, in consistent units as

$$S = \phi c_t h \rho g . \qquad (6.31)$$

When total compressibility, c_t, is in units of 1/psi, thickness, h, is in units of ft, fluid density, ρ, is in units of g/cm^3, and gravitational acceleration, g, is set equal to 980.665 cm/s^2, Eq (6.31) becomes

$$S = 0.4335 \phi c_t h \rho . \qquad (6.32)$$

The INTERPRET code follows a similar procedure in superimposing line-source solutions for the drawdown and recovery periods. It displays the combined drawdown-recovery results in a linear-linear plot showing observed and simulated data. The INTERPRET analysis is subject to the same assumptions of aquifer homogeneity and isotropy as that of Ramey (1980).

6.3 Slug-Test Analysis

Slug-test data are analyzed by a method first presented by Cooper et al. (1967) for slug tests and adapted to DSTs by Ramey et al. (1975). The method is used for calculating the transmissivity of a homogeneous, isotropic, confined, porous medium of uniform thickness that is fully penetrated by a well. To initiate a slug-withdrawal test, a hydraulic gradient is established around the well by swabbing the fluid from the tubing with the test interval shut-in and then opening the test interval to the tubing. The problem is described mathematically in radial geometry by the diffusivity equation

$$\frac{\partial^2 h}{\partial r^2} + \frac{1}{r} \frac{\partial h}{\partial r} = \frac{S}{T} \frac{\partial h}{\partial t} , \qquad (6.33)$$

where, in consistent units,

h   = hydraulic head differential (at radius r and time t) (L)

r   = radius from well center (L)
t   = elapsed time (T)
S   = formation storativity
T   = formation transmissivity (L^2/T).

This equation describes nonsteady, radial flow of groundwater.

The solution to this equation used for analysis of slug-test (or DST flow-period) data is presented in the form of curves of [H/H$_o$] and [(H$_o$ − H)/H$_o$] versus the dimensionless time parameter β for each of several values of α, where in consistent units

$$\beta = Tt/r_c^2 \qquad (6.34)$$

$$\alpha = r_s^2 S/r_c^2 , \qquad (6.35)$$

and

H$_o$ = initial (maximum) head differential (L)
H   = head differential at time t (L)
t   = time elapsed since test began (T)
r$_s$ = radius of borehole (L)
r$_c$ = inside radius of tubing string (L).

Plots of the quantities [H/H$_o$] and [(H$_o$ − H)/H$_o$] versus t are made on semi-log and log-log paper, respectively, of the same scale as the type curves. Semi-log plotting and type curves are best used when a minimum of ~70% recovery has occurred. For lesser degrees of recovery, log-log plotting techniques provide a more definitive type-curve fit (Ramey et al., 1975). The type curves are placed over the test data plots and translated horizontally with the horizontal axes coincident until a best fit is achieved. In this position an arbitrary match point is chosen, and the corresponding values of α and β are read from the type curve, and t is read from the data plot. The transmissivity (T) is then calculated from the following rearrangement of Eq (6.34), using the coordinates of the match point, as

$$T = \frac{r_c^2 \beta}{t} . \qquad (6.36)$$

The vertically averaged hydraulic conductivity, K, can be calculated from

$$K = T/b , \qquad (6.37)$$

where

b   = thickness of tested interval, L.

When static formation pressures are unknown, they may be approximated from flow-period or slug tests in the following manner. A log-log plot of $(H_o - H)/H_o$ versus elapsed time is prepared, using a "best-guess" value of the static formation pressure to calculate H_o and H. At late time, the data should become asymptotic to the $(H_o - H)/H_o$ value of 1.0. If the data become asymptotic to a lower value, the "best-guess" static formation pressure estimate was too high and should be revised downward. If the data exceed the $(H_o - H)/H_o$ value of 1.0, the estimate was too low and should be revised upward. In general, Horner extrapolations of buildup data, when possible, provide greater resolution in estimating static formation pressures than do slug-test interpretations.

6.4 Pressure-Pulse Test Analysis

Pressure-pulse tests were first described by Bredehoeft and Papadopulos (1980). The solution technique is similar to that developed by Cooper et al. (1967) for slug tests. The only difference between the two methods is that water *fills* a tubing string of radius r_c in a slug test, whereas water is only *compressed* in an isolated interval of the borehole in a pressure-pulse test. Analytically, the solution technique for pressure-pulse tests is the same as that derived for slug tests, with the r_c^2 terms in Eqs (6.34), (6.35), and (6.36) replaced by $V_w C_w \rho_w g / \pi$, where in consistent units

V_w = volume of water within the pressurized section of the system (L^3)

C_w = compressibility of water (LT^2/M)

ρ_w = density of water (M/L^3)

g = gravitational acceleration (L/T^2).

With this substitution, and subject to the constraint that $\alpha \leq 0.1$ [see Eq (6.35)], the analysis proceeds as described in Section 6.3, Slug-Test Analysis.

6.5 Drill-Stem Test Analysis

Drill-stem tests (DSTs) consist of flow periods and buildup periods, each requiring different analytical approaches. DST flow periods are exactly analogous to rising-head slug tests, and data from them may be analyzed as described in Section 6.3, Slug-Test Analysis. Slug tests, because of their greater duration, typically provide more definitive results than do DST flow periods. DST buildup periods are analogous to pumping-test recovery periods, and data from them may be analyzed as described in Section 6.2.1 for a pumping well.

7. Test Results

Portions of four formations were tested in DOE-2: the Dewey Lake Red Beds and the Rustler, Salado, and Bell Canyon Formations. Table 7-1 summarizes the tests performed. Results of the tests are summarized in Table 7-2 and discussed below. Except for data from the 1986 Culebra pumping test, all test data were published in Mercer et al. (1986) and INTERA Technologies (1986). Data from the 1986 Culebra pumping test are contained in Appendix A of this report.

7.1 Dewey Lake Red Beds

Testing of the Dewey Lake Red Beds began September 13, 1984, and concluded September 14, 1984 (Table 7-1). The original test zone selected was the lower Dewey Lake from 490 ft deep to the bottom of the hole at 641 ft, ~2 ft into the Rustler Formation. When a good packer seat could not be obtained at 490 ft, the packer was moved down to where the hole had a slightly smaller diameter. The final test interval was from 539 to 641 ft.

The Dewey Lake constant-head, borehole-infiltration test was originally set up with a pump to supply a constant pressure and a totalizing flow meter to measure the flow rate into the formation (Figure 5-1). This meter required a minimum of 0.25 gallons per minute (gpm) of flow to make the internal turbine turn. When it became apparent that the formation would not accept fluid at that rate, the pump and flow meter were removed from the system. The injection-system connections were removed from the tubing string, and the tubing was filled to the top, ~7 ft above ground surface. As the fluid level dropped in the tubing, water was added from a graduated cylinder every 10 to 20 min to maintain a constant head on the system.

After 1 hr, a total of 58 mL of water had been added to the tubing. The test was terminated at this time for two reasons: (1) at an apparent inflow rate of ~1 mL/min, even a very small leak somewhere in the system could introduce a very large error in the flow measurement; and (2) because of the low infiltration rate observed, continuing the test until reaching steady-state conditions was deemed impractical, especially considering that an unknown volume of rock had to be saturated, and the infiltration rate would decrease further as saturation was approached.

Table 7-1. DOE-2 Test Summary

Zone	Lithology	Depth (ft)	Test Interval Transducer Depth (ft)	Test	Test Date	Start Time	End Time	Pressure Before Test (psia)	Start Pressure (psia)	End Pressure (psia)	q_f[1] (BPD)	t_p*[2] (hr)
Dewey Lake	siltstone/ claystone	539–641	531.8	Constant-Head	9/14/84	02:08	03:08	—	—	—	0.009	—
Forty-niner	siltstone/ claystone/ anhydrite/ gypsum	664–686	644.4	FFL[3]	10/15/84	10:37:54	11:38:10	176.3[5]	7.3[5]	8.4[5]	0.16	1.22
				FBU[4]	10/15/84	11:38:18	21:07:00	—	17.4[5]	175.2[5]	—	—
				Slug	10/15-16/84	21:12:05	08:15:00	175.2[5]	14.7[5]	31.8[5]	—	—
Magenta	dolomite	700–722	680.9	FFL	10/13/84	16:29:08	17:22:20	184.1[5]	7.0[5]	9.1[5]	0.08	4.9
				FBU	10/13-14/84	17:22:29	05:15:00	—	18.8[5]	188.9[5]	—	—
				Slug	10/14-15/84	09:18:40	08:45:00	174.7[5]	6.9[5]	41.8[5]	—	—
Tamarisk	clay/ siltstone/ anhydrite/ gypsum	796–817	776.3	FFL/Slug	10/12-13/84	22:09:40	09:38:30	271.4[5]	122.0[5]	112.2[5]	—	—
				FBU	10/13/84	09:39:10	12:35:00	—	136.2[5]	133.7[5]	—	—
Culebra(I)	dolomite	824–846	804.8	FFL	10/12/84	12:32:05	12:39:00	178.0[5]	61.6[5]	102.0[5]	54.0	0.134
				FBU	10/12/84	12:39:15	13:00:40	—	103.9[5]	175.6[5]	—	—
				SFL[6]	10/12/84	13:01:10	13:08:25	175.6[5]	107.1[5]	140.0[5]	41.8	0.141
				SBU[7]	10/12/84	13:08:30	16:00:35	—	142.0[5]	187.2[5]	—	—
				Slug	10/12/84	16:01:17	16:52:00	187.2[5]	47.3[5]	186.4[5]	—	—
Culebra(Ia)	dolomite	824–846	810[8]	Pumping	2/19-3/12/85	17:00:00	17:00:00	197.1[5]	197.1[5]	65.6[5]	213	504.0
				Recovery	3/12-13/85	17:00:00	10:00:00	—	65.6[5]	196.6[5]	—	—
Culebra (1986)	dolomite	824–846	711.0	Pumping	6/30-7/4/86	09:00:00	13:00:00	151.9[5]	149.0[5,9]	122.1[5]	1190	100.0
				Recovery	7/4-12/86	13:00:00	01:00:00	—	125.3[5,9]	149.5[5]	—	—

[1]q_f = final flow rate, in barrels per day
[2]t_p* = modified production time
[3]FFL = first flow period
[4]FBU = first buildup period
[5]psig; psig ≈ psia − 10.5

[6]SFL = second flow period
[7]SBU = second buildup period
[8]below top of casing
[9]first reading after pump on/off

(continued)

Table 7-1 (concluded).

Zone	Lithology	Depth (ft)	Test Interval Transducer Depth (ft)	Test	Test Date	Start Time	End Time	Pressure Before Test (psia)	Start Pressure (psia)	End Pressure (psia)	q_f[1] (BPD)	t_p*[2] (hr)
Rustler-Salado	claystone/ siltstone/ halite	945–967	925.6	FFL/Slug	10/11-12/84	19:00:55	09:00:00	384.7[5]	103.9[5]	93.6[5]	—	—
				FBU	10/12/84	09:20:00	09:30:00	—	348.8[5]	347.2[5]	—	—
MB 138-139	halite/ anhydrite/ clay	2195–2309	2176.94	FFL	5/19/85	10:20:15	10:41:00	988.4	241.0	243.1	0.37	0.95
				FBU	5/19-20/85	10:41:00	10:00:09	—	243.1	445.6	—	—
Salado	halite/ anhydrite	1040–3095	1022.33	Pulse 1	5/21/85	14:18:15	23:55:00	308.8	181.9	266.2	—	—
				Pulse 2	5/22/85	00:12:30	14:00:02	267.1	405.7	309.3	—	—
Ramsey	sandstone/ siltstone	4138–4180	4120.57	FFL	7/12/85	08:55:38	09:19:50	1825.0	270.5	285.1	5.31	0.472
				FBU	7/12/85	09:19:50	12:11:38	—	285.1	1783.3	—	—
				SFL	7/12/85	12:12:04	13:27:10	1783.3	287.7	324.1	4.49	1.388
				SBU	7/12/85	13:27:10	19:01:44	—	343.3	1765.0	—	—
				Slug	7/12-14/85	19:02:10	07:10:07	1765.0	326.0	1114.0	—	—
Olds	sandstone/ siltstone	4177–4218	4159.19	FFL	7/26/85	08:14:55	08:29:50	1875.6	127.5	141.6	6.60	0.370
				FBU	7/26/85	08:29:50	12:29:52	—	141.6	1848.7	—	—
				SFL	7/26/85	12:30:15	13:00:13	1848.7	143.2	164.1	5.51	0.657
				SBU	7/26-27/85	13:00:13	08:47:50	—	164.1	1843.0	—	—
				Slug	7/27-29/85	08:48:22	07:10:23	1843.0	165.6	980.4	—	—
Hays	sandstone/ siltstone	4220–4325	4206.31	FFL	7/18/85	18:04:00	18:15:06	1872.2	198.9	564.2	277	0.227
				FBU	7/18-19/85	18:15:06	07:37:39	—	832.9	1846.8	—	—
				SFL	7/19/85	07:38:07	07:58:25	1846.8	581.8	1011.4	165	0.447
				SBU	7/19/85	07:58:25	12:24:06	—	1175.9	1838.7	—	—
				Slug	7/19/85	12:24:30	16:40:11	1838.7	194.2	1775.8	—	—

[1]q_f = final flow rate, in barrels per day
[2]t_p* = modified production time
[3]FFL = first flow period
[4]FBU = first buildup period
[5]psig; psig ≈ psia − 10.5

[6]SFL = second flow period
[7]SBU = second buildup period
[8]below top of casing
[9]first reading after pump on/off

Table 7-2. DOE-2 Test Results

Zone	Depth (ft)	Test	kh (md-ft)	k (md)	T (ft²/day)	K (ft/day)	S	s	h_{ext} (ft msl)
Dewey Lake	539-641	Constant-Head	—	—	—	—	—	—	—
Forty-niner	664-686	FBU	1.1	4.9×10^{-2}	2.5×10^{-3}	1.1×10^{-4}	—	—	<3187
		Slug	4.5	0.21	1.1×10^{-2}	4.8×10^{-4}	—	—	—
Magenta	700-722	FBU	0.6	0.03	1×10^{-3}	7×10^{-5}	—	—	<3178
Tamarisk	796-817	FBU	—	—	—	—	—	—	—
Culebra(I)	824-846	Slug	—	—	—	—	—	—	3034
Culebra(Ia)		Pumping							
DOE-2	824-846	Recovery	>8500	>380	>22	>1.0	—	31	3045
H-6b	604-627	DD & Rec	21 500	930	61	2.7	6×10^{-6}	—	—
Culebra (1986)		Pumping							
DOE-2	824-846	DD & Rec	31 100	1410	89	4.0	—	−4.7	3045
H-6b	604-627	DD & Rec	21 500	930	61	2.7	6×10^{-6}	—	—
WIPP-13	701-724	DD & Rec	25 200	1100	72	3.1	3×10^{-6}	—	—
Rustler-Salado	945-967	Slug	—	—	—	—	—	—	—
MB 138-139	2195-2309	FBU	$<3 \times 10^{-2}$	$<3 \times 10^{-4}$	$<6 \times 10^{-5}$	$<6 \times 10^{-7}$	—	—	>2160
Salado	1040-3095	Pulse	—	—	—	—	—	—	—
Ramsey	4138-4180*	FBU	2.4	8.4×10^{-2}	5.4×10^{-3}	1.9×10^{-4}	—	1.2	—
		SBU	2.5	8.8×10^{-2}	5.7×10^{-3}	2.0×10^{-4}	—	1.0	<3092
		Slug	2.6	9.4×10^{-2}	6.0×10^{-3}	2.1×10^{-4}	—	—	—
Olds	4177-4218†	FBU	3.1	0.10	7.0×10^{-3}	2.3×10^{-4}	—	2.0	—
		SBU	2.9	9.8×10^{-2}	6.6×10^{-3}	2.2×10^{-4}	—	2.0	<3111
		Slug	3.3	0.11	7.6×10^{-3}	2.5×10^{-4}	—	—	—
Hays	4220-4325‡	FBU	240	2.4	0.56	5.6×10^{-3}	—	0.8	—
		SBU	230	2.3	0.53	5.3×10^{-3}	—	0.6	<3077
		Slug	240	2.4	0.55	5.5×10^{-3}	—	—	—

*Effective thickness 4144 – 4172 ft
†Effective thickness 4187 – 4217 ft
‡Effective thickness 4255 – 4325 ft

The observed small inflow rate was taken as an indication that the permeability of the lower Dewey Lake is low enough to rule out the lower Dewey Lake in the vicinity of DOE-2 as a significant transport pathway in event of a repository breach. Further quantification of the lower Dewey Lake hydraulic properties was deemed unwarranted.

7.2 Rustler Formation

Seven sets of tests were conducted in the Rustler Formation in three phases: (1) the Phase I testing of the Forty-niner Member, the Magenta Dolomite Member, the Tamarisk Member, the Culebra Dolomite Member, and the unnamed member and Rustler-Salado contact; (2) the Phase Ia testing of the Culebra; and (3) the 1986 testing of the Culebra.

7.2.1 Forty-niner Member (DST 664-686)

The Forty-niner Member was tested between depths of 664 and 686 ft, an interval containing all the clay and siltstone within the Forty-niner (670.0 to 680.9 ft) and gypsum and anhydrite above and below. Testing of the Forty-niner was performed October 15 and 16, 1984 (Table 7-1), and consisted of one flow period, one buildup period, and a slug test (Figure 7-1).

The apparent pressure response to testing was somewhat erratic. A relatively high degree of noise is superimposed on the pressure trends for all three transducers shown in Figure 7-1. The noise is significant because the low permeability of the unit did not allow incremental changes in the pressure signal always to be of a greater magnitude than that of the noise. This problem renders analysis, particularly of the pressure derivative, difficult and inconclusive.

The FBU was analyzed and simulated by using the code INTERPRET. A log-log dimensionless plot of the pressure data, pressure-derivative data, and simulations is presented in Figure 7-2. A seven-point derivative was used to overcome some of the effects of noise. The simulations deviate from the data, particularly the pressure-derivative data, to an undesirable degree, but this was the best fit obtainable. The peak and stabilization levels of the derivative are well matched, even if the shapes of the data and simulation differ, indicating a reasonable pressure and curve

match. Hence, the permeability-thickness value obtained, 1.1 md-ft (Table 7-2), is probably reliable. This value corresponds to an average permeability of the entire tested interval of 4.9 $\times$ 10^{-2} md. The corresponding groundwater units are a transmissivity of 2.5 $\times$ 10^{-3} ft^2/day and a hydraulic conductivity of 1.1 $\times$ 10^{-4} ft/day. No value of wellbore skin was calculated because the uncertainties in the porosity and compressibility of the Forty-niner are too great.

The final five derivative points on Figure 7-2 show a sharp decrease in value. This drop was caused when the pressure data stabilized too quickly, apparently because of what Grisak et al. (1985) term a "pressure skin" on the wellbore. Pressure skins develop as wells are drilled and as they stand open before testing. As drilling fluid circulates during drilling, it exerts a fluid pressure on the exposed formations corresponding to the weight of the drilling-fluid column in the wellbore. In most formations, this pressure exceeds the natural static formation fluid pressure. As a result, an overpressurized zone (or pressure skin) develops in the formation around the wellbore. The magnitude and extent of this pressure skin depend on a variety of factors, including the duration and magnitude of the pressure differential and the hydraulic properties of the affected formation. Once the formation is isolated from the overpressure, the pressure skin begins to dissipate. When hydraulic tests are performed while a pressure skin still exists, however, the test data may be influenced by dissipation of the pressure skin.
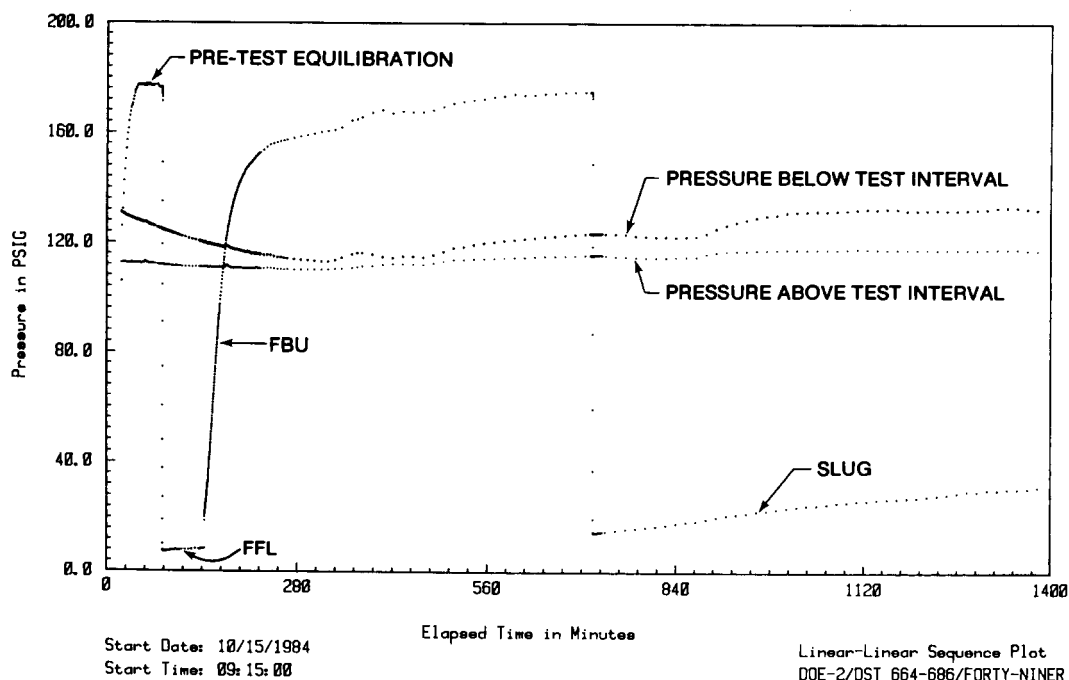

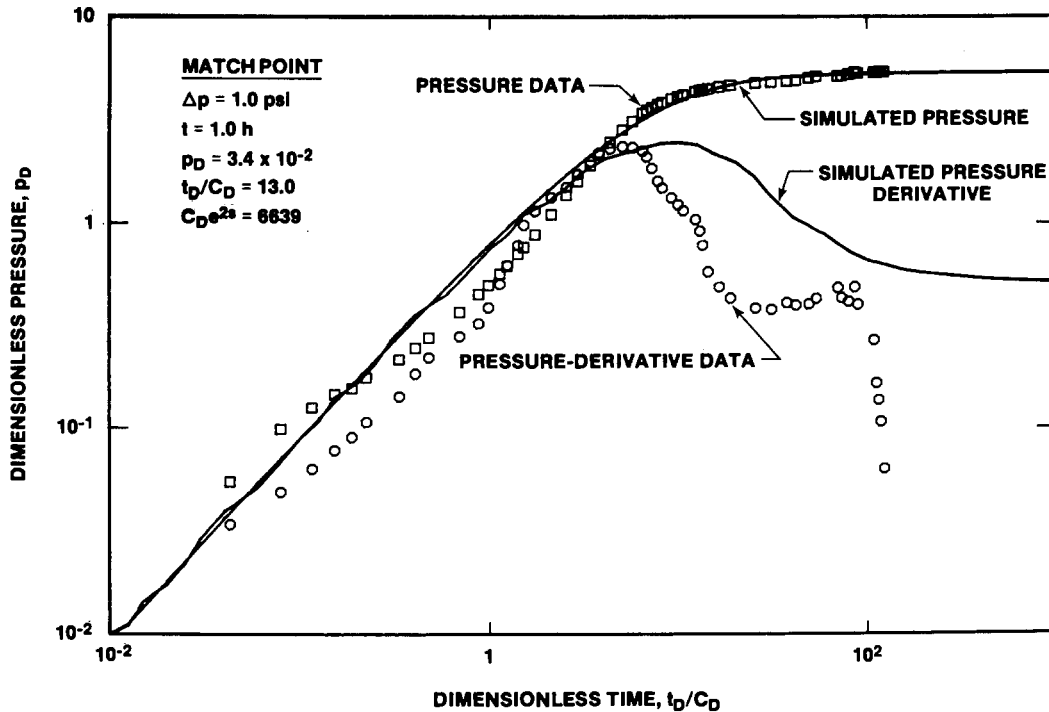**Figure 7-1.** Forty-niner Test Sequence Plot

Figure 7-2. Forty-niner FBU Log-Log Plot With INTERPRET Simulation

During the Forty-niner test, the buildup appears to have been driven, in part, by the pressure skin, which had been imparted to the formation during the 1-month period when the interval was open to the wellbore before testing. This pressure skin caused the pressure to build toward a level above the natural formation pressure. As the pressure skin dissipated and the natural formation pressure began to drive the response, the pressure began to stabilize, and the pressure derivative began to decrease (Figure 7-2). Had the buildup period been longer, the pressure might have reached a maximum and begun to decrease if the pressure skin had been enough to raise the pressure above the natural formation pressure.

The existence of this type of pressure skin invalidates Horner-type extrapolations to estimate static formation pressures. In these cases, the late-time data on a Horner plot will show an overall concave-downward curvature rather than a straight line (Figure 7-3). If a straight line is fit through any portion of the rising limb of the curve, it will extrapolate to a pressure at least partly reflective of the pressure skin as it then existed and not to the natural formation pressure. When this type of response is observed, only an upper bound can be put on the natural formation pressure; no accurate estimate is possible.

Figure 7-3 shows the Horner plot for the Forty-niner FBU. The concave-downward curvature is evident, along with an irregular, very late-time, upward deviation that also begins to level out. The reason for this deviation is unknown. An upward deviation at late time could be expected if the pressure skin had been *lower* than the natural formation pressure, but in that case the pressure curve should steepen, not level out rapidly, as it does in this instance. Some of the irregularity in the late-time rise may be caused by noise in the data-acquisition system.

The latest data on Figure 7-3 extrapolate to a pressure of ~178 psig at infinite time. This represents, for the reasons outlined above, the maximum possible static formation pressure for the Forty-niner Member. With the transducer at a depth of 644.4 ft and a fluid-pressure gradient in the borehole from drilling fluid of 0.52 psi/ft (SG = 1.2), this pressure corresponds to a formation pressure of 197 psig at the base of the claystone/siltstone portion of the Forty-niner, 681 ft deep. In an open borehole containing clean Forty-niner fluid, with an assumed specific gravity of 1.01 (assumed to be similar to that of the Magenta; see Section 7.2.2), 194 psig corresponds to a fluid level ~231 ft below land surface, or at an elevation of ~3187 ft above sea level. Again, this represents the maximum possible level for Forty-niner fluid.
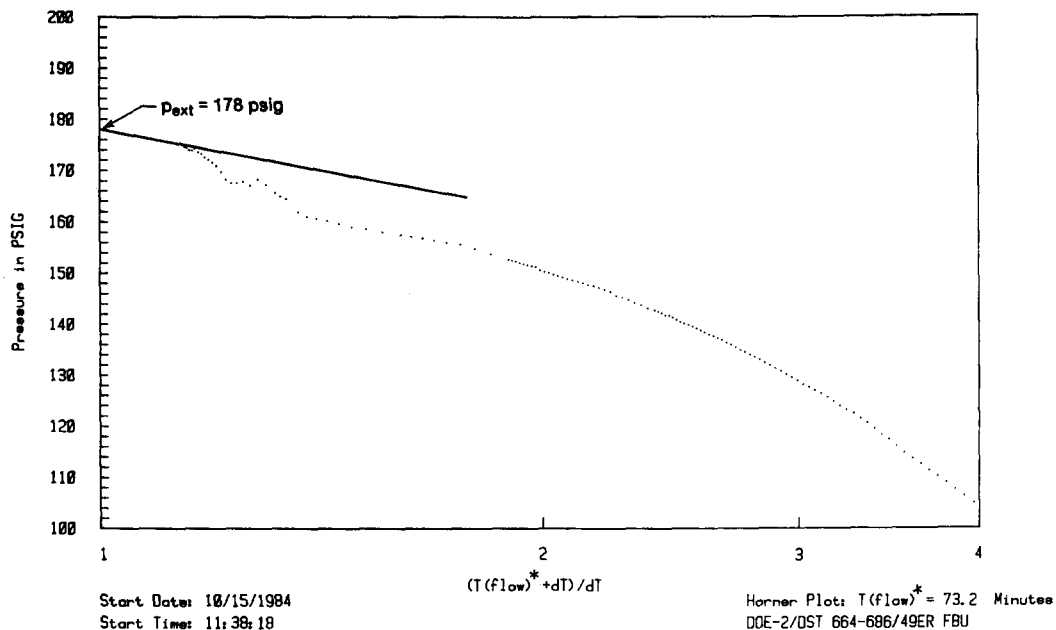
Figure 7-3. Forty-niner FBU Horner Plot

The Forty-niner slug-test data, along with the best-fit type curve, are shown in Figure 7-4. As with the FBU, noise in the data makes the type-curve fit significantly less than ideal. Several curves appeared to fit the data equally well. The intermediate curve selected provided a transmissivity value of 1.1×10^{-2} ft^2/day (Table 7-2). This value corresponds to an average hydraulic conductivity of the entire tested interval of 4.8×10^{-4} ft/day. The corresponding petroleum units are a permeability-thickness product of 4.5 md-ft, and a permeability of 0.21 md. Other apparently valid type-curve fits could change these values by $\pm 25\%$.

The slug-test analysis provided permeability estimates about four times higher than those of the buildup analysis. Neither analysis was particularly definitive; hence, no reason exists to select one over the other. Inasmuch as both analyses provide a similar order of magnitude of permeability, the disagreement is not serious.

7.2.2 Magenta Dolomite Member (DST 700-722)

The Magenta Dolomite Member extends from 698.7 to 722.4 ft deep. Because of restrictions in test-tool dimensions, the Magenta was tested only between depths of 700 and 722 ft. Thus, the testing did not include the actual upper and lower contacts of the Magenta. Testing of the Magenta began October 13,

1984, and concluded October 15, 1984 (Table 7-1). Testing consisted of one flow period, one buildup period, and a slug test (Figure 7-5).

The flow period began with a flow rate of $\sim$0.03 gpm (0.9 BPD), and then dropped off to a final flow rate of $\sim$0.002 gpm (0.08 BPD). A flow rate of this latter magnitude is difficult to quantify accurately, introducing a high degree of uncertainty in all subsequent analyses. The large change observed in the flow rate also required using the modified production time [Eq (6.25)] in buildup analysis.

The buildup period was analyzed and simulated with the code INTERPRET. A log-log dimensionless plot of the pressure data, pressure-derivative data, and simulations is presented in Figure 7-6. A five-point derivative was used to smooth the noise in the data. The derivative data decrease more rapidly than the simulation and do not stabilize. As discussed above, this type of decrease in the derivative is probably caused by pressure-skin effects.

The permeability-thickness value obtained from the INTERPRET simulation is 0.6 md-ft (Table 7-2). This corresponds to a permeability of 0.03 md when divided by the test-interval thickness of 22 ft. The corresponding groundwater units are a transmissivity of $\sim$1 $\times$ 10^{-3} ft^2/day and a hydraulic conductivity of $\sim$7 $\times$ 10^{-5} ft/day. Again, the uncertainty in these values is high. No value of wellbore skin was calculated because of uncertainties in the porosity and compressibility of the Magenta.

MATCH POINT

$\alpha \approx 10^{-10}$
$\beta \approx 1.0$
$t = 940$ min
$r_c = 0.0832$ ft

$\alpha \approx 10^{-10}$

MATCH POINT

Start Date: 10/15/1984
Start Time: 21:12:10

ELAPSED TIME, minutes

Slug Test Plot
DOE-2/FORTY-NINER SLUG
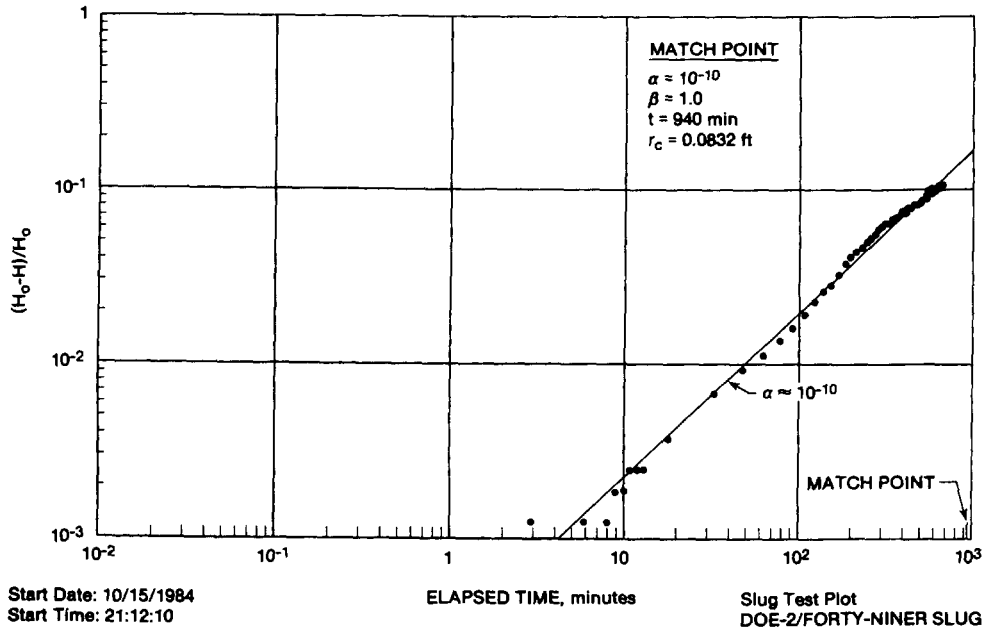
Figure 7-4. Forty-niner Slug Test Plot

Start Date: 10/13/1984
Start Time: 15:05:00

Elapsed Time in Minutes

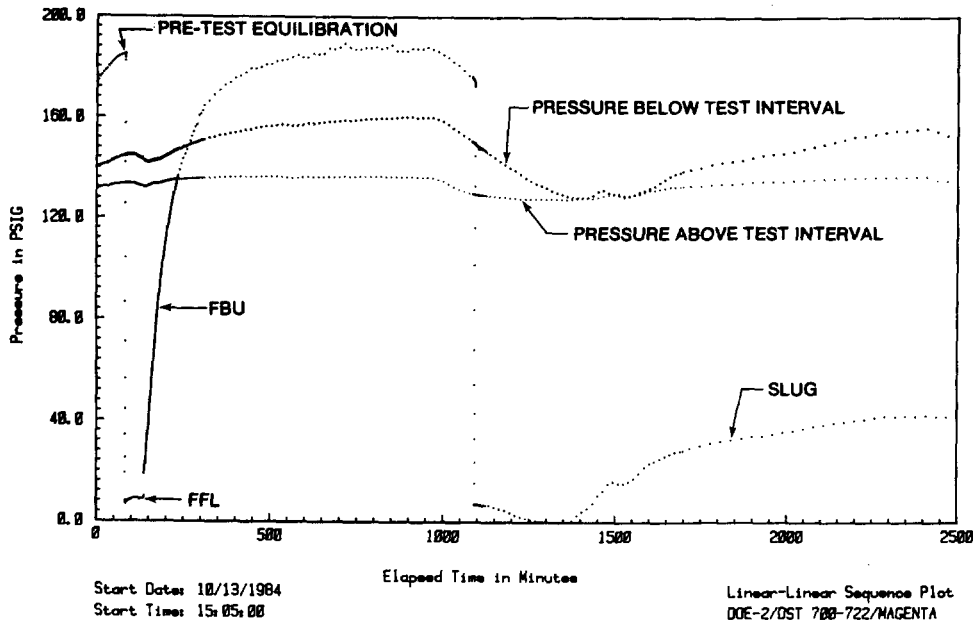Linear-Linear Sequence Plot
DOE-2/DST 700-722/MAGENTA

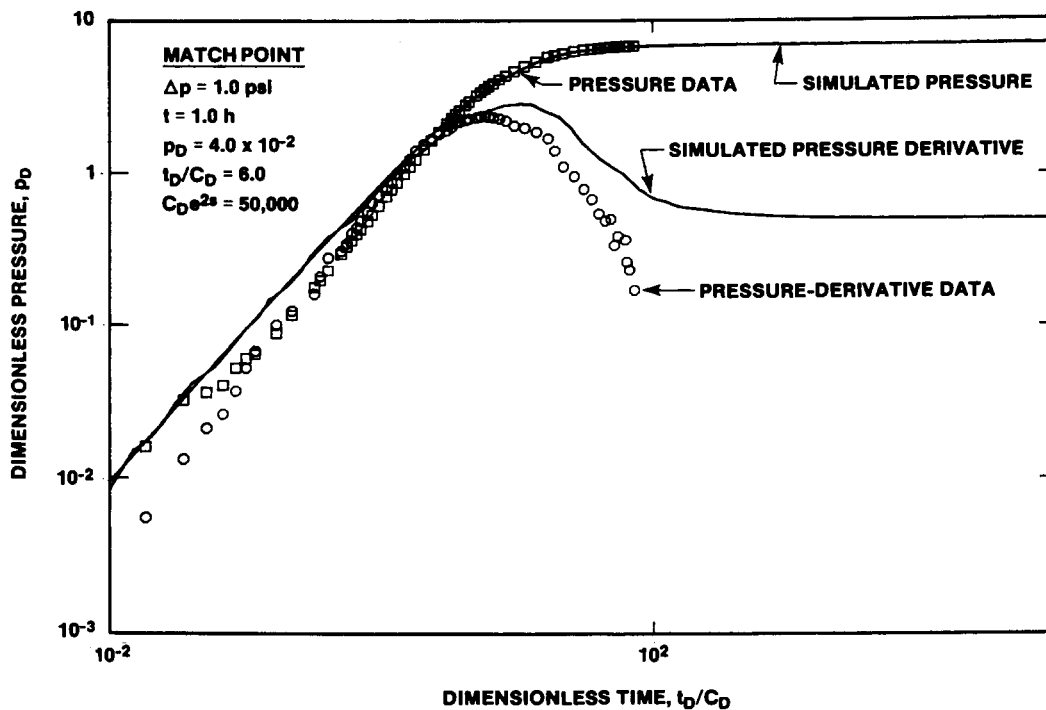**Figure 7-5.** Magenta Test Sequence Plot

40

Figure 7-6. Magenta FBU Log-Log Plot With INTERPRET Simulation

Figure 7-7 shows the Horner plot of the buildup period, exclusive of the late-time pressure decline seen in Figure 7-5. The concave-downward shape caused by pressure-skin effects is evident, as it was in the Forty-niner FBU Horner plot (Figure 7-3), indicating the impossibility of reliable extrapolation to the natural formation pressure. The late-time data extrapolate to a pressure of ~190 psig at infinite time, representing an upper bound on the Magenta pressure. With the transducer at a depth of 680.9 ft and a fluid-pressure gradient in the borehole from drilling fluid of 0.511 psi/ft (measured SG = 1.18), 190 psig corresponds to a formation pressure of ~211 psig at the base of the Magenta, 722.4 ft deep. In an open borehole containing clean Magenta fluid (SG = 1.01, Mercer (1983) for H-5a and H-6a), 211 psig corresponds to a fluid level ~240 below land surface or at an elevation of ~3178 ft above sea level. Again, this represents the maximum possible level for Magenta fluid of the specified density.

Mercer (1983) lists the elevation of the Magenta fluid at H-6a and H-5a as 3056 ft and 3162 ft, respectively. DOE-2, being roughly midway between H-6a and H-5a, should have a Magenta fluid level of ~3110 ft. Hence, the estimate presented above could be ~70 ft (30 psi) too high.

All three transducers showed pressure trends during the Magenta testing that seemed to bear no relationship to the tests themselves (Figure 7-5). Often, these trends seemed to be parallel for all the transducers. The last 4 hr of the buildup period, for example, were marked by declines in the pressures measured by the transducers. These trends were probably caused by transducer "drift"; i.e., a nonconstant relationship between pressure-induced strain and transducer output. This drift could be caused by several factors. The fact that the drift of all three transducers was nearly parallel indicates that the drift may have had a source in an overall system problem, perhaps in the power supply, and not in the individual transducers.

The transducer drift affected test interpretation in varying degrees. A decline in the Magenta interval pressure toward the end of the buildup period is consistent with the hypothesized pressure-skin effects discussed above and with the expected natural formation pressure. The observed decline in Magenta pressure, however, appears to be too rapid. Considering that the other two transducers showed pressure declines over exactly the same period, the observed decline in Magenta pressure cannot be trusted.
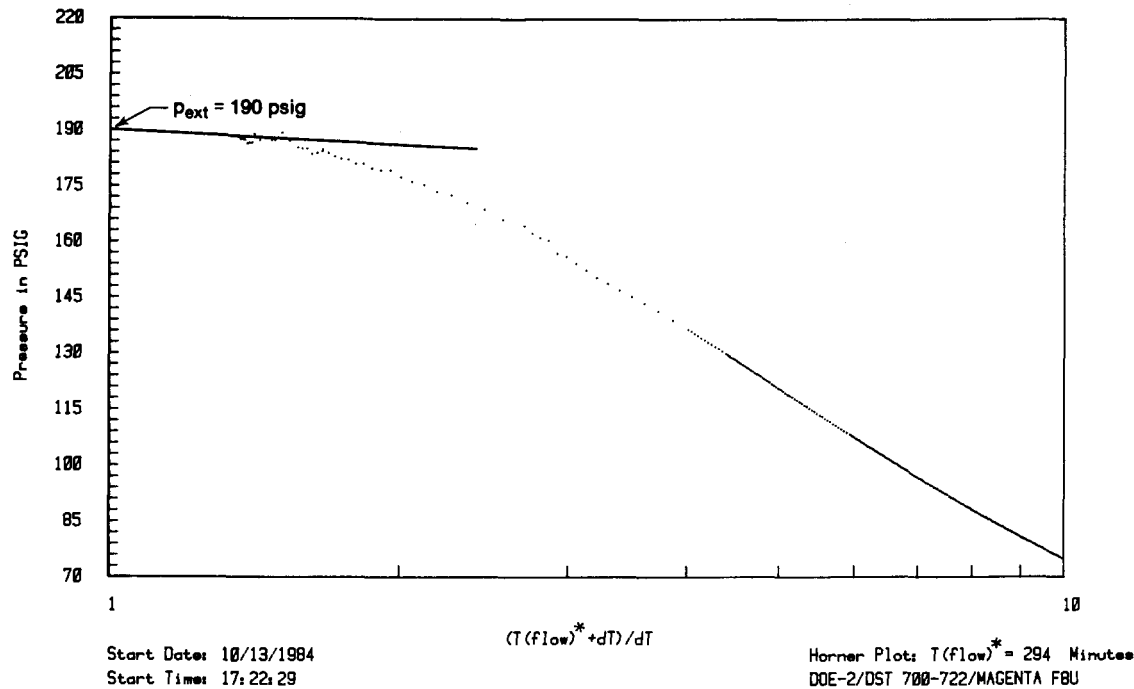
41

Figure 7-7. Magenta FBU Horner Plot

The slug-test data were affected to an even greater degree. After an initial period of little apparent flow, similar to the flow period response, the transducer readings began to decline. Eventually they went to negative values before reversing and finally showing a fairly consistent upward trend. This behavior must have been caused by a system malfunction because no hydraulic system should respond in this manner. As a result, the slug-test data are totally uninterpretable.

7.2.3 Tamarisk Member (DST 796-817)

The Tamarisk Member was tested between the depths of 796 and 817 ft, an interval containing all the clay and siltstone within the Tamarisk (798.3 to 804.9 ft, 811.3 to 811.9 ft deep), sandwiched between layers of gypsum and anhydrite. Testing of the Tamarisk began October 12, 1984, and concluded October 13, 1984 (Table 7-1). A DST consisting of one flow period and one buildup period was attempted (Figure 7-8). With the test interval isolated from the tubing by a valve (shut-in) packer (Figure 5-3), the fluid was bailed from the tubing. The valve packer was deflated to initiate the flow period, but no fluid entered the tubing. After 11.5 hr, the pressure had not risen steadily, but had oscillated slightly and had suffered a net loss of ~10 psi. Reinflating the valve packer to begin the "buildup" period caused an immediate 24-psi rise in pressure as the fluid in the test interval was

compressed slightly. Over the subsequent 3-hr "build-up" period, the pressure again oscillated, with a net loss of ~2.5 psi.

These decreases in pressure could be explained if the initial pressure during the flow period was greater than the natural fluid pressure within the Tamarisk. No data are available on fluid pressures in the Tamarisk at the WIPP site, but Tamarisk pressures could be expected to be intermediate between those of the overlying Magenta and those of the underlying Culebra. At the beginning of the flow period, the test-interval pressure was 122 psi, measured at a depth of 776.3 ft. The estimate of the natural Magenta fluid pressure presented above, 211 psi, when extrapolated down to a depth of 776.3 ft (assuming a specific gravity of 1.01), comes to ~235 psi. The natural Culebra fluid pressure is 208 psi (see Section 7.2.4). Extrapolating this pressure up to a depth of 776.3 ft and assuming a specific gravity of 1.04 (Westinghouse, 1985) gives a pressure of 177 psi. Hence, the pressure at the start of the flow period was well below both the Culebra and Magenta pressures and, by inference, below that of the Tamarisk as well.

The question remains why the pressure during the test not only did not increase, but actually decreased. The most tenable answer is that the apparent decreases in pressure were caused by transducer drift and not by actual changes in pressure. In any case, we

may conclude that the failure of the Tamarisk either to produce fluid or to pressurize when isolated was caused by a very low permeability and possibly a low degree of interconnected porosity. The Tamarisk in the vicinity of DOE-2 does not appear to be capable of playing a significant fluid-transport role in any repository breach scenario.

7.2.4 Culebra Dolomite Member

The Culebra Dolomite Member was tested in three separate episodes. First, drill-stem and slug tests were performed in the open hole after drilling (Phase I). After reaming the hole, we ran a 3-wk pumping test in the open hole (Phase Ia). Finally, after additional reaming, casing, perforation, and acidization, a 100-hr pumping test was conducted in 1986.

7.2.4.1 Phase I (DST 824-846)

The Culebra Dolomite Member was tested between the depths of 824 and 846 ft, which includes all but a fraction of the upper foot of the unit. Culebra testing occurred October 12, 1984 (Table 7-1), and consisted of two flow periods, two buildup periods, and one slug test (Figure 7-9).

The pressure response during the Culebra testing was very rapid. After the flow periods, 99% recovery was attained within 10 s. Consequently, no data are available to analyze for the FBU and SBU. The flow periods and slug test also showed very rapid responses. These tests are uninterpretable because recovery from the slug removal occurred more rapidly than the

theory of flow through porous media predicts. Figure 7-10 shows the pressure response during the slug test, along with the steepest (highest-permeability) type curve available. The pressure reaches 100% recovery after ~35 min. In theory, the pressure should approach 100% recovery asymptotically as time goes to infinity.

The pressure behavior exhibited during these tests indicated that the well was closely connected to a very high permeability and/or high storage zone within the Culebra. Further testing, of a type capable of placing a larger stress on the Culebra, was warranted. A long-term pumping test was selected as the most appropriate method of stressing the Culebra. This became the Phase Ia testing, described in Section 7.2.4.2.

The stabilized Culebra pressure before and after the slug test was ~187 psig. With the transducer at a depth of 804.8 ft and a fluid-pressure gradient in the borehole of 0.52 psi/ft (SG = 1.2), 187 psig corresponds to a formation pressure of 208 psig at the base of the Culebra, 846 ft deep. In an open borehole containing clean Culebra fluid with a specific gravity of 1.04 (Westinghouse, 1985), 208 psig corresponds to a fluid level ~384 ft below ground surface, or at an elevation of ~3034 ft above sea level. Mercer (1983) lists the elevation of the Culebra fluid at H-6b and H-5b as 3049 ft and 3021 ft, respectively. DOE-2, being roughly midway between H-6b and H-5b, should have a Culebra fluid level of ~3035 ft. Hence, the estimate presented above appears reasonable.
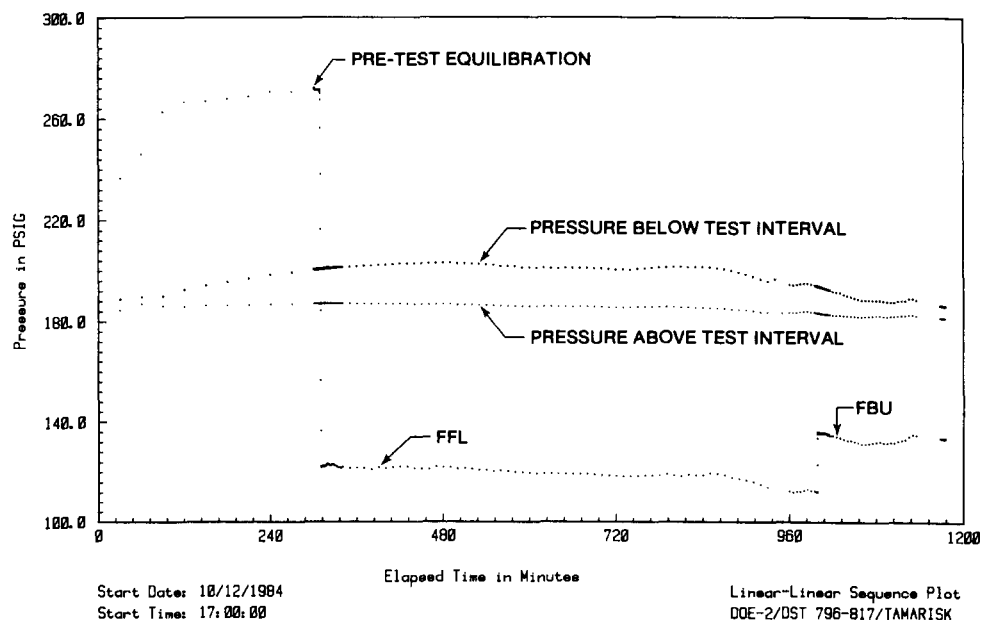

Start Date: 10/12/1984
Start Time: 17:00:00

Linear-Linear Sequence Plot
DOE-2/DST 796-817/TAMARISK

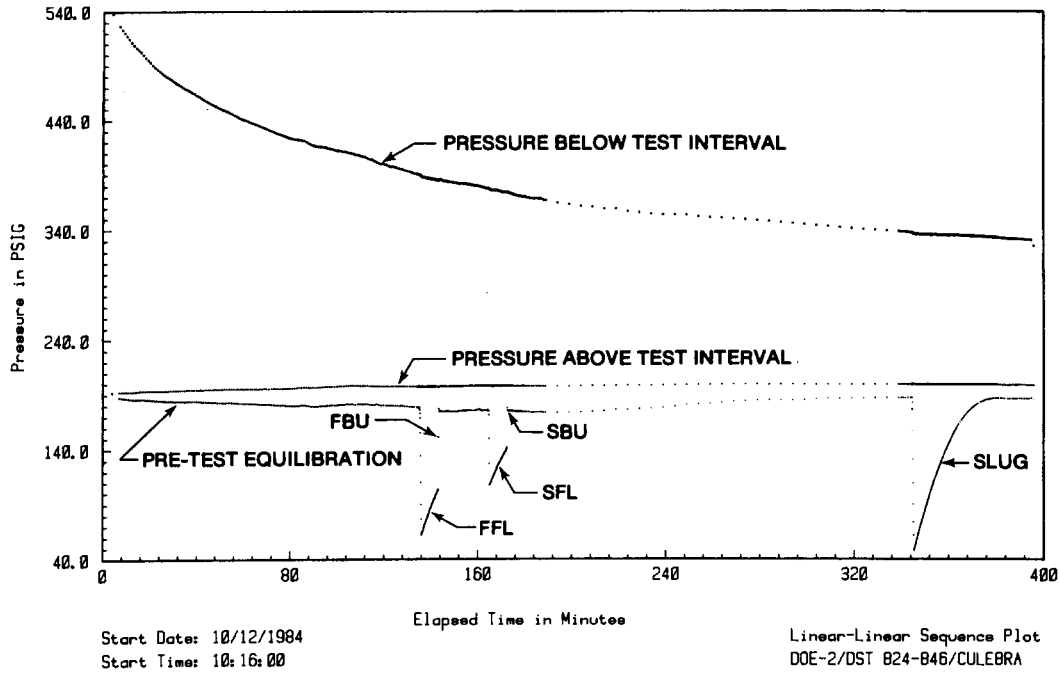**Figure 7-8.** Tamarisk Test Sequence Plot

Figure 7-9. Culebra Test Sequence Plot
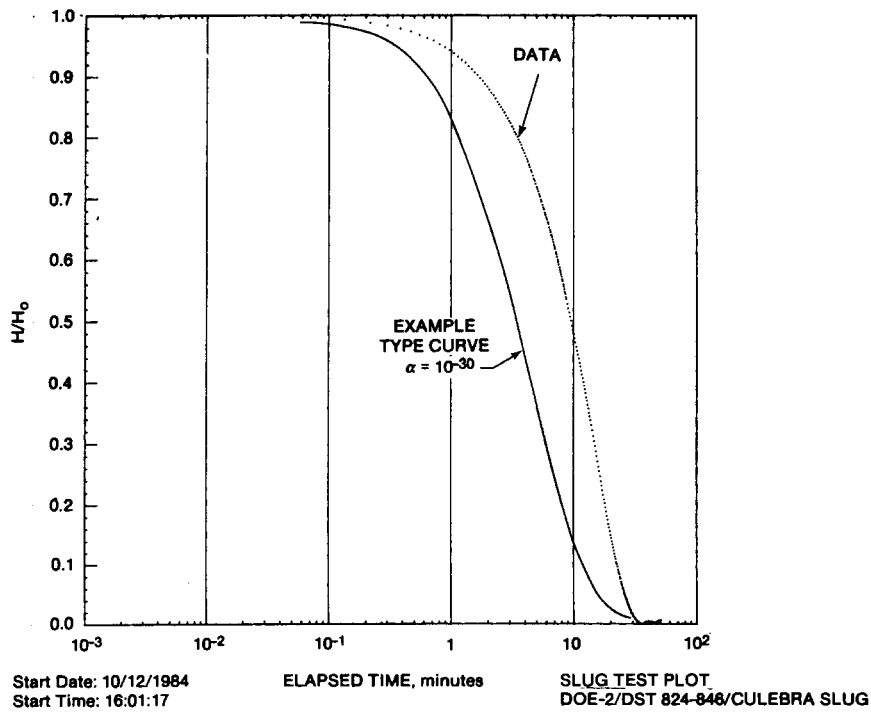
Figure 7-10. Culebra Slug Test Plot

44

When the bottom straddle packer was inflated below the Culebra as the test equipment was being set up, the packer expansion compressed the fluid below. This caused an immediate pressure rise, which decayed steadily during the Culebra testing (Figure 7-9). This bottom-hole pressure decline neither influenced, nor was influenced by, the Culebra testing.

7.2.4.2 Phase Ia (Pumping Test)

When the Phase I drilling and testing was completed, DOE-2 was reamed to a diameter of 7.875 in. to a depth of 981 ft, and left standing open. Later, a Culebra pumping test lasting exactly 3 wk was conducted at DOE-2 from February 19 to March 12, 1985. About 187,900 gal were pumped during this period, at an average rate of ~6.21 gpm (213 BPD). After the pumping period, pressure recovery was monitored at DOE-2 for 17 hr, by which time 99.6% recovery had occurred. Fluid pressures were also monitored during the pumping period and for 28 days of recovery, at the nearest other then-existing Culebra wells, H-5b and H-6b (Figure 1-1).

DOE-2 Response

During the pumping period, the Culebra fluid pressure at DOE-2 declined for the first several hours and then oscillated between ~60 and 65 psig for the balance of the test (Figure 7-11). The oscillation was caused largely by flow-rate fluctuations, particularly early in the test, between ~5.1 and 6.6 gpm. The stabilization at the 60- to 65-psig level is an indication that steady-state (or pseudosteady-state) conditions were reached. Theoretically, steady-state conditions are never reached while pumping an infinite, fully confined aquifer. The fact that such conditions were reached indicated the presence of a recharge, or constant-pressure, boundary close to the well. The data interpretation presented below aids in the boundary conceptualization.

No definitive analysis of the drawdown data is possible because of the pressure stabilization and oscillation that occurred. The early-time data could fit any number of type curves, and the late-time derivative data are unusable because of the random oscillation. The recovery-period data are better, but are also somewhat restricted in their utility. The following discussion is based on an analysis made with the INTERPRET code.
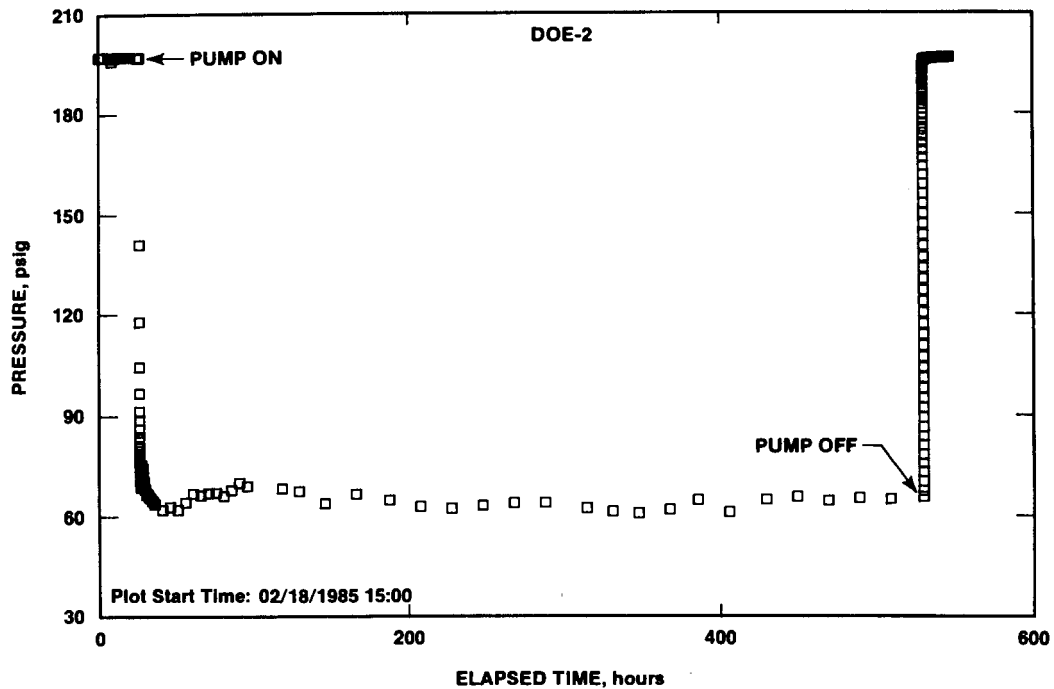
Figure 7-11. Phase Ia Culebra Pumping Test Sequence Plot

Figure 7-12 presents a log-log dimensionless plot of the recovery pressure data, pressure-derivative data, and simulations. The data show an extremely sharp transition from wellbore-storage and skin-affected data (unit slope) to boundary-affected data (stabilized pressure, declining derivative), with little or no infinite-acting aquifer response (gradually stabilizing pressure, constant derivative) in between. This rapid transition is indicative of a well with substantial wellbore damage, i.e., a very high positive skin factor. The low permeability of the skin impedes the flow of water into the borehole. As a result, the pressure in the formation beyond the skin is significantly higher than that in the borehole, and pressure recovery in the borehole is controlled largely by the properties of the "skin," not by the properties of the surrounding aquifer.

Considering that the hole was initially cored using only brine as the circulating fluid and that the hole was then reamed, a very high positive skin factor is difficult to rationalize. Nothing that was done during drilling should have created a high degree of damage.

The pressure type curve presented in Figure 7-12 represents the highest values of $C_D e^{2s}$, and therefore skin factor (s), published by Gringarten et al. (1979). Even so, this simulated-pressure curve cannot match the extent of wellbore-storage and skin domination of the data or stabilize as sharply when wellbore-storage effects terminate. A curve with a higher value of $C_D e^{2s}$, if available, would provide a better match because it would allow quicker transition from wellbore storage to boundary effects. Matching to a higher curve would increase the permeability-thickness estimate, but probably by less than an order of magnitude. The given match provides a permeability-thickness product of 8500 md-ft (Table 7-2). This corresponds to a permeability of 380 md when divided by the thickness of the Culebra. The corresponding groundwater units are a transmissivity of 22 ft²/day and a hydraulic conductivity of 1.0 ft/day. Again, these are minimum values. The skin value obtained from this match is a very high +31. A well so badly damaged that it did not produce at all, regardless of the properties of the surrounding aquifer, would have a skin factor of $+\infty$.

Figure 7-12. Phase Ia Culebra Pumping Test Recovery Log-Log Plot With INTERPRET Simulation

The simulated match to the pressure-derivative data is also presented in Figure 7-12. As with the pressure data, neither the extent of wellbore-storage and skin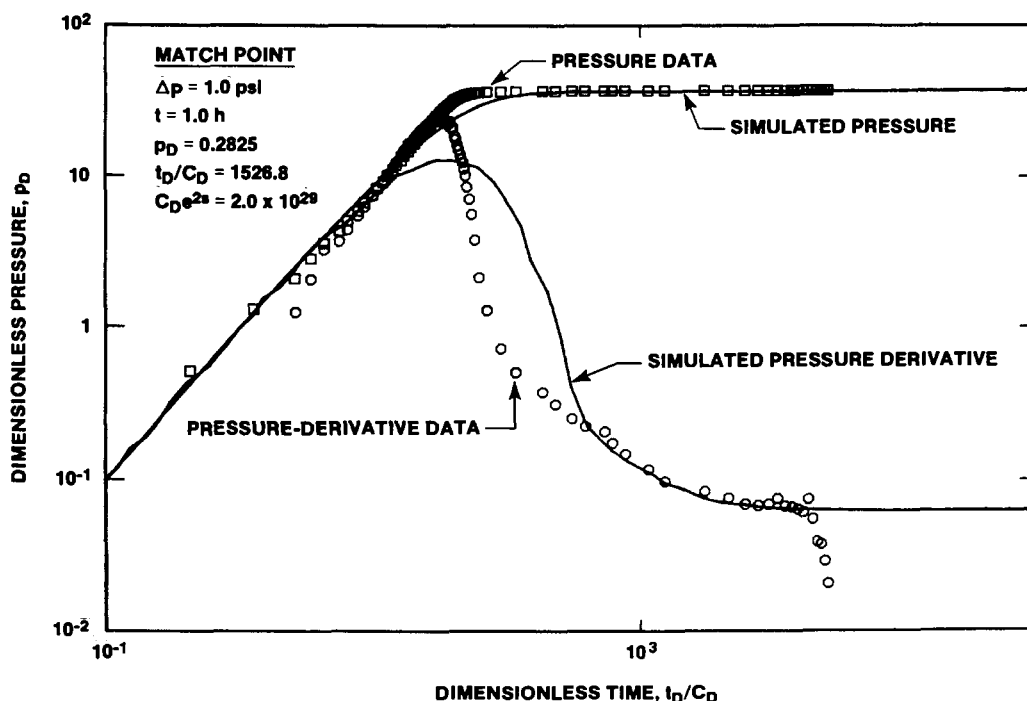 domination nor the rapid pressure stabilization (in this case indicated by a rapidly declining derivative) could be duplicated by using INTER-PRET. Matching the later time behavior required including two boundaries—a constant-pressure boundary close to the well and a fractional no-flow boundary farther from the well. The constant-pressure boundary was included by putting a recharge well injecting at the same rate as DOE-2 was being pumped at a dimensionless distance of 500. The constant-pressure boundary represents a zone of higher permeability close to the well. The fractional no-flow boundary was included by putting a discharge well pumping at one-eighth the rate at DOE-2 at a dimensionless distance of 5000. The fractional no-flow boundary represents a decrease in Culebra permeability at some distance from DOE-2.

The dimensionless boundary distances are related to actual distances by Eq (6.26). If a matrix porosity value of 15% and a total system compressibility of 2 × 10^{5} psi^{-1} are used, the distances to the constant-pressure and no-flow boundaries are ~50 and 170 ft, respectively. These distances are inversely proportional to the square roots of the porosity and compressibility. Hence, if the actual porosity or compressibility of the Culebra is smaller than the value used, the distance to the boundaries would increase. Matching the data to a higher type curve (greater value of $C_D e^{2s}$) would also increase the distance to boundaries. This method provides no information on the orientation of the boundaries. Observation-well data are required to determine boundary locations.

This analysis was performed assuming that the Culebra behaves hydraulically at DOE-2 as a single-porosity system. Core evidence alone indicates that treating the Culebra as a fractured system or a double-porosity system would be more appropriate, but any fracture-flow or double-porosity effects that might be present are obscured by the wellbore-storage and skin effects. In general, this analysis has a high degree of uncertainty because of the problems mentioned above. The 1986 test, discussed below, provided much more definitive, and defendable, results than did the Phase Ia test.

The stabilized Culebra pressure before and after the Phase Ia pumping test was ~197 psig (Figure 7-11). With the transducer at a depth of 810 ft and a specific gravity of 1.04 (Westinghouse, 1985), 197 psig corresponds to a formation pressure of 213 psig at the base of the Culebra, 846 ft deep. In an open borehole containing clean Culebra fluid, 213 psig corresponds to a fluid level ~373 ft below ground surface, or at an elevation of ~3045 ft above sea level. This value is slightly higher than the 3034 ft estimated from the Phase I data, but still between the Culebra fluid levels presented by Mercer (1983) for wells H-6b and H-5b.

H-5b Response

Well H-5b is ~10,595 ft from DOE-2 in the direction S 81° E (Figure 1-1). A plot of the pressure at H-5b during the DOE-2 pumping test is presented in Figure 7-13. Noise in the data obscures any uniform pressure trend and also makes it difficult to define a precise static pressure before the test. Also, while the pressure appears to have dropped during the pumping period, the maximum drawdown is only ~0.4 psi. Furthermore, no actual recovery of pressure is evident after the pump was turned off. Given these factors, whether or not H-5b actually responded to the DOE-2 pumping is problematic. Certainly, no reliable quantitative interpretation of the data is possible.

H-6b Response

Well H-6b is ~10,150 ft from DOE-2 in the direction S 85° W (Figure 1-1). A plot of the H-6b drawdown and recovery response to the DOE-2 pumping test is presented in Figure 7-14. The maximum drawdown recorded was only 1.2 psi. With such a small magnitude of pressure change, transducer noise visibly "smeared" the pressure response. This noise also rendered unrecognizable any boundary effects that might be present in the data.

The best-fit log-log type-curve match is presented in Figure 7-15. This match provides a permeability-thickness product of 21,500 md-ft (Table 7-2) and a porosity-compressibility-thickness product of 1.3 × 10^{5} ft/psi. Corresponding groundwater units are a transmissivity of 61 ft^2/day and a storativity of 6 × 10^{6}. Again, these values are representative of the average Culebra properties between DOE-2 and H-6b, assuming the Culebra is homogeneous and isotropic.
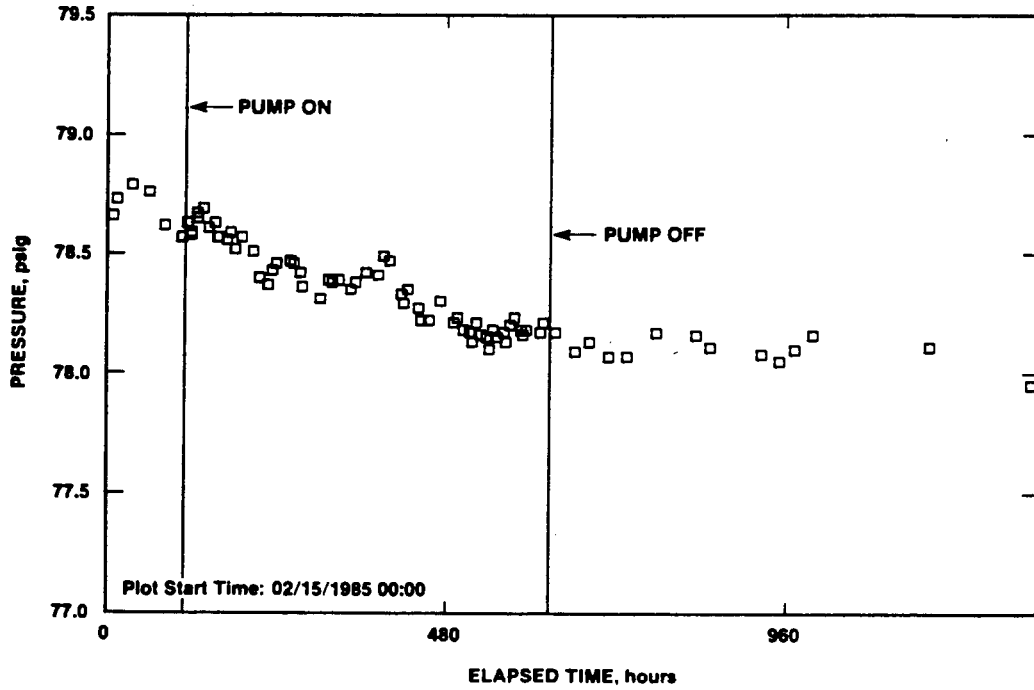
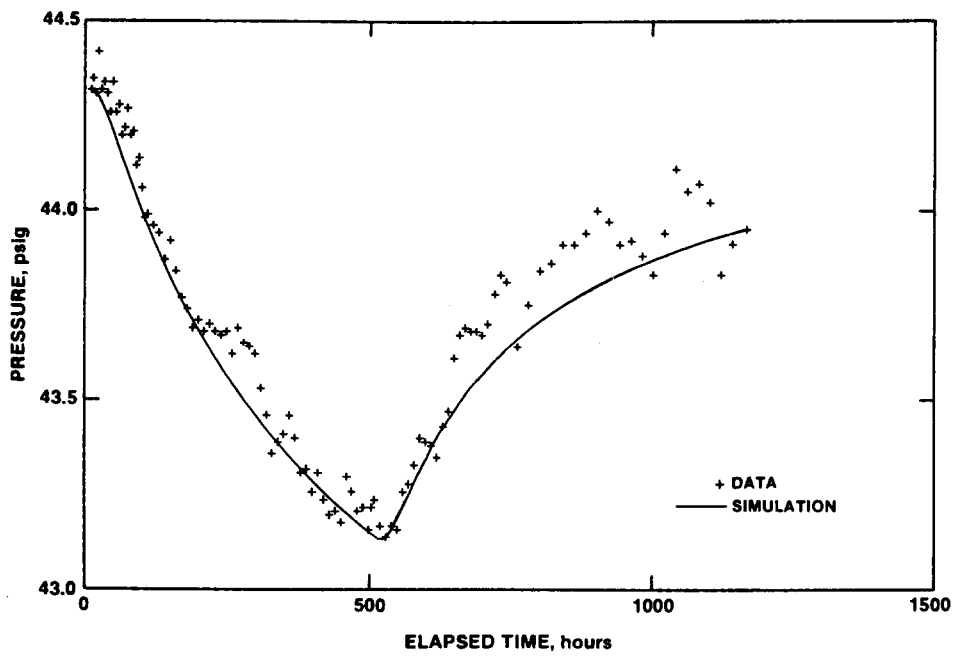**Figure 7-13.** H-5b Response to Phase Ia DOE-2 Culebra Pumping Test

Figure 7-14. H-6b Response to Phase Ia DOE-2 Culebra Pumping Test With INTERPRET Simulation
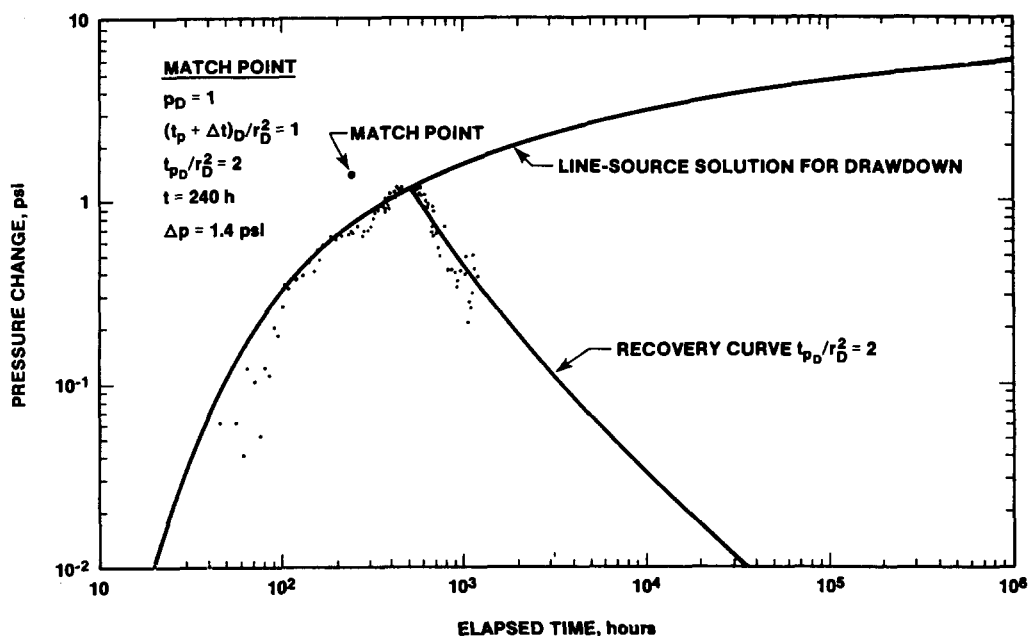
Figure 7-15. Log-Log Plot of H-6b Response to Phase Ia DOE-2 Culebra Pumping Test

Gonzalez (1983) gives the transmissivity of the Culebra at the H-6 pad as 69 ft^2/day and the storativity as 2×10^{-5}. His transmissivity value and that from the present test are in reasonable agreement, but the present storativity is lower than that reported by Gonzalez by a factor of 3. A lower storativity means that H-6b responded faster to the DOE-2 pumping than might have been expected. This relatively rapid response was likely caused by heterogeneities within the Culebra. The transmissivity of the Culebra is less east of DOE-2 at H-5 than it is west of DOE-2 at H-6 (Mercer, 1983). Hence, when DOE-2 was pumped, more water was probably derived from the more-permeable west than from the less-permeable east. This would result in H-6b drawing down more rapidly than it would have if DOE-2 were pumping from a homogeneous system, as the analytical method assumes. Because of this disparity between actual field conditions and the assumptions of the analytical method, the calculated storativity is probably lower than the actual storativity of the Culebra between DOE-2 and H-6b.

The linear-linear simulation generated by INTERPRET using the log-log match to Ramey's type curve is shown in Figure 7-14. In general, the fit is good. Deviations of the simulation from the late-time recovery data are probably caused by a combination of noise and Culebra heterogeneity.

The permeability-thickness product obtained from the H-6b data is almost three times greater than

the minimum value obtained from the DOE-2 data. This indicates how low the permeability-thickness product estimated from the DOE-2 data alone may be.

7.2.4.3 1986 Testing

A pumping test of the Culebra dolomite lasting 100 hr was conducted from June 30 to July 4, 1986 (Table 7-1). About 207,700 gal were pumped over this period, at an average rate of ~34.6 gpm (1190 BPD). After the pumping period, pressure recovery was monitored at DOE-2 for 292 hr. Pumping at H-6b for the WIPP Water Quality Sampling Program (WQSP), however, began ~169 hr into the recovery period and shortly thereafter affected the recovery at DOE-2. Hence, only the first 180 hr of recovery data from DOE-2 are usable for analysis. After 180 hr of recovery, 91% recovery had occurred. Water levels were monitored in Wells H-5b, H-6b, WIPP-12, WIPP-13, and WIPP-18 (Figure 1-1) during the DOE-2 pumping and recovery periods. Wells H-6b and WIPP-13 showed definite responses to the test, while WIPP-12 and WIPP-18 responded only slightly, if at all. H-5b showed no apparent response to the test.

DOE-2 Response

DOE-2 behaved hydraulically in a much more ideal way during the 1986 pumping test than it did during the Phase Ia pumping test. The acidization of the well after perforation apparently removed the high positive skin that so dominated the Phase Ia

response. The sustainable yield of the well increased from 6.2 to 34.6 gpm, drawdown did not stabilize during pumping, and recovery did not occur as rapidly as during both the Phase I and Phase Ia testing (Figure 7-16). Because of the improvement in behavior, the interpretation of the 1986 test is much more certain.

The DOE-2 response during the 1986 pumping test was that of a well in a double-porosity medium with restricted interporosity flow. The effects of a no-flow boundary (or a decrease in transmissivity) at some distance from the well were also evident in the response. Figure 7-17 shows a log-log plot of the drawdown data, along with the final INTERPRET simulation of the data. The match shown produced a permeability-thickness product of 31,100 md-ft (Table 7-2). This value reduces to a vertically averaged permeability of 1410 md when divided by the Culebra thickness of 22 ft. The corresponding groundwater units are a transmissivity of 89 ft2/day and a hydraulic conductivity of 4.0 ft/day, respectively. Assuming that the Culebra porosity is 15%, that the fluid viscosity is ~1.0 cp, and that the total system compressibility is ~2×10^{-5} psi^{-1}, the skin factor is ~-4.7 (Table 7-2). This skin factor, indicating enhanced near-well permeability, is entirely appropriate for an acidized well in a fractured formation (Gringarten, 1984).

The storativity ratio, ω, was 0.10 for this test, indicating that 90% of the water produced came from the matrix, and only 10% from the fractures. The interporosity flow coefficient, λ, was ~8×10^{-8}. Without independent information on matrix geometry, this λ value indicates only that the matrix permeability is probably 5 to 7 orders of magnitude lower than the fracture permeability.

To achieve the fit to the late-time data shown in Figure 7-17 required including a no-flow boundary at a dimensionless distance of 150,000 in the simulation. This dimensionless distance is related to actual distance by Eq (6.26). Using a matrix porosity of 15% and a total system compressibility of 2×10^{-5} psi^{-1}, we found the no-flow boundary to be ~3100 ft from DOE-2. In the field, this boundary probably is not absolute. Rather, the effects are probably caused by the decrease in transmissivity known to occur between DOE-2 and H-5 (Figure 1-1).

Figure 7-18 shows how the parameters chosen to best fit the drawdown data also fit the recovery data. In an ideal system, the fit would be exact. In this system, the fit is very close, indicating that the model chosen is an appropriate approximation to the actual system. Included in Figure 7-16 is the linear-linear simulation of the entire test generated by INTERPRET from the log-log drawdown match parameters. Again, the overall fit to the entire test is excellent.
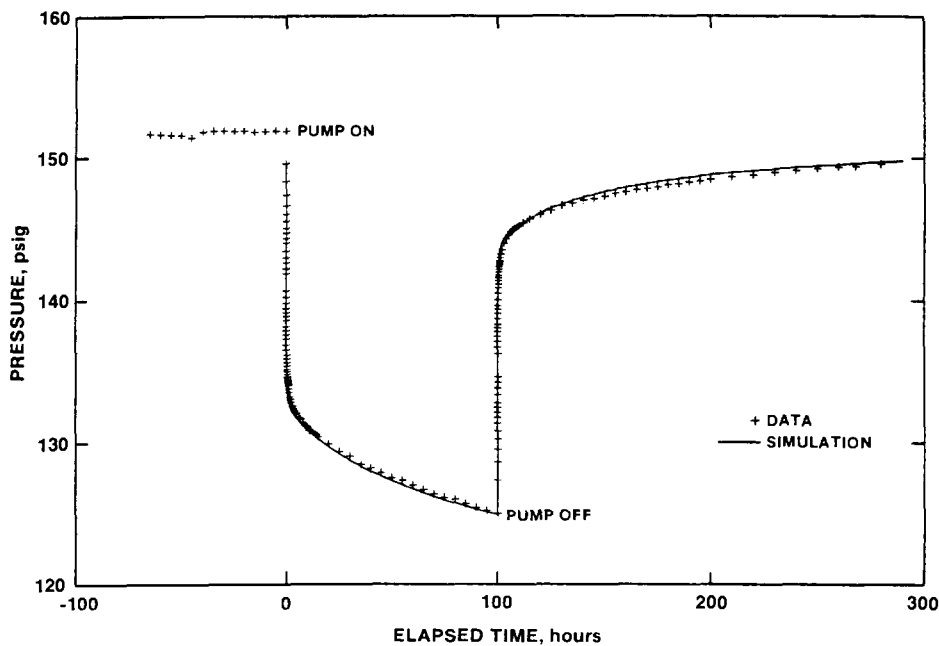
Figure 7-16. 1986 Culebra Pumping Test Sequence Plot With INTERPRET Simulation
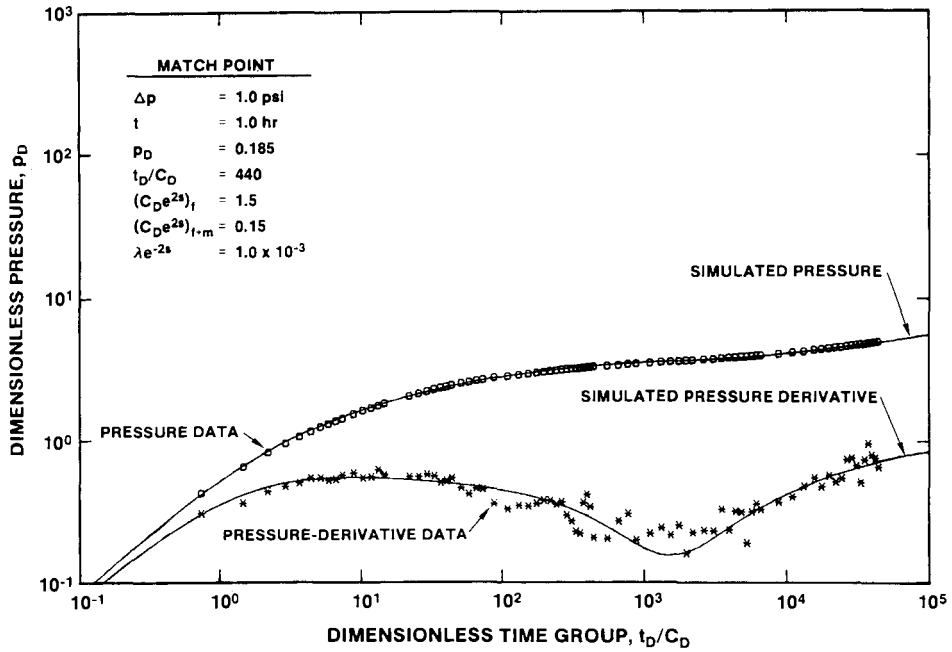
Figure 7-17. 1986 Culebra Pumping Test Drawdown Log-Log Plot With INTERPRET Simulation
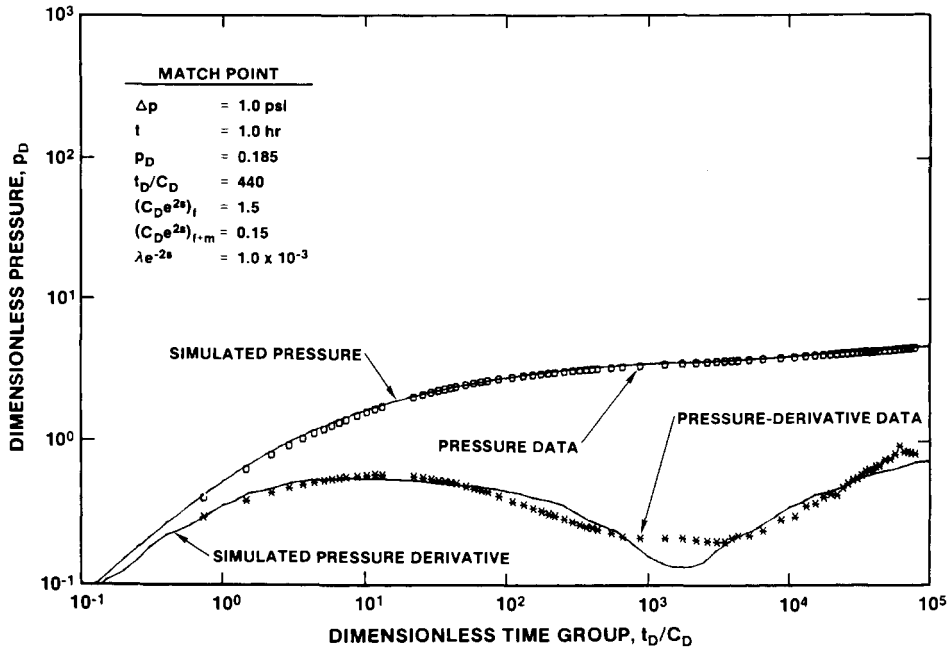
Figure 7-18. 1986 Culebra Pumping Test Recovery Log-Log Plot With INTERPRET Simulation

The stabilized Culebra pressure before the 1986 pumping test was ~151.9 psig (Figure 7-16). With the transducer at a depth of 709.8 ft and a specific gravity of 1.04 (Westinghouse, 1985), 151.9 psig corresponds to a formation pressure of ~213 psig at the base of the Culebra, 846 ft deep. This is the same as the static pressure estimated from the Phase Ia test data (Section 7.2.4.2) and corresponds to a static fluid level ~373 ft below ground surface, or at an elevation of ~3045 ft above sea level.

H-6b Response

Well H-6b is ~10,150 ft from DOE-2 in the direction S 85° W (Figure 1-1). Water levels were measured in H-6b during the DOE-2 pumping period and during ~91 hr of recovery, until activities associated with the WQSP began in the well. Water levels in H-6b responded to the beginning and ending of pumping at DOE-2 within 1 day.

A plot of the H-6b drawdown and recovery response to the DOE-2 pumping test, converted to pressures using a specific gravity of 1.04 (Westinghouse, 1985), is presented in Figure 7-19. Also shown is the best line-source solution fit obtained using INTERPRET to analyze the data. This fit provides a

permeability-thickness product of 21,500 md-ft and a porosity-compressibility-thickness product of 1.3 × 10^{-5} ft/psi (Table 7-2). Corresponding groundwater units are a transmissivity of 61 ft^2/day and a storativity of 6 × 10^{-6}. These values are representative of the average Culebra hydraulic properties between DOE-2 and H-6b.

These values are identical to those obtained from the interpretation of the H-6b response to the Phase Ia pumping test at DOE-2 (Section 7.2.4.2), even though the behavior of DOE-2 differed considerably in the two tests. The agreement of these two sets of results indicates that observation-well responses are not affected by wellbore skin or inefficiencies in the pumping well.

WIPP-13 Response

Well WIPP-13 is ~4835 ft from DOE-2 in the direction S 45° W (Figure 1-1). Water levels were measured in WIPP-13 during the DOE-2 pumping period and during ~188 hr of recovery before they were affected by the WQSP pumping at H-6b. Water levels in WIPP-13 responded to the beginning and ending of pumping at DOE-2 within ~2 hr.
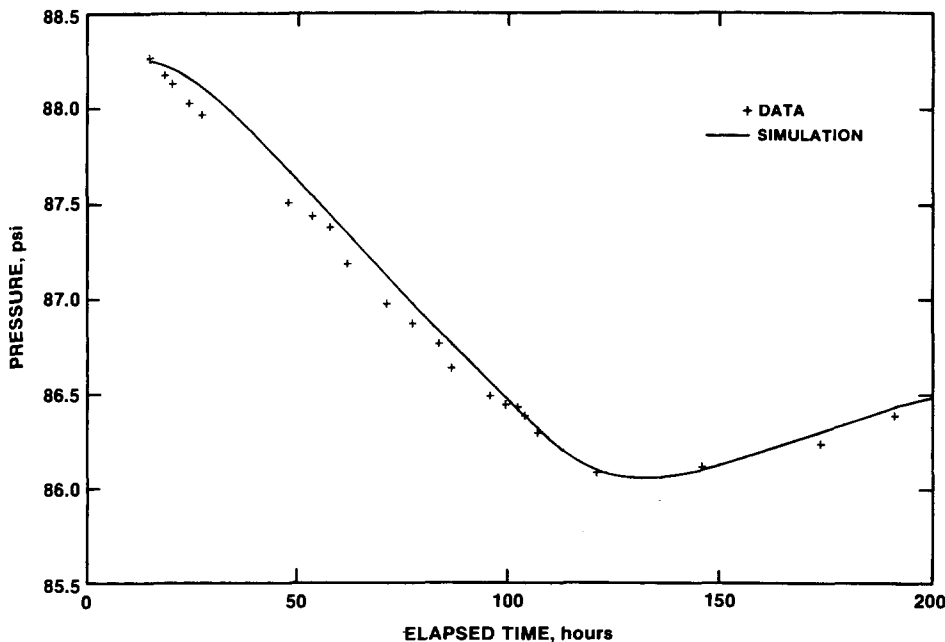
Figure 7-19. H-6b Response to 1986 DOE-2 Culebra Pumping Test With INTERPRET Simulation

A plot of the WIPP-13 drawdown and recovery response to the DOE-2 pumping test, converted to pressures using an assumed specific gravity of 1.04, is presented in Figure 7-20. Also shown is the best line-source solution fit obtained using INTERPRET to analyze the data. This fit provides a permeability-thickness product of 25,200 md-ft and a porosity-compressibility-thickness product of 7.3×10^{-6} ft/psi (Table 7-2). Corresponding groundwater units are a transmissivity of 72 ft²/day and a storativity of 3×10^{-6}. These values are representative of the average Culebra hydraulic properties between DOE-2 and WIPP-13.

The line-source solution fit to the WIPP-13 data shown in Figure 7-20 was chosen because it fit the times at which drawdown and recovery responses began and also fit the magnitude of the maximum drawdown observed. The *shape* of the simulation, however, does not fit the data very well, particularly the recovery data. In general, the observed response is more linear than the simulated response. This type of behavior was also observed in the responses of wells DOE-1 and H-11b1 to the pumping of H-3b2 during the H-3 multipad test at the WIPP site (Beauheim, 1986). The observed response is believed due to fractures and other inhomogeneities controlling fluid flow within the Culebra dolomite, factors that are not taken into account in creating the line-source solution simulations. The low storativity value obtained, 3×10^{-6}, also indicates that fracture flow may play an

important role in the observed response because fracture porosity, and hence storage, is typically much lower than that of a porous medium.

WIPP-12 Response

Well WIPP-12 is ~5835 ft from DOE-2 in the direction S 0.4° E (Figure 1-1). WIPP-12 was acidized in late May 1986 in an attempt to improve the wellbore-Culebra connection. After this acidization, WIPP-12 was left filled to the surface with fluid. The water level in WIPP-12 was still dropping as it equilibrated with the Culebra pressure when pumping began in DOE-2. This decline in water level continued throughout the DOE-2 pumping and recovery periods (Figure 7-21). The rate of decline appears to have increased toward the end of the DOE-2 pumping period, perhaps in response to the pumping, but the data are not adequate for analysis.

WIPP-18 Response

Well WIPP-18 is ~6970 ft from DOE-2 in the direction S 1° E (Figure 1-1). At the time of the DOE-2 pumping test, WIPP-18 was equilibrating from well-development activities performed in mid-May 1986. A slight downward trend in water level was apparent before and during the DOE-2 pumping, which increased after the pump was turned off (Figure 7-22). This roughly indicates a 4- to 5-day response time for WIPP-18 to pumping at DOE-2; but beyond that, the data are not adequate for analysis.
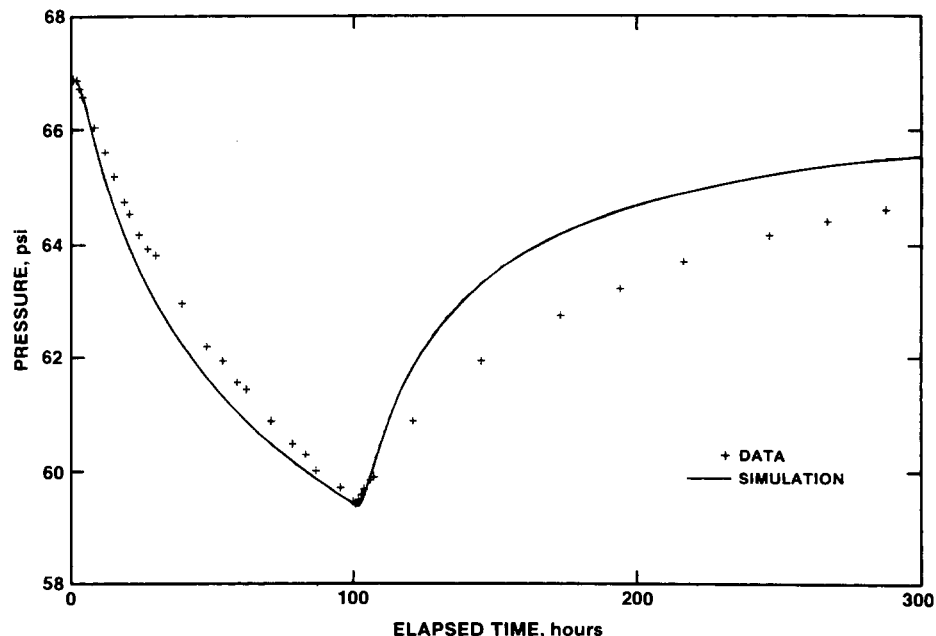
Figure 7-20. WIPP-13 Response to 1986 DOE-2 Culebra Pumping Test With INTERPRET Simulation
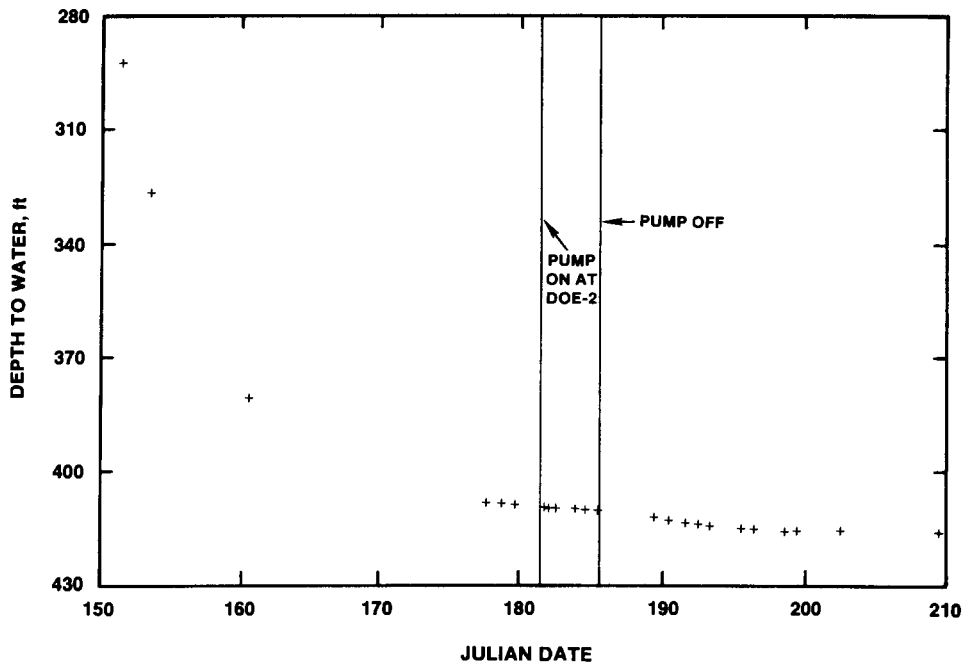
Figure 7-21. WIPP-12 Water Levels During 1986 DOE-2 Culebra Pumping Test
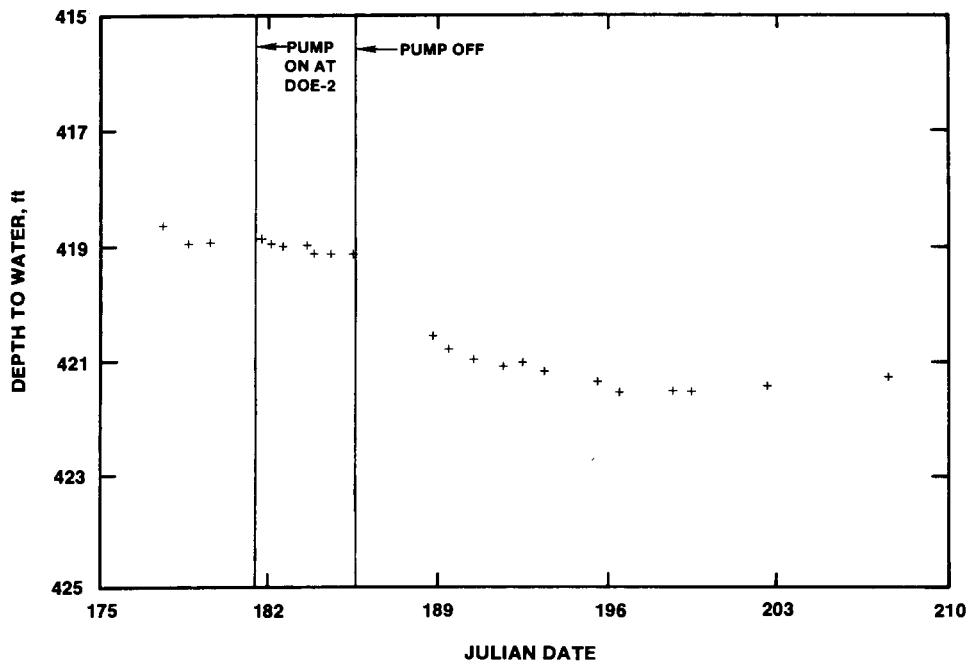
Figure 7-22. WIPP-18 Water Levels During 1986 DOE-2 Culebra Pumping Test

H-5b Response

Well H-5b is ~10,595 ft from DOE-2 in the direction S 81° E (Figure 1-1). At the time of the DOE-2 pumping test, the water level in H-5b was still recovering from WQSP pumping in May 1986. The recovery trend does not appear to have been affected by the pumping at DOE-2 (Figure 7-23).

Discussion

The Culebra dolomite at DOE-2 behaves hydraulically as a double-porosity system, with the major permeability provided by fractures and the major storage provided by matrix porosity. Independent evidence for fracturing of the Culebra at DOE-2 is the broken nature of the core, poor core recovery, and the acoustic-televiewer log run in the hole by the USGS. Fracturing, and fracture-flow effects, have also been noted at H-6b (Gonzalez, 1983). The high permeability interpreted for the H-6b to DOE-2 path, and the rapid response time between those two wells, indicate that the two wells have a high degree of fracture interconnection. Similar conclusions can be drawn for the WIPP-13 to DOE-2 path.

DOE-2, H-6b, and WIPP-13 all lie in an area noted by Snyder (1985) where halite has been dissolved from the Rustler member beneath the Culebra. Subsidence of the Culebra after this dissolution may

have resulted in the fracturing that so strongly affects the hydraulic response of the Culebra in this area. WIPP-12, WIPP-18, and H-5b, by contrast, lie in an area where halite has not been dissolved beneath the Culebra (Snyder, 1985). These wells showed a delayed, lower magnitude (to undetectable) response to the DOE-2 pumping. Mercer (1983) reports the Culebra transmissivity at H-5b as 0.2 ft^2/day. Recent well-development work at WIPP-12 and WIPP-18 indicates that the Culebra also has a low transmissivity at those locations. Hence, the presence or absence of halite dissolution beneath the Culebra, and the accompanying presence or absence of fracturing in the Culebra, appears to be the factor governing the hydraulic response of the Culebra in the vicinity of DOE-2.

7.2.5 Unnamed Member and Rustler-Salado Contact (DST 945-967)

The unnamed member of the Rustler, and the Rustler-Salado contact, were tested between 945 and 967 ft deep. The Rustler-Salado contact is at 960.9 ft. The bottom 16 ft of the Rustler Formation consist of claystone, while the upper 6 ft of the Salado consist of siltstone and halite. Testing of this zone began October 11, 1984, and ended October 12, 1984 (Table 7-1).
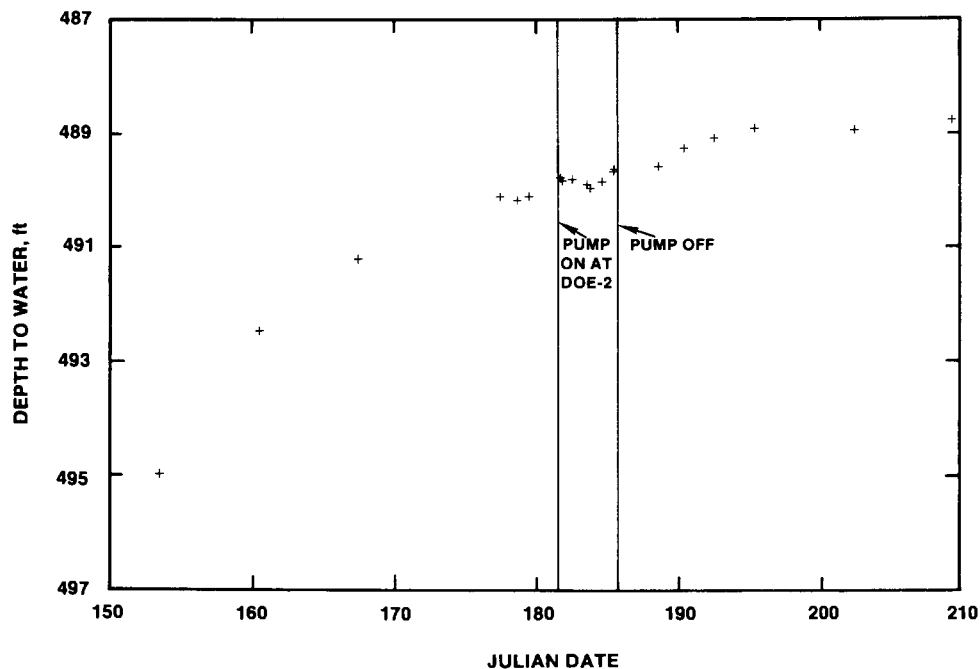
Figure 7-23. H-5b Water Levels During 1986 DOE-2 Culebra Pumping Test

Testing began by deflating the valve packer with the tubing partially bailed to initiate a flow period (Figure 7-24). After 1 hr, no appreciable fluid had entered the tubing, and the test was converted to a long-term slug test. The flow period/slug test lasted a total of 14 hr. The pressure oscillated slightly during this period, with a net loss of ~11 psi. The valve packer was then reinflated to isolate the interval and to see if the pressure would build-up. The valve-packer inflation caused an immediate pressure increase of ~255 psi as the water in the test interval was compressed. This pressure began to decay slowly, and the test was terminated.

As discussed with respect to the Tamarisk tests, the decrease in pressure during the Rustler-Salado contact testing could be explained if the initial pressure during the flow period was greater than the natural *in situ* fluid pressure. At the beginning of the flow period at DOE-2, the test-interval pressure was ~104 psi, measured at a depth of 925.6 ft. Extrapolating this pressure to the Rustler-Salado contact depth of 961 ft, using a fluid density of 1.21 g/cm^3, gives a pressure of ~123 psi. Mercer (1983) lists the depth to water from the Rustler-Salado contact zone at H-6c, ~two mi west of DOE-2, as 410.5 ft, with a fluid density of 1.21 g/cm^3. This water level corresponds to a pressure of ~163 psi at the depth of the Rustler-Salado contact in H-6c, 721 ft. Mercer (1983) indicates that the head at the Rustler-Salado contact increases

to the east from H-6; hence, the pressure at DOE-2 should be *greater* than the 163 psi measured at H-6c, not less.

As with the Tamarisk testing, the question remains as to why the pressure dropped during the test instead of rising. Again, the most tenable answer is that the apparent decrease in pressure was caused by transducer drift as the pressure remained static, not by an actual decrease in pressure. Regardless of the uncertainty caused by transducer drift, the Rustler-Salado contact zone at DOE-2 appears to have very low permeability and possibly very low interconnected porosity. It does not appear to be capable of playing a significant role in any repository breach scenario.

Figure 7-24 shows changes in the bottom-hole pressure during the Rustler-Salado contact testing that appear to parallel pressure changes in the test interval. The large-magnitude (30 to 35 psi) changes in the bottom-hole pressure were caused by expansion and compression of the bottom-hole fluid in response to slight shifts in the bottom straddle packer as the pressure in the test interval above changed when the valve packer was deflated and inflated. The lower magnitude changes in the bottom-hole pressure are probably related to transducer drift. The fact that these changes parallel those in the test interval indicates that the drift may have a source in the power supply system shared by the transducers.
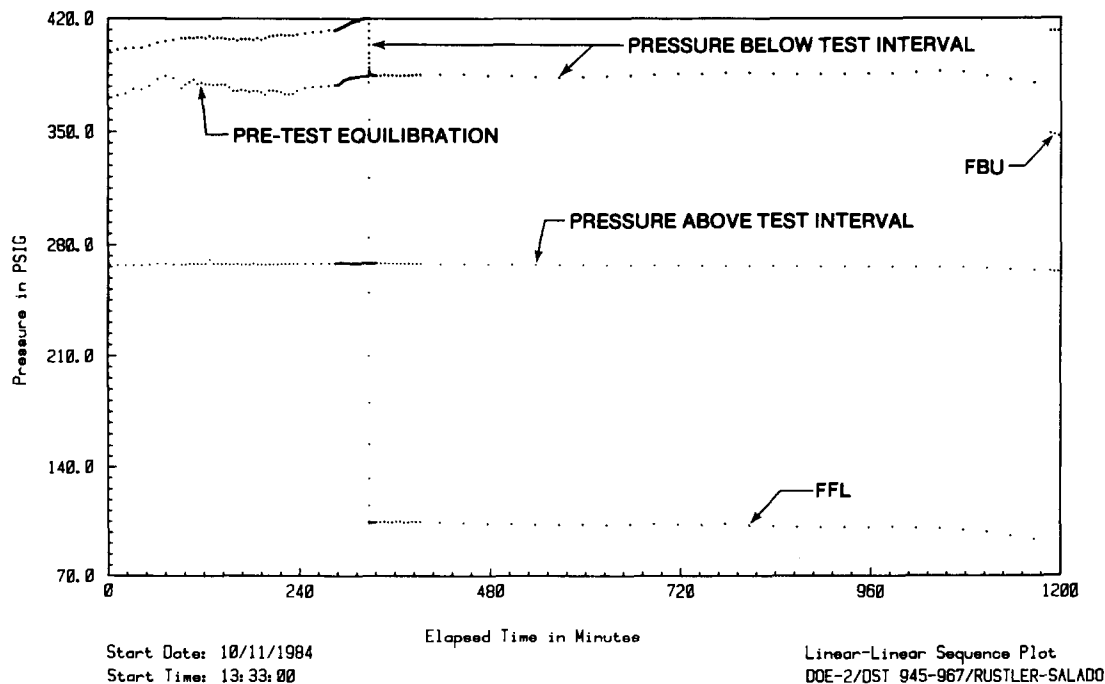
Figure 7-24. Rustler-Salado Test Sequence Plot

7.3 Salado Formation

Two sets of tests were conducted in the Salado Formation: one set covering the interval from Marker Bed 138 to Marker Bed 139, which includes the repository horizon, and another set spanning essentially the entire Salado.

7.3.1 Marker Beds 138 to 139 (DST 2195-2309)

A section of the mid-Salado from 2195 to 2309 ft deep was tested on May 19 and 20, 1985 (Table 7-1). This interval included Marker Beds 138 and 139 and the intervening WIPP facility horizon. The testing consisted of a 21-min flow period followed by a 23.3-hr buildup period (Figure 7-25).

The pressure recovery during the buildup period never stabilized into the infinite-acting radial flow necessary for a definitive analysis. This is shown on the Horner plot of the buildup (Figure 7-26) as a steadily steepening curve. As a result, the only infor-

mation obtainable is a maximum permeability (permeability decreases as the curve on the Horner plot steepens) for the interval and a minimum formation pressure (extrapolated pressure increases as the curve steepens). The permeability-thickness product obtained from the Horner analysis is $\sim 3 \times 10^{-2}$ md-ft (Table 7-2). When divided by the total interval thickness (114 ft), this converts to a permeability of $\sim 3 \times 10^{-4}$ md (0.3 μd). Corresponding groundwater units are a transmissivity of $\sim 6 \times 10^{-5}$ ft^2/day and a hydraulic conductivity of $\sim 6 \times 10^{-7}$ ft/day. Again, these are maximum values.

The last few points on the Horner plot (Figure 7-26) extrapolate to a pressure of 499 psia (489 psig) at infinite time. With the transducer at a depth of 2190.9 ft and a fluid pressure gradient in the borehole of 0.524 psi/ft (SG = 1.21), also representative of clean Salado brine, a pressure of 489 psig corresponds to a natural fluid level ~ 1260 ft below ground surface, or at an elevation of ~ 2160 ft above sea level. Again, these represent minimum pressure and fluid levels.
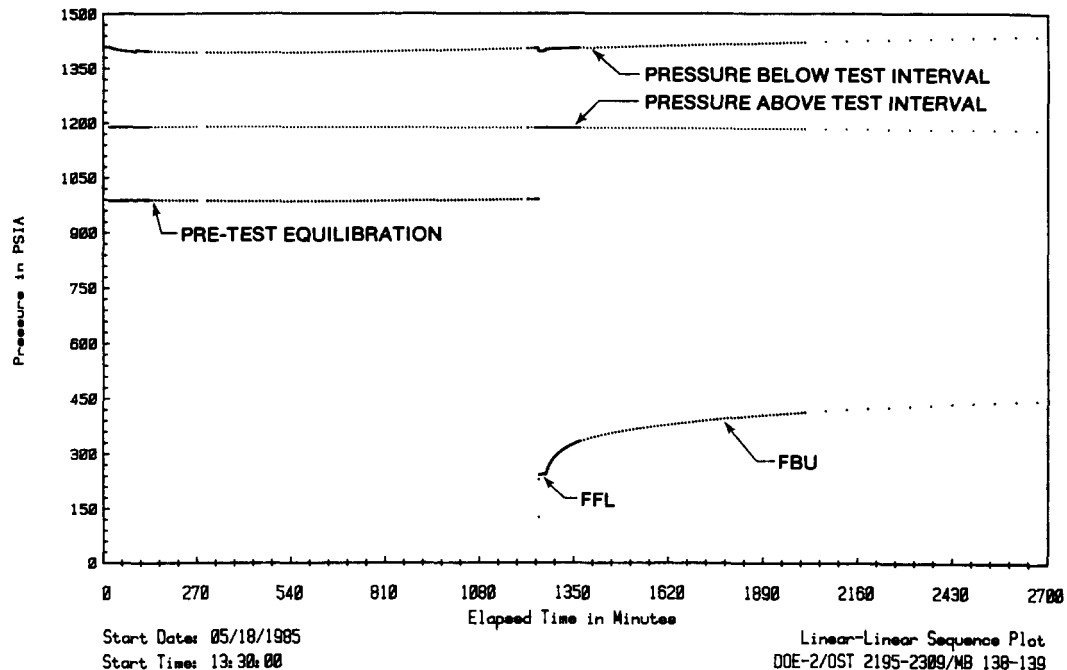
Figure 7-25. Marker Beds 138-139 Test Sequence Plot
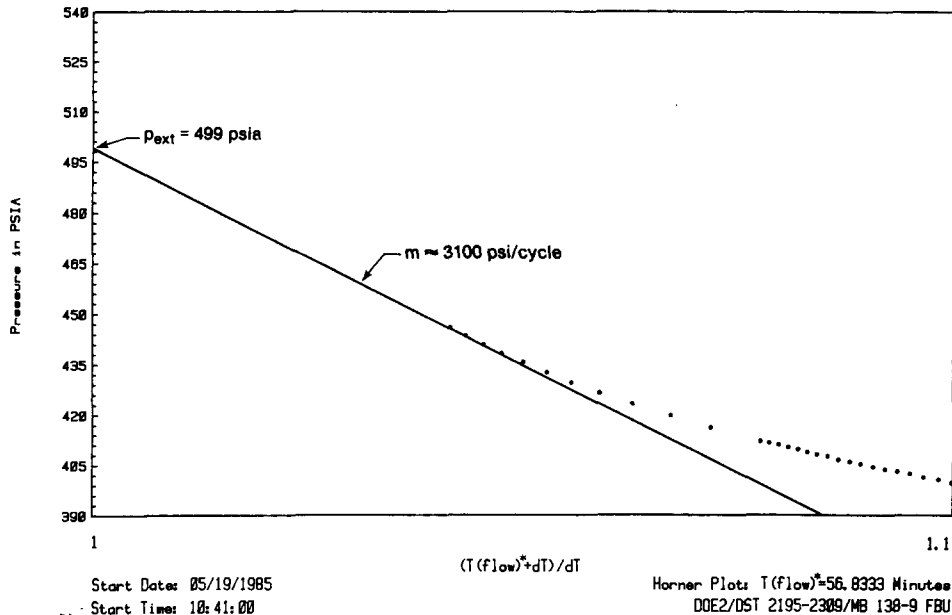
Figure 7-26. Marker Beds 138-139 FBU Horner Plot

During the Marker Beds 138 – 139 testing, the bottom-hole pressure initially dropped and then rose ~50 psi (Figure 7-25). This pressure response was probably not related to formation pressure because later testing of the entire Salado did not detect pressures of this magnitude. Instead, the pressure response was probably caused by temperature changes that exactly paralleled the pressure changes in the isolated interval (Figure 7-27). The drilling fluid used in drilling DOE-2, and the test equipment, were probably not in thermal equilibrium with the formation rock and fluid. A shut-in borehole interval in a very low-permeability medium such as halite behaves, in the short term, as a closed system. Hence, when the temperature of the fluid dropped initially, probably as the fluid cooled the DST tool, the pressure dropped. Later, as the formation heated the drilling fluid, the fluid pressure rose. Over a longer period of time, the pressure would have dissipated through the lower Salado. Similar thermally induced pressure responses have also been observed in testing of low-permeability crystalline rocks (Grisak et al., 1985). No temperature trends were evident in the test-interval data.

7.3.2 Salado Formation (DST 1040-3095)

The entire Salado Formation, except for the upper 79 ft, and the upper 12 ft of the Castile Formation were tested in an interval extending from a single packer at 1040 ft to the bottom of the hole, 3095 ft deep. The tests were performed from May 21 to 22, 1985 (Table 7-1), and consisted of a 9.5-hr pulse-withdrawal test followed by a 13.8-hr pulse-injection test (Figure 7-28). The primary objective of the tests was to determine whether zones existed in the Salado that could cause pressure buildups at the wellhead such as those observed at Cabin Baby-1 and WIPP-12 (Mercer, 1986). The secondary objective of the tests was to obtain information on bulk Salado hydraulic properties.

When the packer was inflated and the Salado interval shut-in, the interval was overpressurized relative to any expected Salado pressure. To relieve this overpressure, we partially swabbed the tubing, opened the interval briefly to the tubing to reduce the pressure, and then shut in the interval again. In response, the test interval pressure built up rapidly and then began a slow, steady decrease (Figure 7-28). This pressure-trend reversal was caused by the dissipation of the pressure skin that had been imparted to the Salado while the hole was open and filled with fluid. Formal testing began after the rate of pressure decline had dropped to ~2 psi/hr.
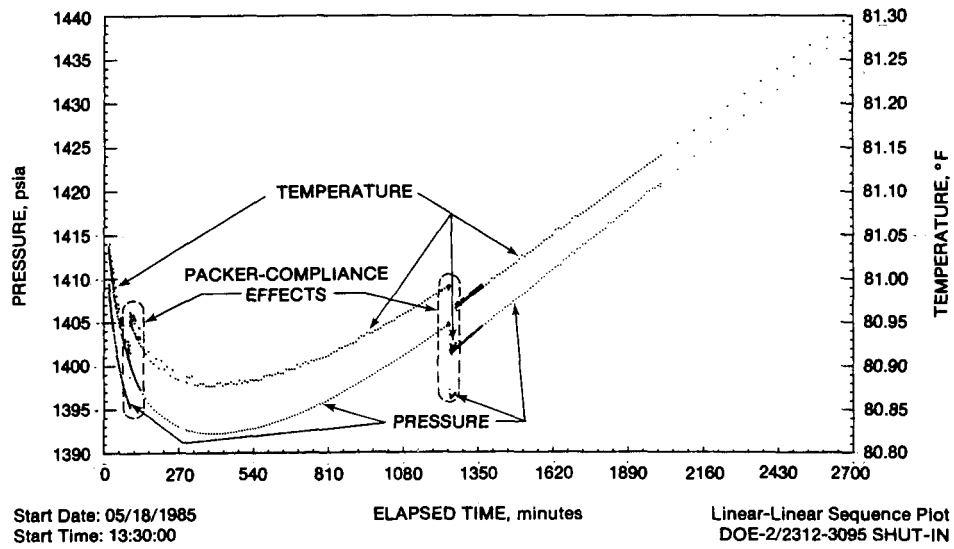
Figure 7-27. Bottom-Hole Temperature and Pressure During Marker Beds 138-139 Testing
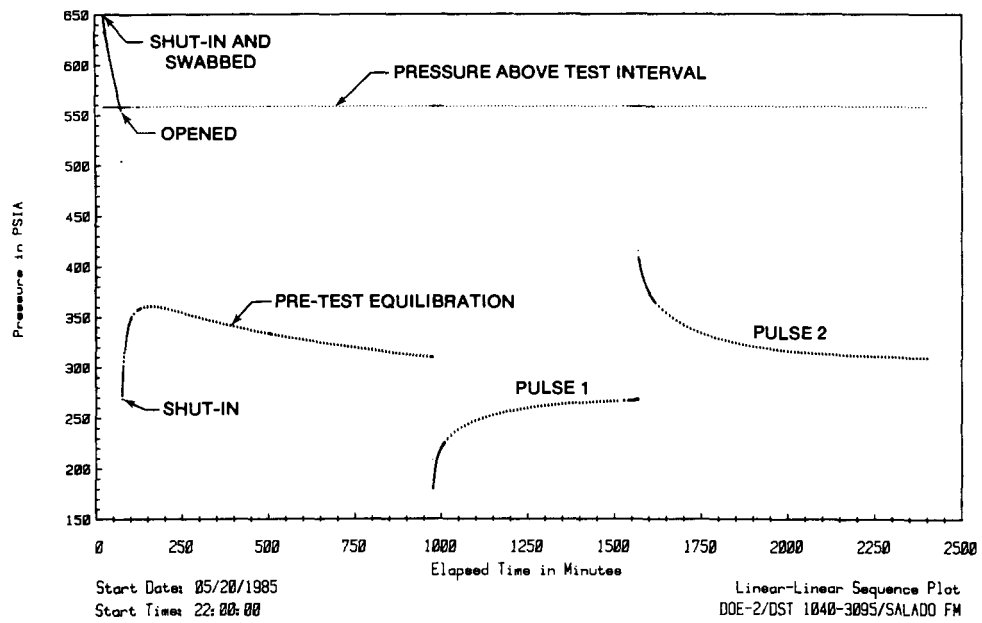
Figure 7-28. Salado Test Sequence Plot

Both the pulse-withdrawal and pulse-injection tests appeared to be successful in the field. Analyzing the data, however, revealed several peculiarities in the responses. To get the pulse-test data to "tail" at the appropriate points to match the tails on the semi-log type curves required very careful static-pressure selection. A difference of only 2 psi resulted in significantly poorer fits. The best-fit static pressures for the two tests were, however, quite different. The semi-log plot for the pulse-withdrawal test, Test 1 (Figure 7-29), was prepared using a static formation pressure of 270 psia, whereas the semi-log plot of the pulse-injection test, Test 2 (Figure 7-30), was prepared using a static formation pressure of 305 psia. No single pressure could produce reasonable plots for both tests. Also, even with the best-fit tails, the data fit the overall type curves poorly, particularly the data from the pulse-withdrawal test (Figure 7-29).

The observed pressure response is similar to that expected when testing a relatively small, finite volume rather than an infinite-acting system. A pulse-withdrawal test removes a small quantity of fluid from the system, and so a closed system would recover to a pressure slightly below the pretest static pressure. A subsequent pulse-injection test would add a small quantity of fluid to the system, and thus the pressure should recover to a value slightly higher than it

reached after the pulse withdrawal. No fit to type curves derived for infinite-acting systems would be expected. This theoretical behavior is entirely consistent with the pressure responses observed during the Salado testing.

A closed system can be conceptualized as a small region around the borehole with enhanced permeability, surrounded by unaffected halite of much lower permeability. The local permeability enhancement could be in response to stress relief around the hole. On the time scale of the tests, the unaffected "natural-permeability" halite may not respond appreciably to the test-induced stresses. Whether or not this particular conceptualization is accurate, if the overall concept of the near-wellbore Salado's behaving as a closed system on the time scale of the tests is correct, analysis of the Salado pulse tests using methods derived for infinite-acting systems would result in meaningless parameter values. For this reason, and because the type-curve matches are so ambiguous, no analysis of the Salado pulse tests is presented.

The only conclusions from the tests are that no high-pressure zones are evident in the Salado at DOE-2, and that the Salado has very low permeability. Accurate Salado pressure data could probably be collected only by isolating the Salado for a period of months.

$P_{static} = 270$ psia

Start Date: 05/21/1985
Start Time: 14:18:15

ELAPSED TIME, minutes

Pulse Test Plot
DOE-2/DST 1040-3095/SALADO P-1
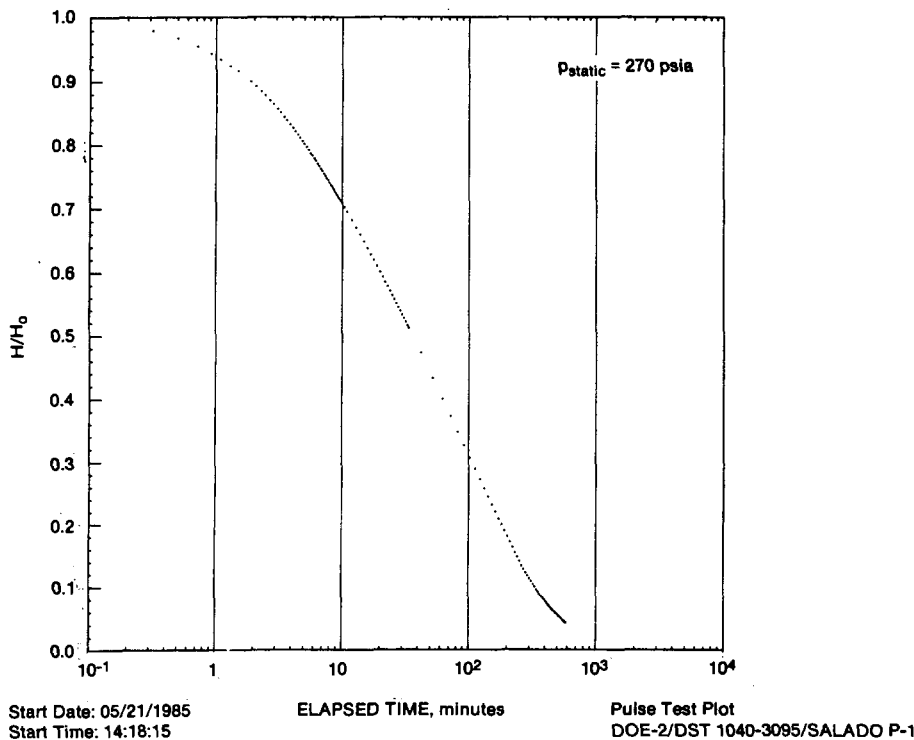
Figure 7-29. Salado Pulse Test 1 Plot
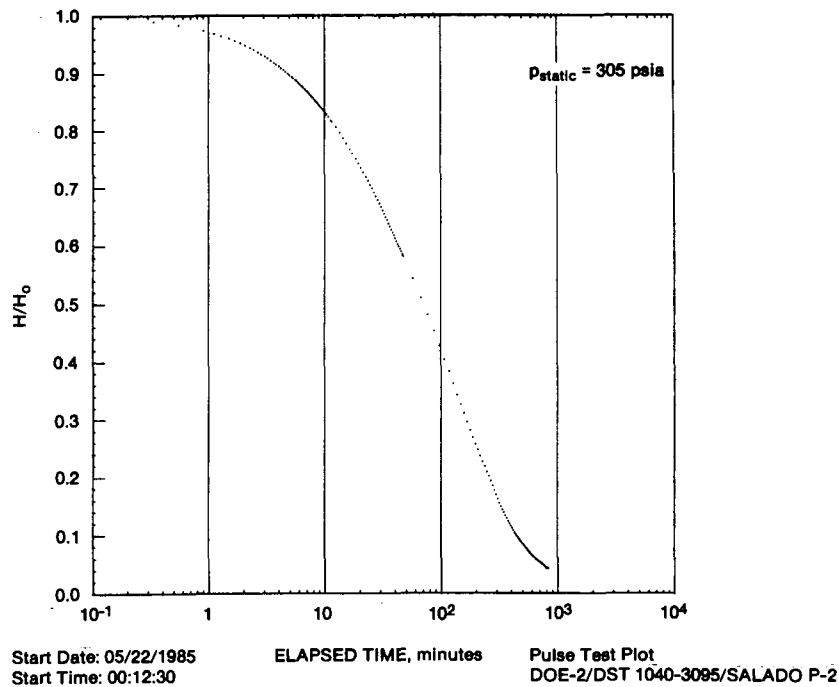
Figure 7-30. Salado Pulse Test 2 Plot

7.4 Bell Canyon Formation

Three sets of tests were conducted in the Bell Canyon Formation: tests of the Ramsey sandstone, the Olds sandstone, and the Hays sandstone. These sandstones are separated by siltstones/claystones of lower permeability that served as packer seats. Analyses of the first and second flow periods (FFLs and SFLs) from each interval are not presented because only a small degree of recovery of the induced pressure differential occurs during a DST flow period. Much greater degrees of recovery occur during slug tests, and therefore the analytical results are more definitive from those tests. Similarly, second buildup periods (SBUs) typically provide more definitive results than do first buildup periods (FBUs) because SBUs typically last longer than FBUs, allowing a greater degree of recovery. Nevertheless, both FBU and SBU analyses are presented below. All of the Bell Canyon intervals tested behaved as homogeneous single-porosity media.

7.4.1 Ramsey Sandstone (DST 4138-4180)

Based on an examination of geophysical logs, the most permeable portion of the Ramsey sandstone appears to be a 28-ft section from 4144 to 4172 ft deep. This zone was tested in a straddled interval extending from 4138 to 4180 ft deep. Tests were conducted from

July 12 to 14, 1985 (Table 7-1), and consisted of two flow periods, two buildup periods, and a slug test (Figure 7-31). The Ramsey tests were hindered by a partial short circuit in the wireline connecting the transducers to the data-acquisition system. The short circuit led to occasional periods of meaningless data. This "noise" was filtered out, leaving visible gaps in the data presented in Figure 7-31. The analysis of the data, however, is not affected by the malfunction.

The FBU and SBU were analyzed and simulated using the code INTERPRET. Log-log dimensionless plots of the FBU and SBU pressure data, pressure-derivative data, and simulations are presented in Figures 7-32 and 7-33, respectively. The FBU and SBU analyses yielded permeability-thickness products of 2.4 and 2.5 md-ft, respectively (Table 7-2). These values correspond to permeabilities of 8.4×10^{-2} and 8.8×10^{-2} md, respectively, when divided by the "effective" Ramsey thickness of 28 ft. The corresponding groundwater units are transmissivities of 5.4×10^{-3} and 5.7×10^{-3} ft^2/day and hydraulic conductivities of 1.9×10^{-4} and 2.0×10^{-4} ft/day for the FBU and SBU, respectively. Assuming the Ramsey porosity is 25%, that the fluid viscosity is ~1.5 cp, and that the total system compressibility is ~6×10^{-6} psi^{-1}, the FBU and SBU skin factors are 1.2 and 1.0, respectively. These values indicate a well with minor wellbore damage (decreased near-well permeability).
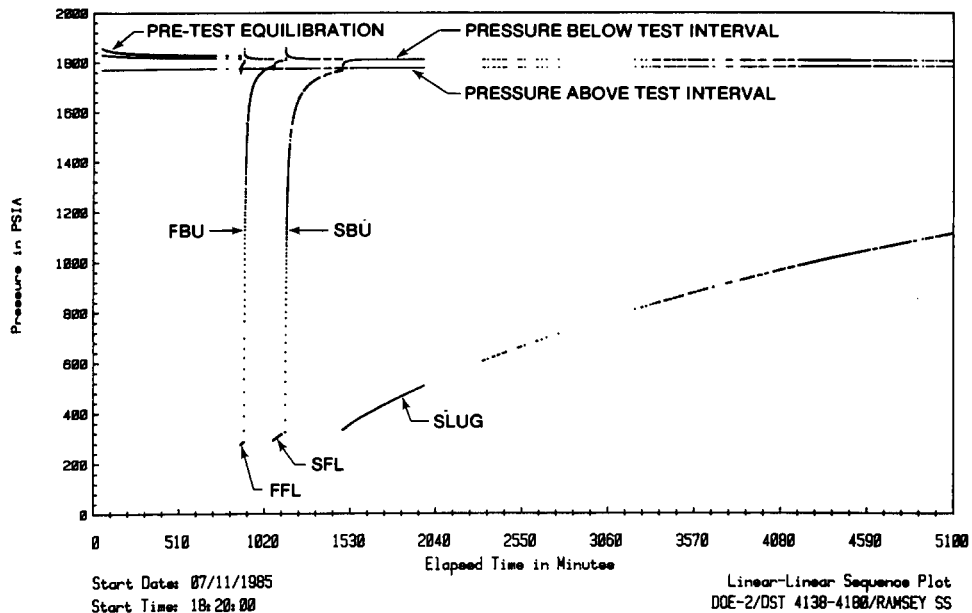
Figure 7-31. Ramsey Test Sequence Plot
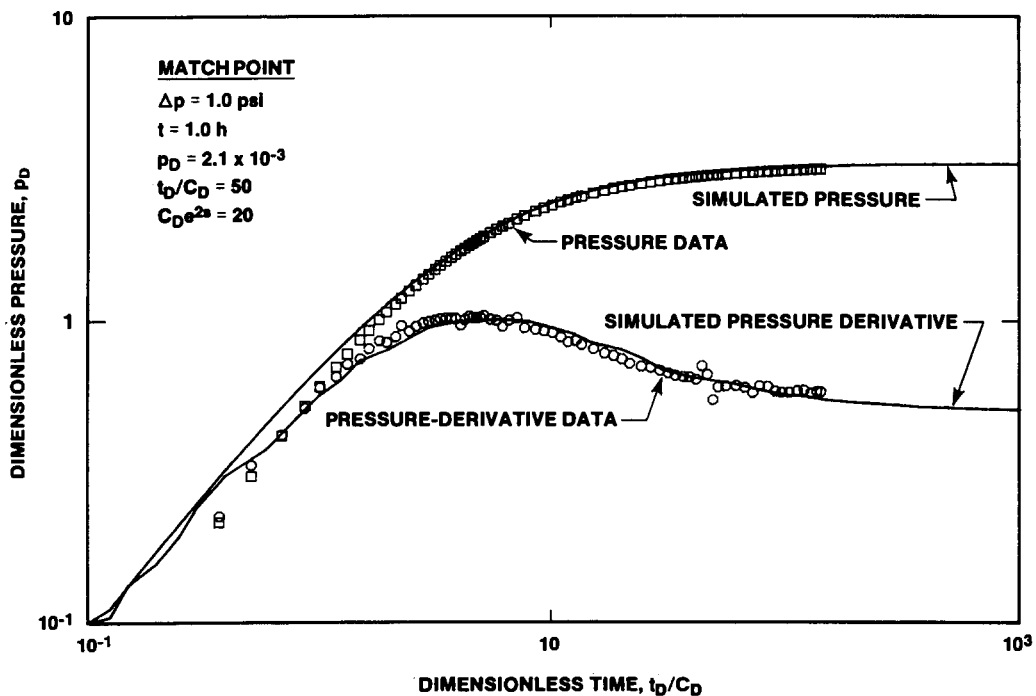
Figure 7-32. Ramsey FBU Log-Log Plot With INTERPRET Simulation
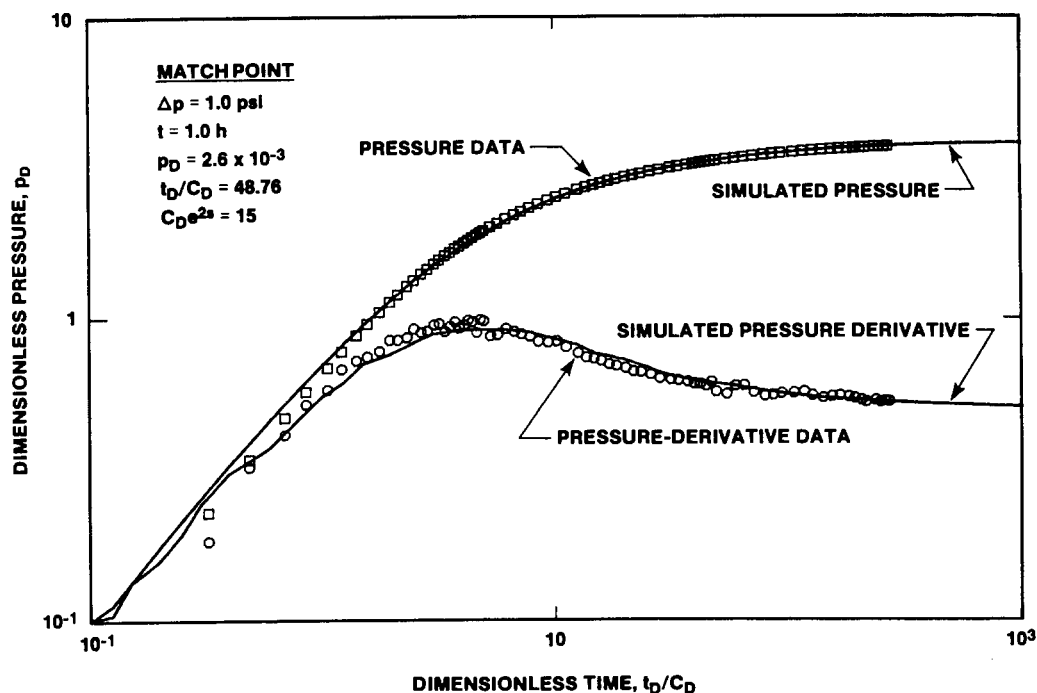
Figure 7-33. Ramsey SBU Log-Log Plot With INTERPRET Simulation

The late-time SBU data are shown in a Horner plot in Figure 7-34. Extrapolating the data trend to infinite time provides a static formation pressure estimate of ~1816 psia (1805 psig). With the transducer at a depth of 4120.6 ft and a fluid pressure gradient in the borehole from drilling fluid of 0.542 psi/ft (assumed SG = 1.25), 1805 psig corresponds to a formation pressure of 1833 psig at the base of the Ramsey, 4172 ft deep. In an open borehole containing clean Ramsey fluid (SG = 1.1), 1833 psig corresponds to a fluid level ~327 ft below land surface, or at an elevation of 3092 ft above sea level. This probably represents the maximum possible level for Ramsey fluid and puts it in the upper Dewey Lake Red Beds, above the estimated Culebra fluid level.

A log-log plot of the Ramsey slug test is presented in Figure 7-35. The best-fit type-curve match gives a transmissivity of 6.0×10^{-3} ft²/day (Table 7-2). When divided by the effective Ramsey thickness of 28 ft, this value gives a hydraulic conductivity of 2.1×10^{-4} ft/day. Corresponding petroleum units are a permeability-thickness product of 2.6 md-ft and a permeability of 9.4×10^{-2} md. These values are in excellent agreement with the results of the buildup analyses presented above.

7.4.2 Olds Sandstone (DST 4177-4218)

Based on an examination of geophysical logs, the most permeable portion of the Olds sandstone appears to be a 30-ft section from 4187 to 4217 ft deep. This zone was tested in a straddled interval extending from 4177 to 4218 ft deep. Tests were conducted from July 26 to 29, 1985 (Table 7-1), and consisted of two flow periods, two buildup periods, and a slug test (Figure 7-36).

The FBU and SBU were analyzed and simulated using the code INTERPRET. Log-log dimensionless plots of the FBU and SBU pressure data, pressure-derivative data, and simulations are presented in Figures 7-37 and 7-38, respectively. The FBU and SBU analyses yielded permeability-thickness products of 3.1 and 2.9 md-ft, respectively (Table 7-2). These values correspond to permeabilities of 0.10 and 9.8×10^{-2} md, respectively, when divided by the "effective" Olds thickness of 30 ft. The corresponding groundwater units are transmissivities of 7.0×10^{-3} and 6.6×10^{-3} ft²/day and hydraulic conductivities of 2.3×10^{-4} and 2.2×10^{-4} ft/day for the FBU and SBU, respectively. Assuming the Olds porosity is 25%, that the fluid viscosity is ~1.5 cp, and that the total system compressibility is $\sim 6 \times 10^{-6}$ psi^{-1}, the FBU and SBU skin factors are both 2.0. These values indicate a well with slight wellbore damage.
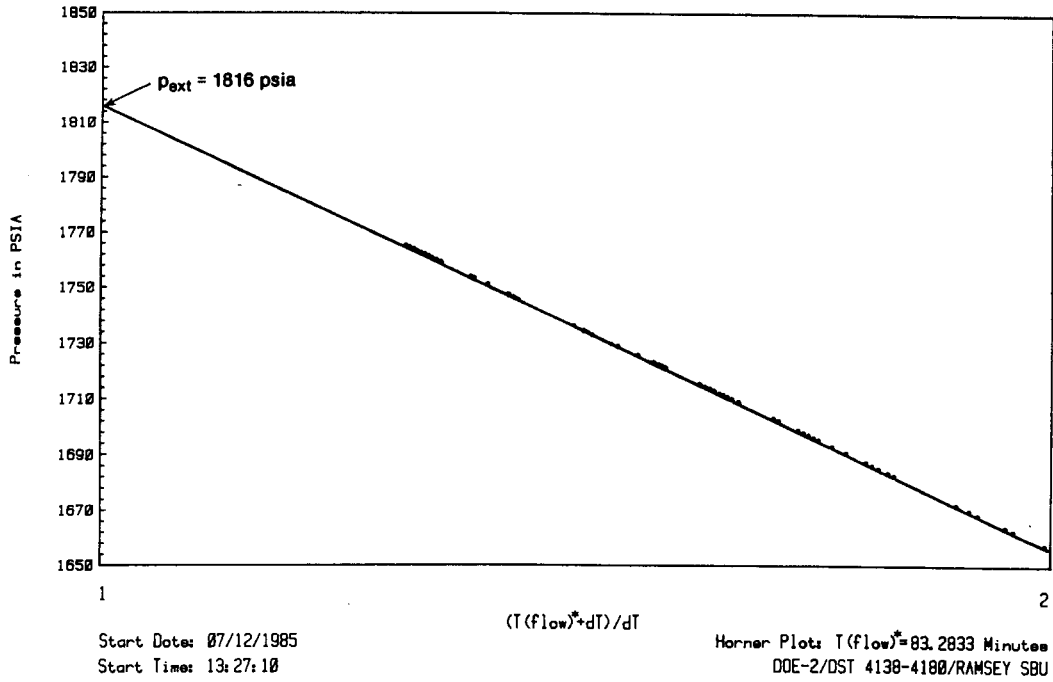
Figure 7-34. Ramsey SBU Horner Plot

In the plot: $p_{ext} = 1816$ psia

X-axis label: $(T(flow)^* + dT)/dT$

Start Date: 07/12/1985
Start Time: 13:27:10

Horner Plot: $T(flow)^* = 83.2833$ Minutes
DOE-2/DST 4138-4180/RAMSEY SBU
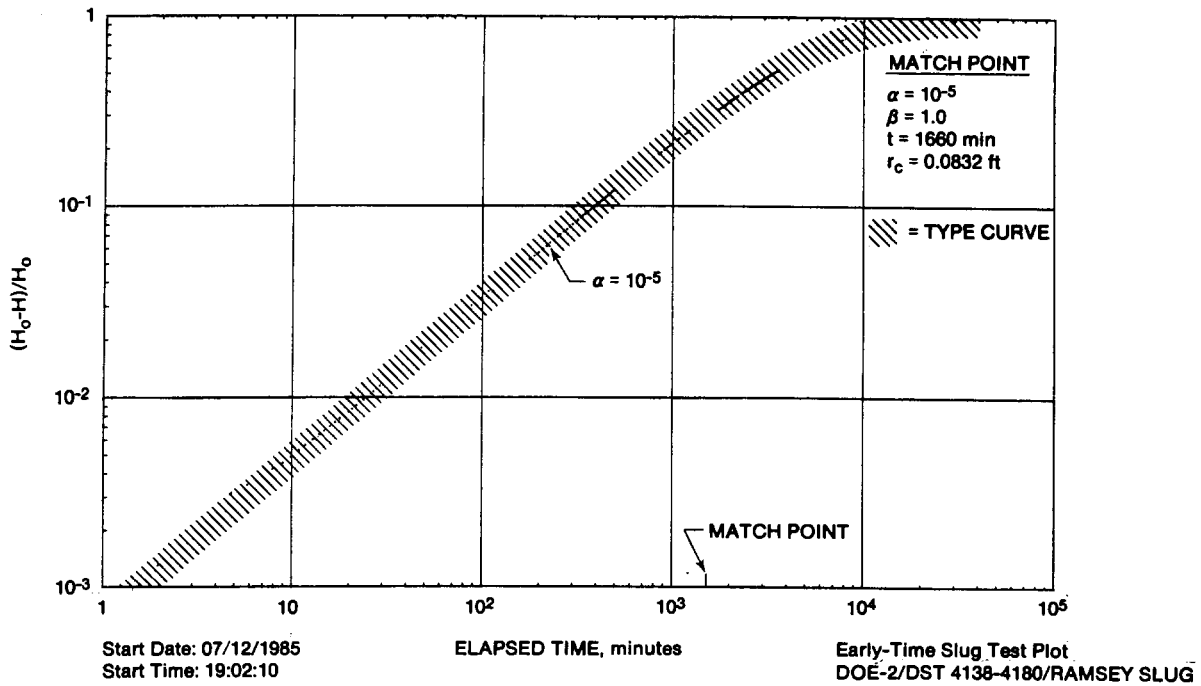
Figure 7-35. Ramsey Slug Test Plot

Y-axis label: $(H_o-H)/H_o$

X-axis label: ELAPSED TIME, minutes

MATCH POINT
$\alpha = 10^{-5}$
$\beta = 1.0$
$t = 1660$ min
$r_c = 0.0832$ ft

= TYPE CURVE

$\alpha = 10^{-5}$

MATCH POINT

Start Date: 07/12/1985
Start Time: 19:02:10

Early-Time Slug Test Plot
DOE-2/DST 4138-4180/RAMSEY SLUG

Figure 7-36. Olds Test Sequence Plot
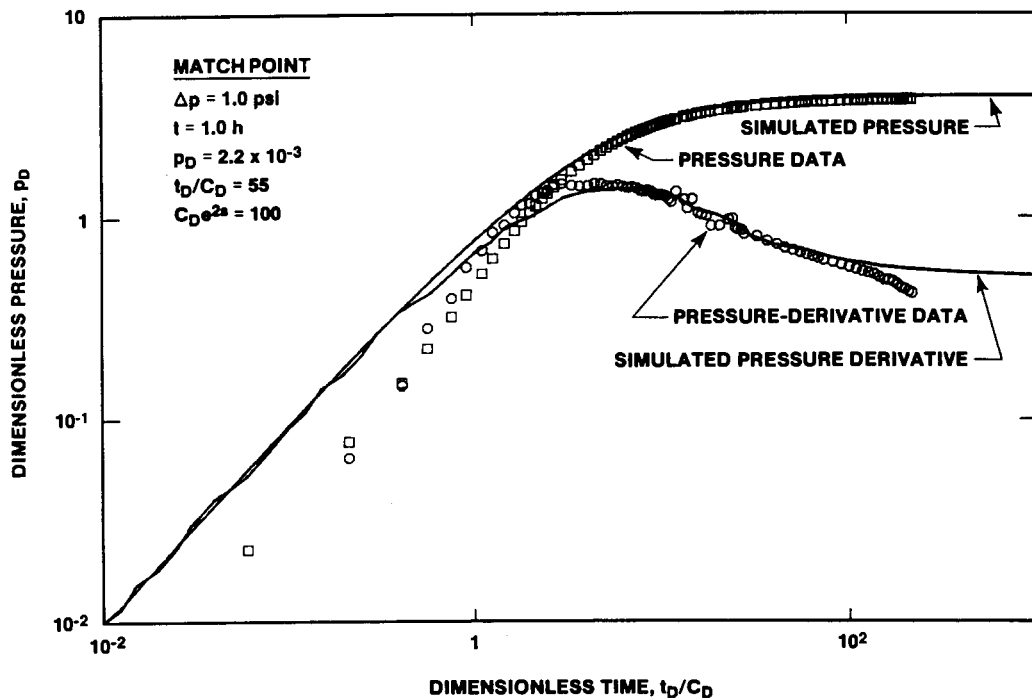
Figure 7-37. Olds FBU Log-Log Plot With INTERPRET Simulation
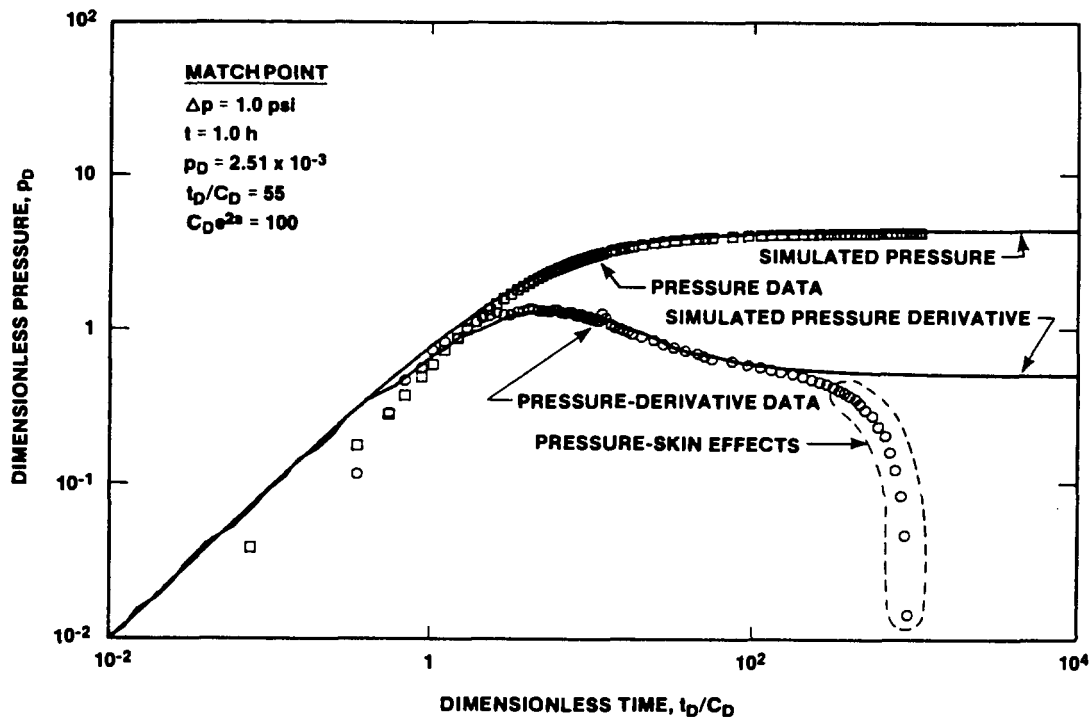
Figure 7-38. Olds SBU Log-Log Plot With INTERPRET Simulation

The log-log plot of the SBU pressure and pressure-derivative data (Figure 7-38), and to a lesser degree the FBU plot (Figure 7-37), show the late-time pressure-derivative data dropping below the simulated curves. The first and second buildups were driven, in part, by the pressure skin that had previously been imparted to the formation. This pressure skin caused the pressures to build to levels above the natural formation pressure. As the pressure skin continued to dissipate, pressures stabilized and, in the case of the SBU, began to drop. Similar pressure-skin effects were not observed during the Ramsey testing, probably because the Ramsey buildup periods were of considerably shorter duration than those of the Olds (See Figures 7-31 and 7-36).

The late-time SBU Horner plot (Figure 7-39) shows the concave-downward curvature and pressure-trend reversal typical of buildups affected by pressure skins. The final pressure, 1843.0 psia (1832.5 psig), is the maximum possible static formation pressure for the Olds sandstone. With the transducer at a depth of 4159.2 ft and a fluid pressure gradient in the borehole from drilling fluid of 0.537 psi/ft (measured SG =

1.24), this pressure corresponds to a formation pressure of 1863.6 psig at the base of the Olds, 4217 ft deep. In an open borehole containing clean Olds fluid (SG = 1.1), 1863.6 psig corresponds to a fluid level ~307 ft below land surface, or at an elevation of 3111 ft above sea level. Again, this represents the maximum possible level for Olds fluid and puts it in the upper Dewey Lake Red Beds, above the estimated Culebra fluid level. Because of the pronounced curvature in the Olds SBU Horner plot (Figure 7-39), this static-fluid-level estimate is probably less accurate than those made for the Ramsey and Hays sandstones.

A log-log plot of the Olds slug test is presented in Figure 7-40. The best-fit type-curve match gives a transmissivity of 7.6×10^{-3} ft^2/day (Table 7-2). When divided by the effective Olds thickness of 30 ft, this value gives a hydraulic conductivity of 2.5×10^{-4} ft/day. Corresponding petroleum units are a permeability-thickness product of 3.3 md-ft and a permeability of 0.11 md. These values are in excellent agreement with the results of the buildup analyses presented above.

66
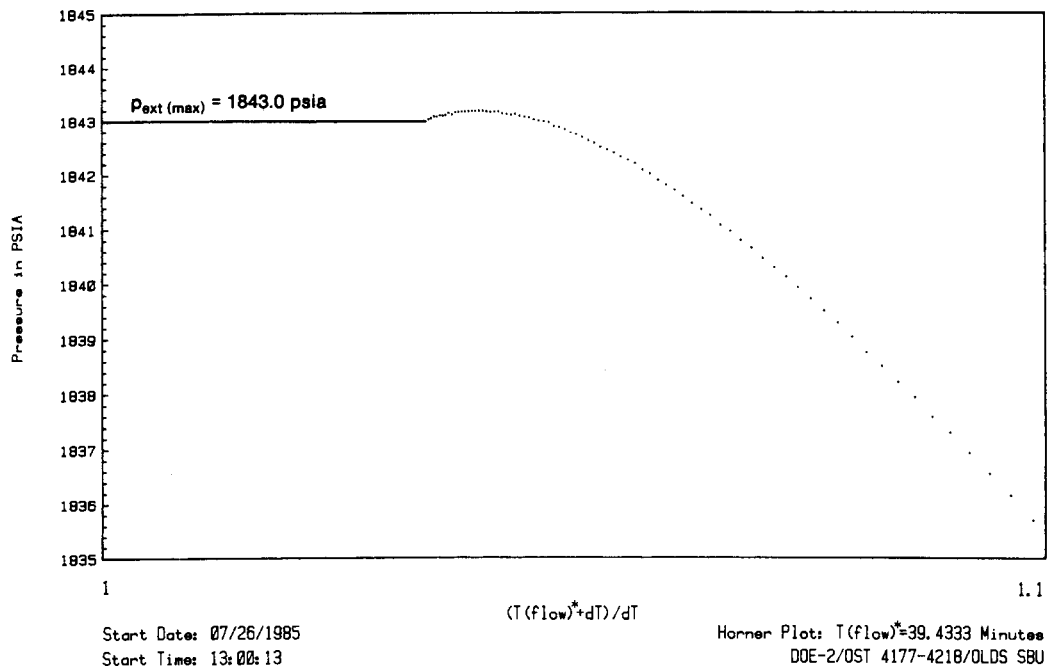
Figure 7-39. Olds SBU Horner Plot
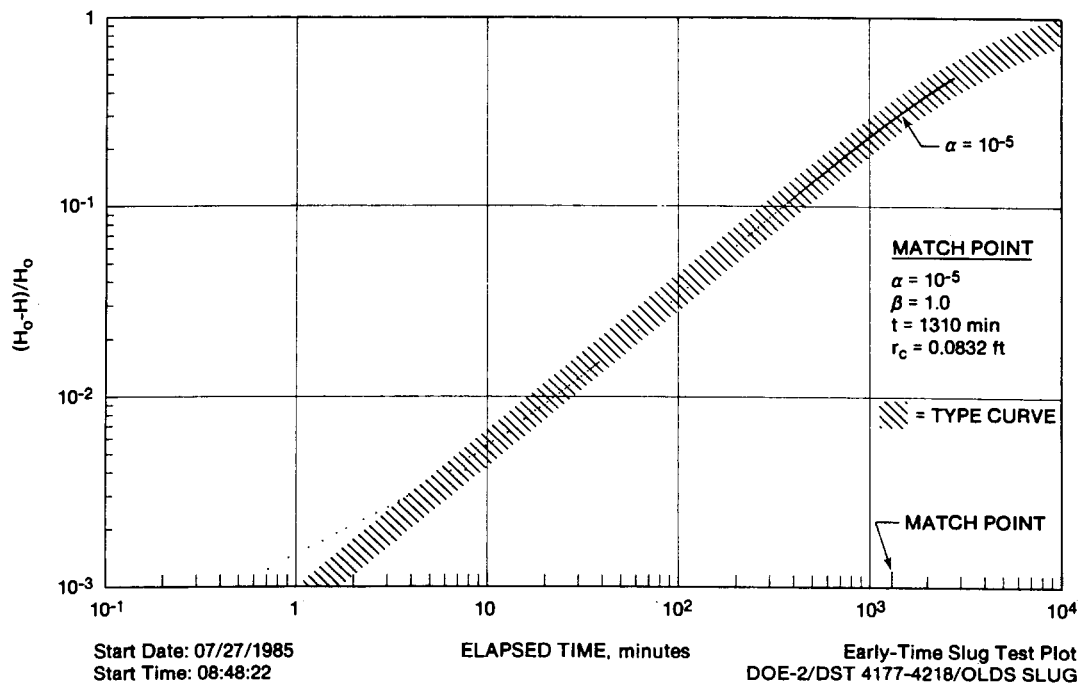
Figure 7-40. Olds Slug Test Plot

7.4.3 Hays Sandstone (DST 4220-4325)

Based on an examination of geophysical logs, the most permeable portion of the Hays sandstone exposed in DOE-2 appears to be the lower 100 ft from 4225 to 4325 ft deep. This zone was tested in a bottom-hole test using a single packer set at 4220 ft, with the bottom of the hole at 4325 ft. Tests were conducted on July 18 and 19, 1985 (Table 7-1), and consisted of two flow periods, two buildup periods, and a slug test (Figure 7-41).

The FBU and SBU were analyzed and simulated using the code INTERPRET. Log-log dimensionless plots of the FBU and SBU pressure data, pressure-derivative data, and simulations are presented in Figures 7-42 and 7-43, respectively. The FBU and SBU analyses yielded permeability-thickness products of 240 and 230 md-ft, respectively (Table 7-2). These values correspond to permeabilities of 2.4 and 2.3 md, respectively, when divided by the "effective" Hays thickness of 100 ft. The corresponding groundwater units are transmissivities of 0.56 and 0.53 ft²/day and hydraulic conductivities of 5.6×10^{-3} and 5.3×10^{-3} ft/day for the FBU and SBU, respectively. Assuming the Hays porosity is 25%, that the fluid viscosity is ~1.5 cp, and that the total system compressibility is

~6×10^{-6} psi^{-1}, the FBU and SBU skin factors are 0.8 and 0.6, respectively. These values indicate a well with very little wellbore damage.

The log-log Hays FBU and SBU plots (Figures 7-42 and 7-43) show the same late-time decline in the pressure derivative as the corresponding Olds plots (Figures 7-37 and 7-38). As was the case with the Olds sandstone tests, the Hays sandstone tests were affected by residual pressure skin. Pressure-skin effects are more pronounced for the Hays FBU than for the SBU because in this instance the FBU lasted considerably longer than the SBU.

On the FBU Horner plot (Figure 7-44), pressure-skin effects are again manifested as a concave-downward curvature of the late-time data. This plot shows only that the static Hays pressure is <1846.8 psia (1836.3 psig). The late-time SBU Horner plot (Figure 7-45) shows a lesser degree of curvature, in part because the test did not last as long as the FBU and perhaps in part because the long FBU served to dissipate a large portion of the pressure skin. The very latest time SBU data extrapolate to a pressure of ~1845.5 psia (1835 psig) at infinite time. This value can be taken as the maximum possible Hays pressure.
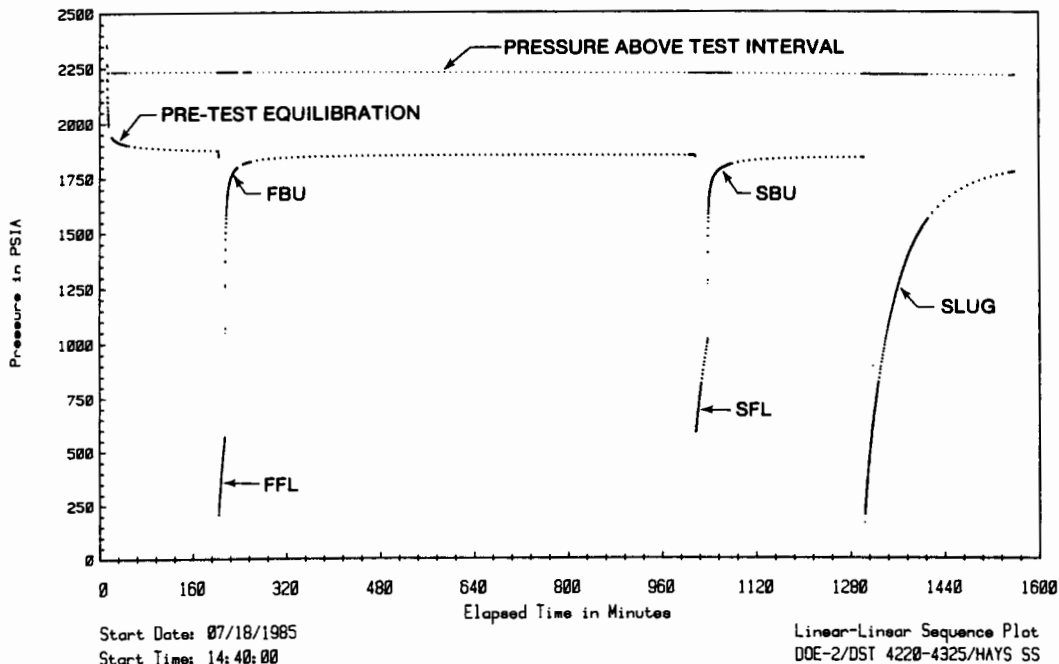
Figure 7-41. Hays Test Sequence Plot
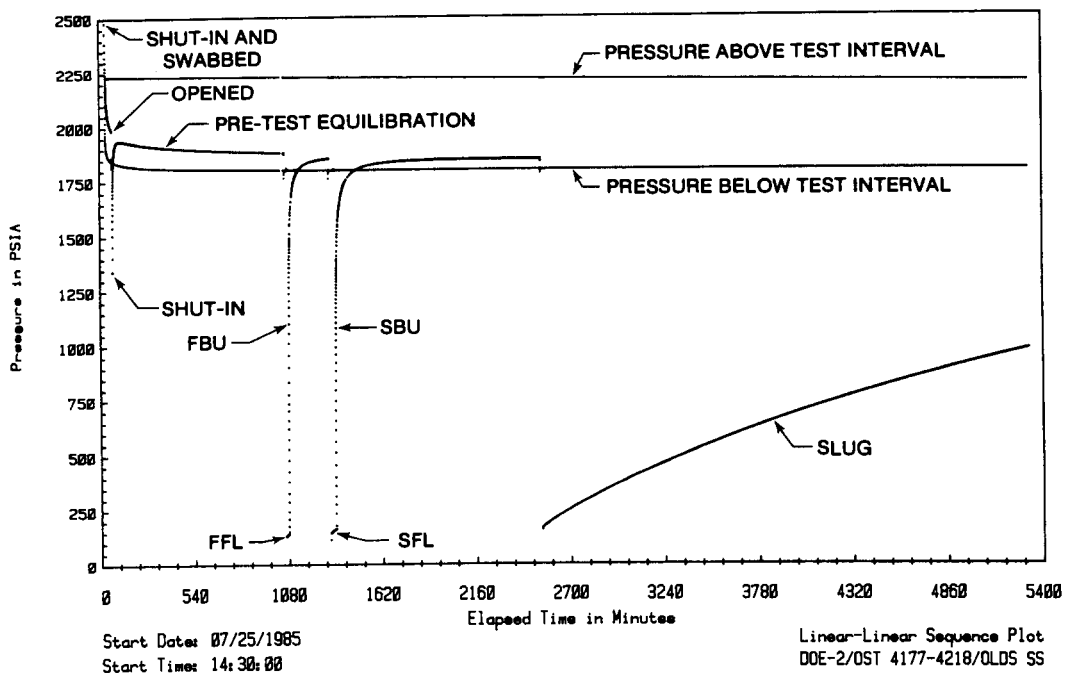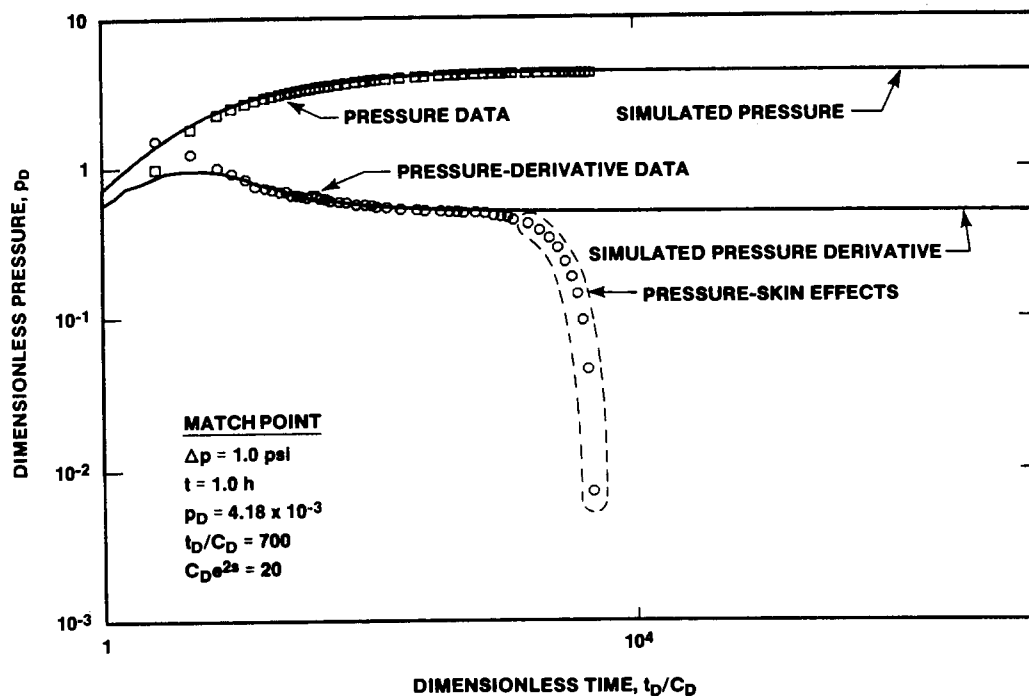
Figure 7-42. Hays FBU Log-Log Plot With INTERPRET Simulation
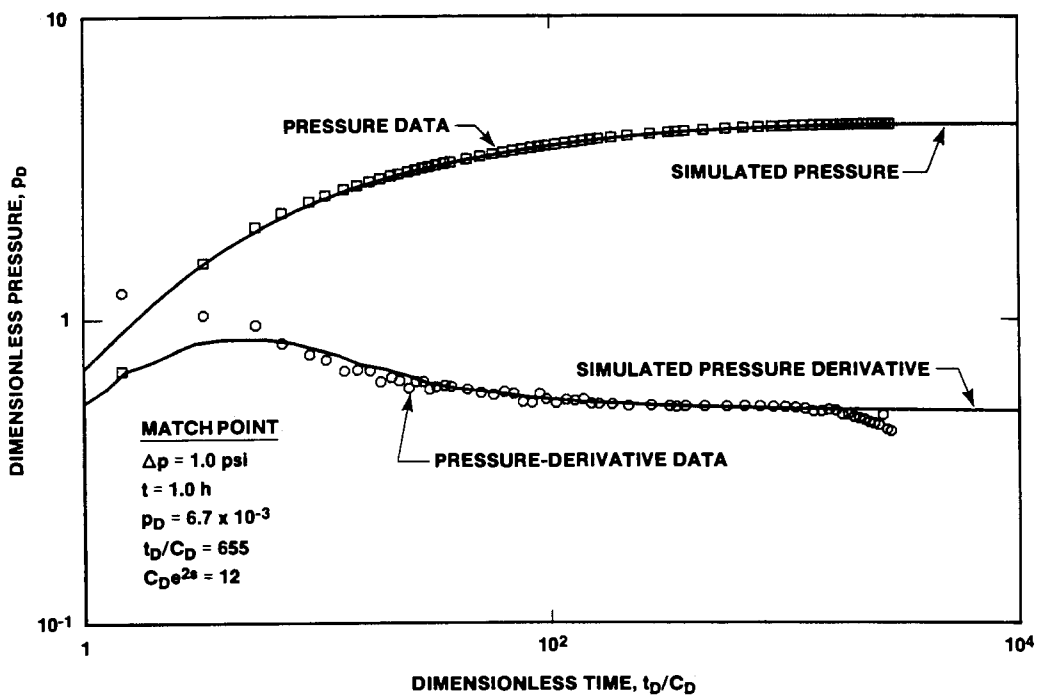
Figure 7-43. Hays SBU Log-Log Plot With INTERPRET Simulation
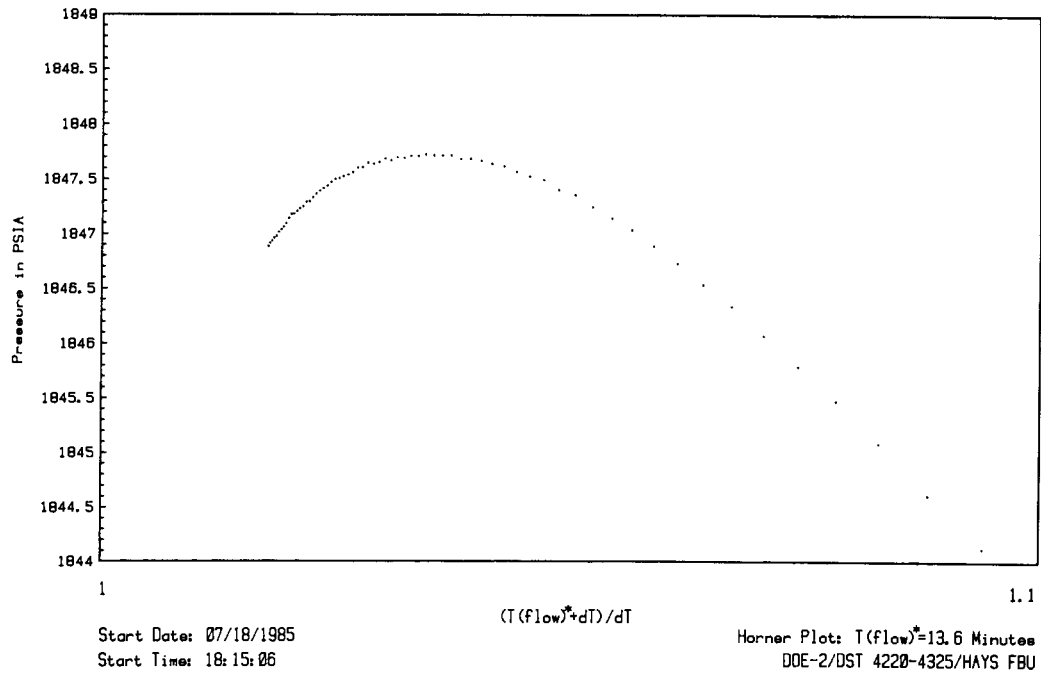
Figure 7-44. Hays FBU Horner Plot
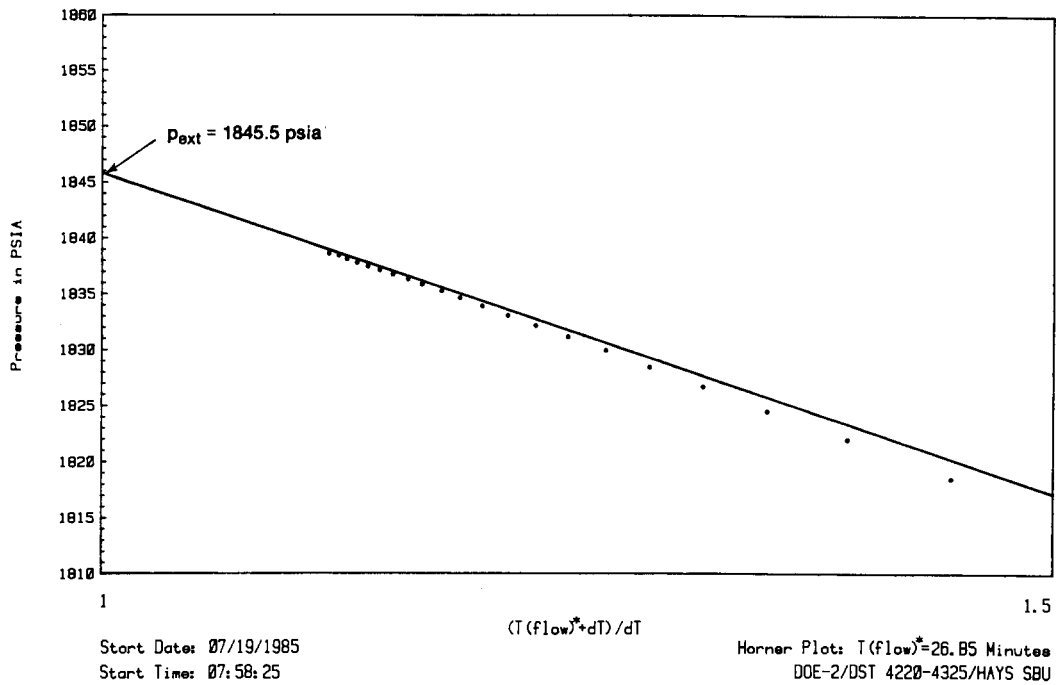
Figure 7-45. Hays SBU Horner Plot

With the transducer at a depth of 4206.3 ft and a fluid pressure gradient in the borehole from drilling fluid of 0.542 psi/ft (measured SG = 1.25), 1835 psig corresponds to a formation pressure of 1899 psig at the base of the Hays, 4325 ft deep. In an open borehole containing clean Hays fluid (SG = 1.1; Mercer et al., 1986), 1899 psig corresponds to a fluid level ~341 ft below land surface, or at an elevation of 3077 ft above sea level. Again, this represents the maximum possible level for Hays fluid and puts it in the upper Dewey Lake Red Beds, above the estimated Culebra fluid level.

A semi-log plot of the Hays slug test is presented in Figure 7-46. The best-fit type-curve match gives a transmissivity of 0.55 ft²/day (Table 7-2). When divided by the effective Hays thickness of 100 ft, this value gives a hydraulic conductivity of 5.5 × 10^{-3} ft/day. Corresponding petroleum units are a permeability-thickness product of 240 md-ft and a permeability of 2.4 md. These values are in excellent agreement with the results of the buildup analyses presented above.

MATCH POINT

$\alpha = 10^{-4.5}$
$\beta = 1.0$
t = 18 min
r_c = 0.0832 ft

/// = TYPE CURVE

$\alpha = 10^{-4.5}$

MATCH POINT
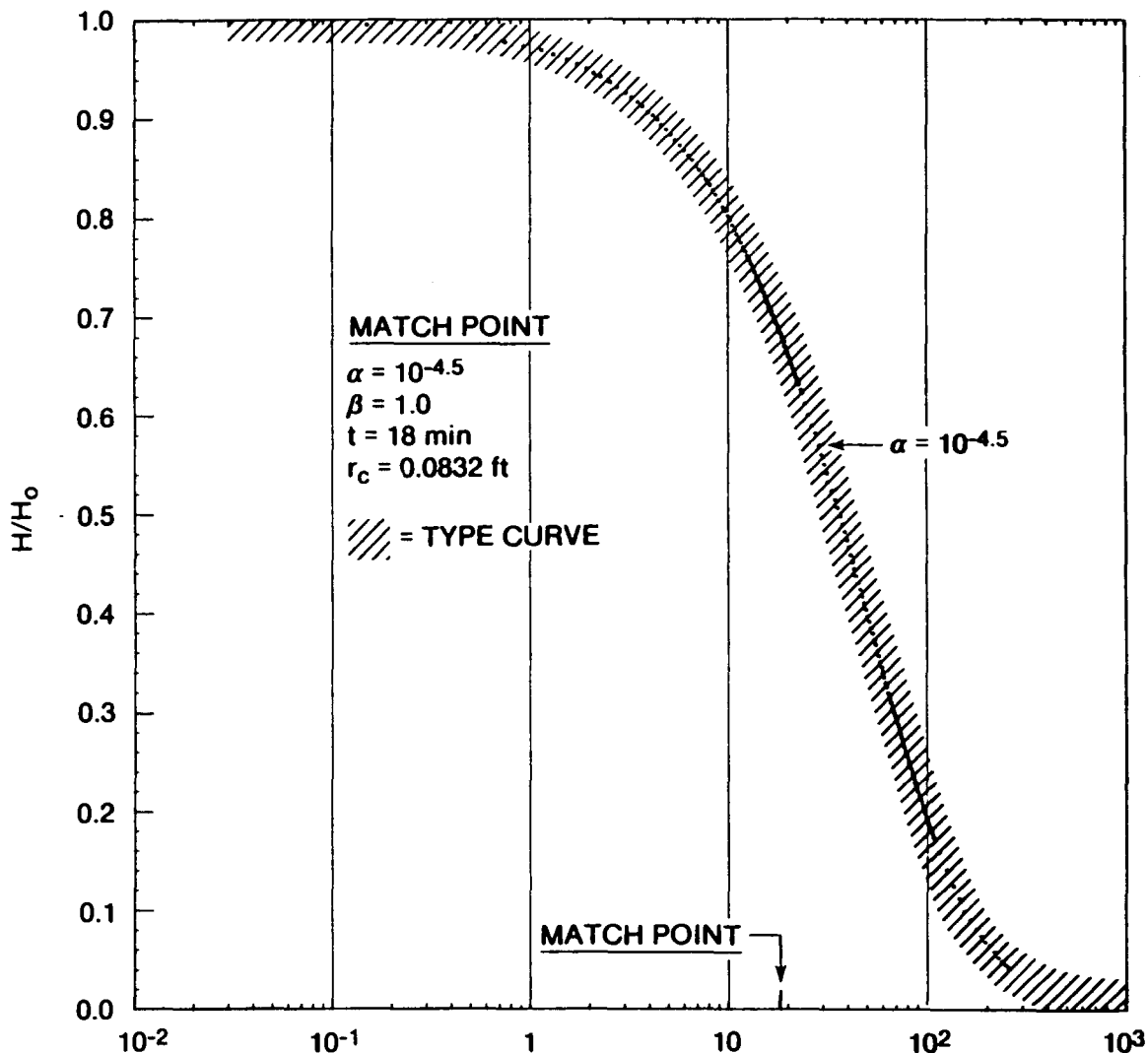
Start Date: 07/19/1985
Start Time: 12:24:30

ELAPSED TIME, minutes

Slug Test Plot
DOE-2/DST 4220-4325/HAYS SLUG

Figure 7-46. Hays Slug Test Plot

7.4.4 Bell Canyon Fluid-Level Measurements

After completion of all Bell Canyon testing in DOE-2, a production-injection packer (PIP) was set near the base of the Castile Formation from 4051.6 to 4057.1 ft deep. The 2.375-in. drill tubing was left attached to the PIP and open to the interval below, forming an observation well completed through the upper Bell Canyon. The Bell Canyon interval was then cleaned by swabbing ~5800 gal of fluid from the tubing. The specific gravity of the fluid removed was monitored during swabbing, and swabbing was terminated when the specific gravity stabilized at 1.1.

Over the subsequent months, the Bell Canyon fluid rose up the tubing as a recovery response to the swabbing. From November 1985 through March 1986, the fluid level in the tubing changed very little, apparently stabilizing ~384 ft below ground surface, at an elevation of ~3034 ft above sea level. This fluid level is 43 to 77 ft below the estimated static fluid levels for the Bell Canyon sandstones. The discrepancy between measured and estimated values is probably due to slight inaccuracies in the specific gravities used in estimating the fluid levels, and possibly to some residual drilling fluid contamination in the borehole.

The observed Bell Canyon fluid level at a depth of 384 ft is ~20 ft lower than the observed Culebra fluid level at DOE-2. Because of the higher specific gravity of the Bell Canyon fluid, however, the Bell Canyon *head* at the elevation of the base of the Culebra is slightly higher than that of the Culebra. This indicates that, in the event of an interconnection between the Bell Canyon and the Culebra, the undisturbed head gradient would drive fluid upward from the Bell Canyon into the Culebra.

If the interconnection were through an uncased borehole, however, salt dissolution in the Salado section would increase the specific gravity of the Bell Canyon fluid so that, *at the elevation of the Culebra*, the Culebra head would be higher than that of the Bell Canyon. In this event, the flow direction would be downward. The long-term flow rate would be governed by a combination of factors, including the transmissivity and storativity of both the Culebra and Bell Canyon and the rate of halite dissolution.

8. Summary and Conclusions

Eleven different zones were tested in Well DOE-2 in five phases of testing between 1984 and 1986. Testing techniques included a constant-head, borehole-infiltration test, drill-stem tests, slug tests, pressure-pulse tests, and multiwell pumping tests. Four of the zones tested—the lower Dewey Lake Red Beds, the Tamarisk Member of the Rustler Formation, the lower unnamed member of the Rustler Formation and Rustler/Salado contact, and the entire Salado Formation—had permeabilities too low to quantify with the equipment and test techniques used. The other zones had permeabilities ranging over six orders of magnitude. No saturated strata were encountered above the Rustler Formation, although parts of the middle Dewey Lake Red Beds appear to have appreciable permeability.

In the Rustler Formation, the Culebra Dolomite Member is the most permeable unit, with a transmissivity of ~90 ft^2/day. The Culebra behaves hydraulically as a double-porosity system, with the major permeability provided by fractures and the major storage provided by matrix porosity. The Culebra at DOE-2 is well-connected hydraulically to the Culebra at Wells H-6b and WIPP-13 to the west, probably by interconnected fractures. Response times between these wells are very short (<1 day/10,000 ft). The Culebra does not appear to be as fractured to the south at Wells WIPP-12 and 18 or to the east at Well H-5b, as indicated by delayed, low-magnitude (or nonexistent) responses to DOE-2 pumping and by low permeabilities interpreted from other tests conducted at those wells. The other Rustler members at DOE-2, which are not known to be fractured and do not display hydraulic responses typical of fractured (or double-porosity) media, have permeabilities three to four orders of magnitude lower than that of the Culebra. Hydraulic heads decrease through the Rustler with increasing depth. This implies that the Tamarisk, and indirectly the Magenta and Forty-niner, could act as a source of recharge for the Culebra.

In the Salado Formation, the interval including Marker Beds 138 and 139 and the WIPP facility horizon has a very low average permeability (<0.3 μd), and showed no evidence over ~2 days of testing of containing high-pressure sources of either brine or gas.

In the Bell Canyon Formation, the Hays sandstone was the most permeable unit tested, with an average permeability of ~2.4 md (0.55 ft/day). The Olds and Ramsey sandstones, overlying the Hays, have permeabilities almost two orders of magnitude lower. Hydraulic heads in the Bell Canyon sandstones could not be quantified precisely enough to define vertical gradients within the Bell Canyon.

In freshwater terms, the observed Bell Canyon head is higher than the hydraulic head of the Culebra dolomite. If the Bell Canyon and Culebra were connected by an open borehole, however, salt dissolution in the Salado section would increase the specific gravity of the Bell Canyon fluid so that, *at the elevation of the Culebra*, the Culebra head would be higher than that of the Bell Canyon. In this event, the flow direction would be downward from the Culebra into the Bell Canyon.

References

Basler, J. A. 1983. *Instrumentation Used for Hydraulic Testing of Potential Water-Bearing Formations at the Waste Isolation Pilot Plant Site in Southeastern New Mexico.* USGS Open-File Report 83-144 (Washington, DC: US GPO), 29 pp.

Beauheim, R. L. *Analysis of Pumping Tests of the Culebra Dolomite Conducted at the H-3 Hydropad at the Waste Isolation Pilot Plant (WIPP) Site.* SAND86-2311 (Albuquerque, NM: Sandia National Laboratories, to be published).

Beauheim, R. L.; Hassinger, B. W.; and Klaiber, J. A. 1983. *Basic Data Report for Borehole Cabin Baby-1 Deepening and Hydrologic Testing.* WTSD-TME-020 (Albuquerque, NM: US DOE).

Bourdet, D., and Gringarten, A. C. 1980. *Determination of Fissure Volume and Block Size in Fractured Reservoirs by Type-Curve Analysis.* SPE 9293 (Richardson, TX: Soc Pet Eng).

Bourdet, D.; Ayoub, J. A.; and Pirard, Y. M. 1984. *Use of Pressure Derivative in Well Test Interpretation.* SPE 12777 (Richardson, TX: Soc Pet Eng).

Bredehoeft, J. D., and Papadopulos, S. S. 1980. "A Method for Determining the Hydraulic Properties of Tight Formations," *Water Resources Research* 16(1):233-38.

Cinco-Ley, H.; Samaniego-V., F.; and Kucuk, F. 1985. *The Pressure Transient Behavior for Naturally Fractured Reservoirs with Multiple Block Size.* SPE 14168 (Richardson, TX: Soc Pet Eng).

Cooper, H. H.; Bredehoeft, J. D.; and Papadopulos, I. S. 1967. "Response of a Finite-Diameter Well to an Instantaneous Charge of Water," *Water Resources Research* 3(1):263-69.

Deruyck, B. G.; Bourdet, D. P.; DaPrat, G.; and Ramey, H. J., Jr. 1982. *Interpretation of Interference Tests in Reservoirs with Double Porosity Behavior—Theory and Field Examples.* SPE 11025 (Richardson, TX: Soc Pet Eng).

de Swaan, A. O. 1976. "Analytical Solutions for Determining Naturally Fractured Reservoir Properties by Well Testing," *Soc Pet Eng J* (June 1976):117-22.

Ehlig-Economides, C. A. 1979. "Well Test Analysis for Wells Produced at a Constant Pressure," PhD Dissertation (Palo Alto, CA: Stanford Univ Dept of Pet Eng), 117 pp.

Freeze, R. A., and Cherry, J. A. 1979. *Groundwater* (Englewood Cliffs, NJ: Prentice-Hall, Inc), 604 pp.

Glover, R. E. 1953. "Flow From a Test-Hole Located Above Groundwater Level," in *Theory and Problems of Water Percolation.* US Bur Rec Eng Mono No. 8 (Washington, DC: US GPO), pp 69-71.

Gonzalez, D. D. 1983. *Groundwater Flow in the Rustler Formation, Waste Isolation Pilot Plant (WIPP), Southeast New Mexico (SENM), Interim Report.* SAND82-1012 (Albuquerque, NM: Sandia National Laboratories), 39 pp.

Gringarten, A. C. 1984. "Interpretation of Tests in Fissured and Multilayered Reservoirs with Double-Porosity Behavior: Theory and Practice," *J Pet Tech* 36(4):549-64.

Gringarten, A. C. 1986. *Computer-Aided Well Test Analysis.* SPE 14099 (Richardson, TX: Soc Pet Eng).

Gringarten, A. C.; Ramey, H. J., Jr.; and Raghavan, R. 1974. "Unsteady-State Pressure Distributions Created by a Well with a Single Infinite-Conductivity Vertical Fracture," *Soc Pet Eng J* 14(4):347-60.

Gringarten, A. C.; Bourdet, D. P.; Landel, P. A.; and Kniazeff, V. J. 1979. *A Comparison Between Different Skin and Wellbore Storage Type Curves for Early-Time Transient Analysis.* SPE 8205 (Richardson, TX: Soc Pet Eng).

Grisak, G. E.; Pickens, J. F.; Avis, J. D.; Belanger, D. W.; Thury, M.; and Schneider, A. 1985. "Principles of Hydrogeologic Investigations at Depth in Crystalline Rock," *Proc Int Assn of Hydrogeologists Memoires* 17(1):52-71 (Tucson, AZ, January 7-12, 1985).

Horner, D. R. 1951. "Pressure Buildup in Wells," *Proc Third World Pet Cong* 2:503-23 (The Hague, Netherlands). Reprinted 1967. "Pressure Analysis Methods," *AIME Reprint Series* 9:45-50 (Richardson, TX: Soc Pet Eng).

INTERA Technologies. 1986. *WIPP Hydrology Program, Waste Isolation Pilot Plant, Southeastern New Mexico, Hydrologic Data Report #3.* SAND86-7109 (Albuquerque, NM: Sandia National Laboratories).

INTERA Technologies and HydroGeoChem. 1985. *WIPP Hydrology Program, Waste Isolation Pilot Plant, Southeastern New Mexico, Hydrologic Data Report #2.* SAND85-7263 (Albuquerque, NM: Sandia National Laboratories).

Jones, C. L.; Bowles, C. G.; and Bell, K. G. 1960. *Experimental Drill Hole Logging in Potash Deposits of the Carlsbad District, New Mexico*. USGS Open-File Report 502 (Washington, DC: US GPO), 25 pp.

Kazemi, H. 1969. "Pressure Transient Analysis of Naturally Fractured Reservoirs with Uniform Fracture Distribution," *Soc Pet Eng J* (Dec 1969):451-62.

Lohman, S. W. 1979. *Ground-Water Hydraulics*. USGS Prof Paper 708 (Washington, DC: US GPO), 70 pp.

Mavor, M. J., and Cinco-Ley, H. 1979. *Transient Pressure Behavior of Naturally Fractured Reservoirs*. SPE 7977 (Richardson, TX: Soc Pet Eng).

Mercer, J. W. 1983. *Geohydrology of the Proposed Waste Isolation Pilot Plant Site, Los Medanos Area, Southeastern New Mexico*. USGS Water-Resources Investigations Rpt 83-4016 (Albuquerque, NM), 113 pp.

Mercer, J. W. 1986. *Compilation of Hydrologic Data From Drilling the Salado and Castile Formations Near the WIPP Site, Southeastern New Mexico*. SAND86-0954 (Albuquerque, NM: Sandia National Laboratories).

Mercer, J. W.; Beauheim, R. L.; Snyder, R. P.; and Fairer, G. M. 1986. *Basic Data Report for Drillhole DOE-2 Drilling and Hydrologic Testing (Waste Isolation Pilot Plant)*. SAND86-0611 (Albuquerque, NM: Sandia National Laboratories).

Moench, A. F. 1984. "Double-Porosity Models for a Fissured Groundwater Reservoir with Fracture Skin," *Water Resources Research* 20(7):831-46.

Narasimhan, T. N., and Kanehiro, B. Y. 1980. "A Note on the Meaning of Storage Coefficient," *Water Resources Research* 16(2):423-29.

Ramey, H. J., Jr. 1980. "A Drawdown and Build-up Type Curve for Interference Testing," *Proc Third Invitational Well-Testing Symp*. LBL-12076 (Berkeley, CA, Mar 26-28, 1980), pp 130-34.

Ramey, H. J., Jr.; Agarwal, R. G.; and Martin, I. 1975. "Analysis of 'Slug Test' or DST Flow Period Data," *J Can Pet Tech* 14(3):37-47.

Snyder, R. P. 1985. *Dissolution of Halite and Gypsum, and Hydration of Anhydrite to Gypsum, Rustler Formation, in the Vicinity of the Waste Isolation Pilot Plant, Southeastern New Mexico*. USGS Open-File Report 85-229 (Washington, DC: US GPO), 11 pp.

Stephens, D. B., and Neuman, S. P. 1980. *Analysis of Borehole Infiltration Tests Above the Water Table*. Reports on Natural Resources Systems, No. 35 (Tucson, AZ: U of Arizona), 211 pp.

Theis, C. V. 1935. "The Relation Between the Lowering of the Piezometric Surface and the Rate and Duration of Discharge of a Well Using Groundwater Storage," *Trans AGU* 2:519-24.

US Bureau of Reclamation. 1974. *Earth Manual*, 2nd ed (Washington, DC: US GPO).

US Bureau of Reclamation. 1977. *Ground Water Manual* (Washington, DC: US GPO).

US Department of Energy. 1983. *Quarterly Geotechnical Field Data Report, October 1983*. WIPP-DOE-177 (Albuquerque, NM: WIPP Project Office).

Warren, J. E., and Root, P. J. 1963. "The Behavior of Naturally Fractured Reservoirs," *Soc Pet Eng J* (Sept 1963):245-55.

Westinghouse Electric Corporation. 1985. *Ecological Monitoring Program Semiannual Report, January-June, 1985*. DOE/WIPP-85-002 (Carlsbad, NM: Waste Isolation Pilot Plant).

APPENDIX A

Pressure and Water-Level Data From 1986 DOE-2 Culebra Pumping Test

Table A-1. DOE-2 Pressures During 1986 DOE-2 Culebra Pumping Test

Day	Hr	Min	S	Elapsed Time (Hr)	Pressure (Psig)	Comments
178	16	10	0	-64.83333	151.66	
178	21	10	0	-59.83333	151.60	
179	2	10	0	-54.83333	151.58	
179	7	10	0	-49.83333	151.57	
179	12	0	0	-45.00000	151.41	
179	17	30	0	-39.50000	151.81	
179	22	30	0	-34.50000	151.87	
180	3	30	0	-29.50000	151.88	
180	8	30	0	-24.50000	151.86	
180	13	0	0	-20.00000	151.88	
180	18	0	0	-15.00000	151.79	
180	23	0	0	-10.00000	151.85	
181	4	0	0	-5.00000	151.89	
181	8	59	54	-0.00167	151.87	
181	9	0	0	0.00000	148.96	PUMP ON
181	9	0	6	0.00167	146.67	
181	9	0	12	0.00333	145.43	
181	9	0	18	0.00500	144.50	
181	9	0	24	0.00667	143.79	
181	9	0	30	0.00833	143.18	
181	9	0	36	0.01000	142.68	
181	9	0	42	0.01167	142.19	
181	9	0	48	0.01333	141.84	
181	9	0	54	0.01500	141.48	
181	9	1	0	0.01667	141.19	
181	9	1	12	0.02000	140.60	
181	9	1	24	0.02333	140.13	
181	9	1	36	0.02667	139.76	
181	9	1	48	0.03000	139.37	
181	9	2	0	0.03333	139.01	
181	9	3	0	0.05000	137.78	
181	9	3	30	0.05833	137.34	
181	9	4	0	0.06667	136.92	
181	9	4	30	0.07500	136.56	
181	9	5	0	0.08333	136.25	
181	9	5	30	0.09167	136.01	
181	9	6	0	0.10000	135.74	
181	9	7	0	0.11667	135.30	
181	9	8	0	0.13333	135.02	
181	9	9	0	0.15000	134.74	
181	9	10	0	0.16667	134.46	
181	9	12	0	0.20000	134.03	

(continued)

Table A-1 (continued).

Day	Hr	Min	S	Elapsed Time (Hr)	Pressure (Psig)	Comments
181	9	15	0	0.25000	133.67	
181	9	18	0	0.30000	133.31	
181	9	21	0	0.35000	133.04	
181	9	24	0	0.40000	132.78	
181	9	27	0	0.45000	132.55	
181	9	30	0	0.50000	132.32	
181	9	33	0	0.55000	132.15	
181	9	36	0	0.60000	131.97	
181	9	39	0	0.65000	131.81	
181	9	42	0	0.70000	131.72	
181	9	45	0	0.75000	131.61	
181	9	48	0	0.80000	131.56	
181	9	51	0	0.85000	131.46	
181	9	54	0	0.90000	131.33	
181	9	57	0	0.95000	131.21	
181	10	0	0	1.00000	131.14	
181	10	15	0	1.25000	130.90	
181	10	30	0	1.50000	130.70	
181	10	45	0	1.75000	130.41	
181	11	0	0	2.00000	130.23	
181	11	30	0	2.50000	130.03	
181	12	0	0	3.00000	129.75	
181	12	30	0	3.50000	129.59	
181	13	0	0	4.00000	129.41	
181	13	30	0	4.50000	129.25	
181	14	0	0	5.00000	129.22	
181	15	0	0	6.00000	128.92	
181	16	0	0	7.00000	128.81	
181	17	0	0	8.00000	128.56	
181	18	0	0	9.00000	128.37	
181	19	0	0	10.00000	128.28	
181	20	0	0	11.00000	128.02	
181	21	0	0	12.00000	127.98	
181	22	0	0	13.00000	127.85	
181	23	0	0	14.00000	127.72	
182	0	0	0	15.00000	127.58	
182	5	0	0	20.00000	127.09	
182	10	0	0	25.00000	126.56	
182	15	0	0	30.00000	126.22	
182	20	31	26	35.52389	125.66	
183	1	0	0	40.00000	125.38	
183	6	0	0	45.00000	125.05	

(continued)

77

Table A-1 (continued).

Day	Hr	Min	S	Elapsed Time (Hr)	Pressure (Psig)	Comments
183	11	0	0	50.00000	124.70	
183	16	0	0	55.00000	124.50	
183	21	0	0	60.00000	124.17	
184	2	0	0	65.00000	123.84	
184	7	0	0	70.00000	123.54	
184	12	0	0	75.00000	123.33	
184	17	0	0	80.00000	123.18	
184	22	0	0	85.00000	122.83	
185	3	0	0	90.00000	122.57	
185	8	0	0	95.00000	122.36	
185	12	59	54	99.99833	122.15	
185	13	0	0	100.00000	125.28	PUMP OFF
185	13	0	6	100.00167	127.44	
185	13	0	12	100.00333	128.70	
185	13	0	18	100.00500	129.60	
185	13	0	24	100.00667	130.30	
185	13	0	30	100.00833	130.88	
185	13	0	36	100.01000	131.39	
185	13	0	42	100.01167	131.82	
185	13	0	48	100.01333	132.21	
185	13	0	54	100.01500	132.56	
185	13	1	0	100.01667	132.88	
185	13	1	12	100.02000	133.43	
185	13	1	24	100.02333	133.91	
185	13	1	36	100.02667	134.32	
185	13	1	48	100.03000	134.69	
185	13	3	0	100.05000	136.30	
185	13	3	30	100.05833	136.77	
185	13	4	0	100.06667	137.16	
185	13	4	30	100.07500	137.51	
185	13	5	0	100.08333	137.81	
185	13	5	30	100.09167	138.08	
185	13	6	0	100.10000	138.32	
185	13	7	0	100.11667	138.72	
185	13	8	0	100.13333	139.07	
185	13	9	0	100.15000	139.37	
185	13	10	0	100.16667	139.61	
185	13	12	0	100.20000	140.02	
185	13	15	0	100.25000	140.50	
185	13	18	0	100.30000	140.87	
185	13	21	0	100.35000	141.15	
185	13	24	0	100.40000	141.39	

(continued)

Table A-1 (concluded).

Day	Hr	Min	S	Elapsed Time (Hr)	Pressure (Psig)	Comments
185	13	27	0	100.45000	141.59	
185	13	30	0	100.50000	141.76	
185	13	35	0	100.58333	142.00	
185	13	40	0	100.66667	142.21	
185	13	45	0	100.75000	142.37	
185	13	50	0	100.83333	142.52	
185	13	55	0	100.91667	142.65	
185	14	0	0	101.00000	142.76	
185	14	15	0	101.25000	143.03	
185	14	30	0	101.50000	143.26	
185	15	0	0	102.00000	143.57	
185	16	0	0	103.00000	144.01	
185	17	0	0	104.00000	144.33	
185	18	0	0	105.00000	144.59	
185	19	0	3	106.00083	144.77	
185	20	0	3	107.00083	144.94	
185	21	0	0	108.00000	145.05	
185	22	0	0	109.00000	145.17	
185	23	0	0	110.00000	145.26	
186	0	0	0	111.00000	145.37	
186	1	0	0	112.00000	145.46	
186	2	0	0	113.00000	145.55	
186	3	0	0	114.00000	145.64	
186	4	0	0	115.00000	145.73	
186	9	0	0	120.00000	146.03	
186	14	0	0	125.00000	146.31	
186	19	0	0	130.00000	146.64	
187	0	0	0	135.00000	146.81	
187	5	0	0	140.00000	147.01	
187	10	0	0	145.00000	147.13	
187	15	0	0	150.00000	147.29	
187	20	0	0	155.00000	147.49	
188	1	0	0	160.00000	147.57	
188	6	0	0	165.00000	147.73	
188	11	0	0	170.00000	147.80	
188	16	0	0	175.00000	147.92	
188	21	0	0	180.00000	148.09	
189	2	0	0	185.00000	148.15	
189	7	0	0	190.00000	148.27	
189	12	0	0	195.00000	148.33	
189	17	0	0	200.00000	148.44	
190	3	0	0	210.00000	148.62	
190	13	0	0	220.00000	148.74	
190	23	0	0	230.00000	148.96	
191	9	0	0	240.00000	149.09	
191	19	0	0	250.00000	149.22	
192	5	0	0	260.00000	149.33	
192	13	0	0	268.00000	149.40	
193	1	0	0	280.00000	149.54	

Table A-2. H-6B Water Levels and Pressures During 1986 DOE-2 Culebra Pumping Test

Day	Hr	Min	Elapsed Time (Hr)	Depth to Water (Ft)	Pressure* (Psi)	Comments
181	12	15	3.250	304.36	88.23	PUMP ON AT
181	13	40	4.667	304.26	88.28	DOE-2 09:00
181	15	37	6.617	304.20	88.31	
181	20	35	11.583	304.43	88.20	
181	23	55	14.917	304.29	88.27	
182	3	30	18.500	304.49	88.18	
182	5	20	20.333	304.59	88.13	
182	9	25	24.417	304.82	88.03	
182	12	30	27.500	304.95	87.97	
182	15	20	30.333	304.88	88.00	
183	9	0	48.000	305.97	87.51	
183	14	45	53.750	306.13	87.44	
183	18	55	57.917	306.26	87.38	
183	23	5	62.083	306.69	87.18	
184	8	25	71.417	307.15	86.98	
184	14	32	77.533	307.38	86.87	
184	20	41	83.683	307.61	86.77	
184	23	40	86.667	307.90	86.64	
185	8	50	95.833	308.23	86.49	
185	12	35	99.583	308.33	86.44	
185	15	30	102.500	308.36	86.43	PUMP OFF AT
185	17	10	104.167	308.46	86.38	DOE-2 13:00
185	20	10	107.167	308.66	86.29	
186	10	0	121.000	309.12	86.09	
186	10	55	121.917	309.05	86.12	
188	14	45	173.750	308.79	86.24	
189	8	10	191.167	308.46	86.38	

*Pressure = [500 ft - Depth to water] * 0.451 psi/ft

Table A-3. WIPP-13 Water Levels and Pressures During 1986 DOE-2 Culebra Pumping Test

Day	Hr	Min	Elapsed Time (Hr)	Depth to Water (Ft)	Pressure* (Psi)	Comments
178	16	15	-64.750	351.57	66.94	PUMP ON AT
179	12	40	-44.333	351.60	66.93	DOE-2 09:00
180	15	0	-18.000	351.31	67.06	
181	8	25	-0.583	351.70	66.88	
181	9	50	0.833	351.70	66.88	
181	11	10	2.167	351.73	66.87	
181	12	0	3.000	352.06	66.72	
181	13	10	4.167	352.39	66.57	
181	17	15	8.250	353.57	66.04	
181	21	0	12.000	354.52	65.61	
182	0	10	15.167	355.44	65.20	
182	3	50	18.833	356.43	64.75	
182	5	40	20.667	356.89	64.54	
182	9	10	24.167	357.71	64.17	
182	12	15	27.250	358.26	63.92	
182	15	5	30.083	358.53	63.80	
183	0	30	39.500	360.40	62.96	
183	9	20	48.333	362.10	62.19	
183	15	0	54.000	362.66	61.94	
183	20	15	59.250	363.51	61.56	
183	23	30	62.500	363.78	61.44	
184	8	15	71.250	364.99	60.89	
184	15	45	78.750	365.87	60.49	
184	20	25	83.417	366.30	60.30	
185	0	0	87.000	366.92	60.02	
185	8	35	95.583	367.58	59.72	
185	13	0	100.000	368.11	59.48	PUMP OFF AT
185	13	55	100.917	368.20	59.44	DOE-2 13:00
185	14	55	101.917	368.04	59.51	
185	16	0	103.000	367.84	59.60	
185	16	55	103.917	367.64	59.69	
185	19	12	106.200	367.28	59.86	
185	20	25	107.417	367.15	59.92	
186	10	20	121.333	364.99	60.89	
187	10	30	145.500	362.66	61.94	
188	14	18	173.300	360.88	62.74	
189	11	20	194.333	359.84	63.21	
190	9	40	216.667	358.79	63.69	
191	15	45	246.750	357.77	64.15	
192	12	10	267.167	357.21	64.40	
193	8	45	287.750	356.75	64.61	

*Pressure = [500 ft - Depth to water] * 0.451 psi/ft

Table A-4. WIPP-12 Water Levels During 1986 DOE-2 Culebra Pumping Test

Day	Hr	Min	Depth to Water (Ft)	Comments
143	15	30	33.00	
147	8	25	175.21	
149	10	0	246.02	
151	10	0	292.65	
153	13	20	326.63	
160	14	15	381.10	
177	13	35	408.50	
178	15	10	408.87	
179	13	40	409.25	
181	16	0	409.80	PUMP ON AT DOE-2
182	1	38	409.95	09:00
182	12	38	410.00	
183	20	25	410.31	
184	13	40	410.49	
185	10	40	410.73	PUMP OFF AT
189	10	30	412.10	DOE-2 13:00
190	10	20	413.16	
191	15	55	413.77	
192	11	35	414.14	
193	8	55	414.50	
195	13	15	415.24	
196	10	50	415.45	
198	14	40	415.81	
199	10	50	416.00	
202	13	10	416.20	
209	12	30	416.12	

Table A-5. WIPP-18 Water Levels During 1986 DOE-2 Culebra Pumping Test

Day	Hr	Min	Depth to Water (Ft)	Comments
177	13	50	418.66	
178	15	20	418.96	
179	13	45	418.96	
181	16	10	418.89	PUMP ON AT DOE-2
182	1	55	418.96	09:00
182	13	45	419.02	
183	13	45	418.99	
183	20	35	419.15	
184	13	45	419.15	
185	10	50	419.15	PUMP OFF AT
188	18	8	420.60	DOE-2 13:00
189	10	0	420.83	
190	10	30	420.99	
191	16	5	421.12	
192	11	40	421.06	
193	9	4	421.22	
195	13	40	421.39	
196	10	45	421.58	
198	14	45	421.55	
199	11	0	421.58	
202	13	30	421.45	
207	12	3	421.32	

Table A-6. H-5B Water Levels During 1986 DOE-2 Culebra Pumping Test

Day	Hr	Min	Depth to Water (Ft)	Comments
153	10	55	494.97	
160	12	15	492.45	
167	11	0	491.20	
177	12	35	490.09	
178	16	0	490.15	
179	13	13	490.09	
181	16	45	489.76	PUMP ON AT DOE-2
181	21	25	489.82	09:00
182	14	17	489.79	
183	14	20	489.89	
183	19	20	489.95	
184	15	2	489.82	
185	9	10	489.63	
185	12	15	489.59	PUMP OFF AT DOE-2
188	15	32	489.56	13:00
190	9	55	489.23	
192	12	30	489.06	
195	10	55	488.90	
202	11	25	488.94	
209	10	35	488.77	

DISTRIBUTION:

US Department of Energy (5)
Office of Civilian Radioactive Waste Management
Office of Geologic Repositories
Attn: Associate Director
      W. J. Purcell, RW-20
      Director, Repository Coordination Div.
      T. H. Isaacs, RW-22
      Director, Engineering & Licensing
      R. Stein, RW-23
      Director, Geosciences & Technology
      R. Stein, Actg., RW-24
      Director, Siting Division
      E. Burton, RW-25
Forrestal Building
Washington, DC 20585

US Department of Energy (3)
Albuquerque Operations
Attn: R. G. Romatowski
      D. L. Krenz
      D. G. Jackson, Director, Public Affairs Division
PO Box 5400
Albuquerque, NM 87185

US Department of Energy (6)
Attn: W. R. Cooper,
      WIPP Project Office (Carlsbad) (2)
      J. Tillman
      A. Hunt, WPO (Carlsbad)
      R. Crawley, WPO (Carlsbad) (2)
PO Box 3090
Carlsbad, NM 88221

US Department of Energy, SRPO (3)
Office of Nuclear Waste Isolation
Attn: J. O. Neff
      R. Wunderlich
      G. Appel
505 King Avenue
Columbus, OH 43201

US Department of Energy (2)
Idaho Operations Office
Nuclear Fuel Cycle Division
Attn: R. M. Nelson
      J. Whitsett
550 Second Street
Idaho Falls, ID 83401

US Department of Energy (2)
Savannah River Operations Office
Waste Management Project Office
Attn: S. Cowan
      W. J. Brumley
PO Box A
Aiken, SC 29801

US Department of Energy (3)
Office of Defense Waste and
  Transportation Management
Attn: J. E. Dieckhoner, DP-122
      L. H. Harmon, DP-121
      A. Follett, DP-121
Washington, DC 20545

US Department of Energy
Research & Technical Support Division
Attn: D. E. Large
PO Box E
Oak Ridge, TN 37830

US Department of the Interior
Attn: E. Roedder
959 National Center
Geological Survey
Reston, VA 22092

US Nuclear Regulatory Commission (2)
Division of Waste Management
Attn: M. Bell
      H. Miller
Mail Stop 623SS
Washington, DC 20555

US Geological Survey
Special Projects
Attn: R. Snyder
MS954, Box 25046
Denver Federal Center
Denver, CO 80255

US Geological Survey
Conservation Division
Attn: W. Melton
PO Box 1857
Roswell, NM 88201

DISTRIBUTION (continued):

US Geological Survey (2)
Water Resources Division
Attn: H. L. Case
        P. Davies
Western Bank Bldg.
505 Marquette NW, #720
Albuquerque, NM 87102

State of New Mexico (3)
Environmental Evaluation Group
Attn: R. H. Neill, Director
320 Marcy Street
PO Box 968
Santa Fe, NM 87503

NM Department of Energy & Minerals
Attn: K. LaPlante, Librarian
PO Box 2770
Santa Fe, NM 87501

New Mexico Bureau of Mines and Mineral
    Resources (2)
Attn: F. E. Kottolowski, Director
        J. Hawley
Socorro, NM 87801

Battelle Pacific Northwest Laboratories
Attn: D. J. Bradley
Battelle Boulevard
Richland, WA 99352

Battelle Memorial Institute (9)
Project Management Division
Attn: W. Carbiener, General Manager (3)
        J. Treadwell
        T. Naymik
        J. Kirchner
        L. Page
        O. Swanson
        ONWI Library
505 King Avenue
Columbus, OH 43201

Bechtel Inc. (2)
Attn: E. Weber
        M. Bethard
PO Box 3965
45-11-B34
San Francisco, CA 94119

IT Corporation (2)
Attn: W. E. Coons
        J. E. Zurkoff
2340 Alamo, SE
Suite 306
Albuquerque, NM 87106

IT Corporation (4)
Attn: W. Patrick
        R. McKinney
        D. Deal
        D. Winstanley
PO Box 2078
Carlsbad, NM 88221

INTERA Technologies, Inc. (3)
Attn: G. E. Grisak
        J. F. Pickens
        G. J. Saulnier
6850 Austin Center Blvd., #300
Austin, TX 78731

INTERA Technologies, Inc.
Attn: W. Stensrud
PO Box 2123
Carlsbad, NM 88221

Martin Marietta Energy Systems, Inc.
Oak Ridge National Laboratory
Attn: J. A. Carter
Box Y
Oak Ridge, TN 37830

Martin Marietta Energy Systems, Inc.
Oak Ridge National Laboratory
Environmental Science
Attn: E. Bondietti
X10 Area, Bldg. 1505, Rm. 322
Oak Ridge, TN 37831

RE/SPEC Inc.
Attn: P. Gnirk
PO 725
Rapid City, SD 57701

RE/SPEC Inc.
Attn: S. W. Key
PO Box 14984
Albuquerque, NM 87191

DISTRIBUTION (continued):

Rockwell International
Atomics International Division
Rockwell Hanford Operations
Attn: W. W. Schultz
PO Box 800
Richland, WA 99352

Serata Geomechanics
Attn: S. Serata
4124 Lakeside Drive
Richmond, CA 94806-1941

G. O. Bachman
Star Route Box 1028
Corrales, NM 87048

Leonard Minerals Co.
Attn: B. Donegan
3202 Candelaria NE
Albuquerque, NM 87107

Peters Technology Transfer
Attn: L. Lantz
PO Box 216
Swarthmore, PA 19081

Stanford University
Department of Geology
Attn: K. B. Krauskopf
Stanford, CA 94305

Vanderbilt University
Department of Environmental and
   Water Resources Engineering
Attn: F. L. Parker
Nashville, TN 37235

Oak Ridge National Laboratory
Attn: J. O. Blomeke
PO Box X
Oak Ridge, TN 37830

US Geological Survey
Water Resources Division
Attn: J. D. Bredehoeft
Western Region Hydrologist
345 Middlefield Road
Menlo Park, CA 94025

K. P. Cohen
928 N. California Avenue
Palo Alto, CA 94303

F. M. Ernsberger
1325 NW 10th Avenue
Gainesville, FL 32601

Johns Hopkins University
Department of Earth Sciences
Attn: H. P. Eugster
Baltimore, MD 21218

University of New Mexico
Department of Geology
Attn: R. C. Ewing
Albuquerque, NM 87131

University of Minnesota
Department of Geological Sciences
Attn: C. Fairhurst
Minneapolis, MN 55455

University of Texas at Austin
Department of Geological Sciences
Attn: W. R. Muehlberger
Austin, TX 78712

D. A. Shock
233 Virginia
Ponca City, OK 74601

National Academy of Sciences
Committee on Radioactive Waste Management
Attn: P. Meyers
2101 Constitution Avenue, NW
Washington, DC 20418

New Mexico Junior College
Pannell Library
Attn: R. Hill
Lovington Highway
Hobbs, NM 88240

New Mexico Tech
Martin Speere Memorial Library
Campus Street
Socorro, NM 87810

New Mexico Tech (2)
Department of Geoscience
Attn: J. Wilson
       D. Stephens
Socorro, NM 87801

DISTRIBUTION (continued):

New Mexico State Library
Attn: I. Vollenhofer
PO Box 1629
Santa Fe, NM 87503

US Geological Survey
Water Resources Division
Attn: P. Hsieh
345 Middlefield Rd.
Menlo Park, CA 94025

University of New Mexico
Zimmerman Library
Attn: Z. Vivian
Albuquerque, NM 87131

Atomic Museum
WIPP Public Reading Room
Attn: G. Schreiner
Kirtland East AFB
Albuquerque, NM 87185

Carlsbad Municipal Library
WIPP Public Reading Room
Attn: L. Hubbard, Head Librarian
101 S. Hallagueno St.
Carlsbad, NM 88220

Thomas Brannigan Library
Attn: D. Dresp, Head Librarian
106 W. Hadley St.
Las Cruces, NM, 88001

Roswell Public Library
Attn: N. Langston
301 N. Pennsylvania Avenue
Roswell, NM 88201

University of Minnesota
Dept. of Energy and Materials Science
Attn: R. Oriani
151 Amundson Hall
421 Washington Ave SE
Minneapolis, MN 55455

Texas A&M University
Center of Tectonophysics
Attn: J. Handin
College Station, TX 77840

University of Arizona (2)
Department of Nuclear Engineering
Attn: J. G. McCray
J. J. K. Daemen
Tucson, AZ 85721

University of Arizona
Department of Hydrology
Attn: S. P. Neuman
Tucson, AZ 85721

University of New Mexico (2)
Geology Department
Attn: D. G. Brookins
Library
Albuquerque, NM 87131

University of Texas at El Paso
Department of Geological Sciences
Attn: D. W. Powers
El Paso, TX 79968

Princeton University
Department of Civil Engineering
Attn: G. Pinder
Princeton, NJ 08504

Scientific Software-Intercomp
Attn: A. C. Gringarten
1801 California, 3rd Floor
Denver, CO 80202

University of California (2)
Lawrence W. Berkeley Laboratory
Attn: J. Long
S. M. Benson
Berkeley, CA 94720

Netherlands Energy Research Foundation ECN (2)
Attn: T. Deboer, Mgr.
L. H. Vons
3 Westerduinweg
PO Box 1
1755 ZG Petten
THE NETHERLANDS

DISTRIBUTION (continued):

1540	W. C. Luth		6332	L. D. Tyler
6000	D. L. Hartley		6332	F. G. Yost
6300	R W. Lynch		6431	P. A. Davis
6310	T. O. Hunter		6431	R. L. Hunter
6311	L. W. Scully		6431	M. D. Siegel
6312	F. W. Bingham		6431	C. D. Updegraff
6314	J. R. Tillerson		7100	C. D. Broyles
6330	W. D. Weart		7120	M. J. Navratil
6330	Sandia WIPP Central Files (700H IND) (2)		7125	R. L. Rutter
6331	A. R. Lappin		7130	J. D. Kennedy
6331	R. L. Beauheim (2)		7133	R. D. Statler
6331	D. J. Borns		7133	J. W. Mercer
6331	M. M. Gonzales		7135	P. D. Seward
6331	A. L. Jensen		8024	P. W. Dean
6331	S. J. Lambert		3141	S. A. Landenberger (5)
6331	K. L. Robinson		3151	W. L. Garner (3)
6331	C. L. Stein		3154-1	C. H. Dalin (28)
6331	D. Tomasko			For DOE/OSTI (Unlimited Release)